

MAGNETOM FLASH

Content

MR Spectroscopy
with *syngo*
Page 8

Perfusion MRI/MRS for
Brain Tumors
Page 22

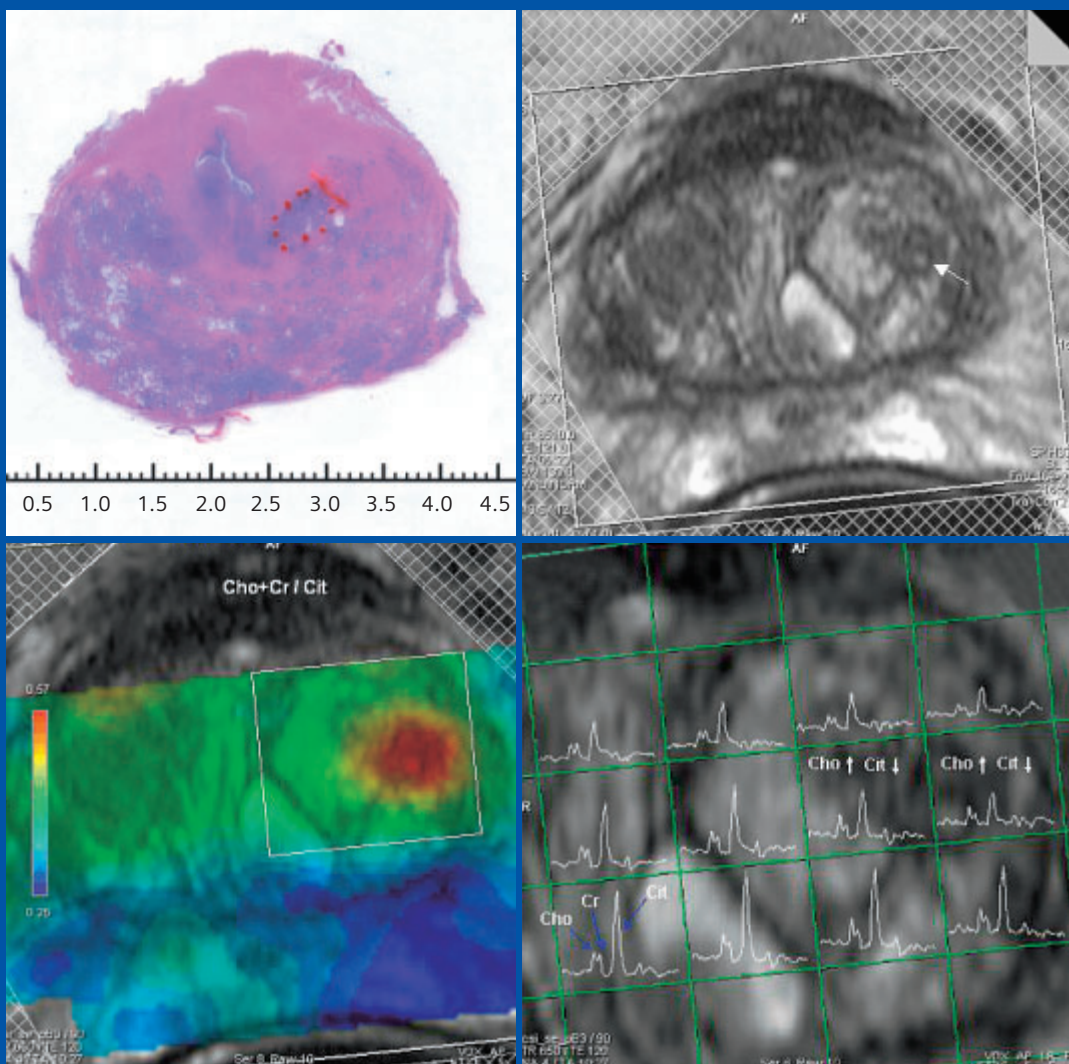
3T MR Spectroscopy
Page 48, 50

Case Reports:
Prostate MRS
Page 58

The Potential of ^1H MRS
of the Breast
Page 64

^{31}P MR Spectroscopy
of the Heart
Page 66, 74

MR Spectroscopy of
Prostate Carcinoma



3rd MAGNETOM World Summit 2004 Cardiac MR Ambassador Meeting 2004

Rottach-Egern, Tegernsee,
Germany

June 23-27, 2004

Dear MAGNETOM User,

We cordially invite you to join our community and attend the 3rd MAGNETOM World Summit and Cardiac MR Ambassador Meeting.

The community of MAGNETOM Users has been growing steadily worldwide over the last years. By providing a platform for socializing and exchanging information, we want to create the path for trans-setting developments in MR.

Both meetings will take place in one of the most beautiful areas of central Europe. We look forward to offering you a traditional Bavarian welcome at the picturesque Tegernsee, one of Germany's hidden treasures.

We look forward to seeing you there.

With warmest regards,

Dr. Heinrich Kolem Dr. Bernd Montag
President MR VP MR Marketing

3rd MAGNETOM World Summit 2004

Wednesday, June 23

6:00 – 8:00 P.M. Welcome Reception

Thursday, June 24

New paradigms

8:30 – 8:40 A.M.	Welcome
8:40 – 9:00 A.M.	MAGNETOM World meets again...
9:00 – 9:20 A.M.	Why Tim – How did it change the applications?
9:20 – 9:40 A.M.	Parallel Imaging with Tim
9:40 – 10:40 A.M.	Whole Body Imaging – Is it already a clinical reality?
10:40 – 11:00 A.M.	Coffee Break
11:00 – 12:00 P.M.	The impact of Tim at NYU
12:00 – 12:30 P.M.	The technology behind Tim
12:30 – 1:00 P.M.	How will Tim affect the future?
1:00 – 2:15 P.M.	Lunch
2:15 – 2:30 P.M.	Exciting Applications in the MAGNETOM World

New advances

2:30 – 3:00 P.M.	Stroke
3:00 – 3:30 P.M.	Coffee Break
3:30 – 4:00 P.M.	Routine iPAT Neuro Applications
4:00 – 4:30 P.M.	Diffusion Tensor Imaging: clinical opportunities
4:30 – 5:30 P.M.	Hands-on: Neuro
7:00 P.M.	Social Event

Friday, June 25

New applications

8:30 – 9:00 A.M.	Ultra High-Field Club News
9:00 – 9:30 A.M.	Prostate Spectroscopy
9:30 – 9:50 A.M.	3T Cartilage Imaging and its clinical value
9:50 – 10:10 A.M.	Breast MR-Perfusion
10:10 – 10:30 A.M.	Kidney Perfusion
10:30 – 10:45 A.M.	Coffee Break
10:45 – 12:30 P.M.	Hands-on: Kidney Perfusion Breast MR-Perfusion Prostate Spectroscopy
12:30 – 1:30 P.M.	Lunch
1:30 – 1:45 P.M.	Exciting Applications in the MAGNETOM World
1:45 – 2:15 P.M.	CMR with the 1 st Tim system and the MAGNETOM Trio
2:15 – 2:45 P.M.	Cardiomyopathy Assessment with CMR
2:45 – 3:15 P.M.	CMR in private practice
3:15 – 4:15 P.M.	Hands-on: Cardiac
4:15 – 4:30 P.M.	Wrap up
6:00 – 8:00 P.M.	Welcome Reception Cardiac MR Ambassador Meeting

Registration fee: Euro 500.00



Hotel Information

This hotel will host the meeting!

Dorint Seehotel Überfahrt

Überfahrtstraße 10,
D-83700 Rottach-Egern
Phone: +49 (0)8022 669-0
Fax: +49 (0)8022 669-1000

Single Occupancy EUR 175.00
Double Occupancy EUR 221.00
www.dorint.com/tegensee

Hotel Bachmair am See

Seestraße 47,
D-83700 Rottach-Egern
Phone: +49 (0)8022 272-0
Fax: +49 (0)8022 272-790

Single Occupancy EUR 140.00
Double Occupancy EUR 190.00
www.bachmair.de

Cardiac MR Ambassador Meeting 2004

Friday, June 25

1:45 – 4:15 P.M.	Cardiovascular MR at the MAGNETOM World Summit
6:00 – 8:00 P.M.	Welcome Reception

Saturday, June 26

8:00 – 8:30 A.M.	Registration
8:30 – 9:15 A.M.	Siemens Talks Siemens update on products and WIPs
9:15 – 10:00 A.M.	Customer Talks How I do a myocardial perfusion exam?
10:00 – 10:45 A.M.	Coffee Break
10:45 – 1:00 P.M.	Working groups in parallel sessions and live demos
	• Sequences and methods: k-space coverage strategies
	• Roles of cardiac CT and MR as non invasive diagnostic tools
	• Pediatric imaging
	• Live demos on syngo 2004A/2004V, Argus and Vessel View
1:00 – 2:30 P.M.	Lunch
2:30 – 4:00 P.M.	Working groups in parallel sessions and CMR hotline
	• CMR with the MAGNETOM Family: system differences
	• Myocardial perfusion
	• Vessel wall/plaque imaging
	• CMR application hotline
4:00 – 4:30 P.M.	Coffee Break
4:30 – 6:00 P.M.	Customer Talks and CMR Young Investigator Award
7:00 P.M.	Social Event

Sunday, June 27

8:30 – 10:00 A.M.	Customer Talks
10:00 – 10:30 A.M.	Coffee Break
10:30 – 12:20 P.M.	Summary of working groups
12:20 P.M.	Closing remarks
12:30 P.M.	Adjourn

Registration fee: Euro 500.00

Fax: +49 (0) 91 31 84-21 42

Mailing address:

ATTN: Christina Spiller
Siemens AG, Medical Solutions
Corporate Communications
Henkestr. 127, D-91052 Erlangen
Germany

MAGNETOM World Summit Registration Form

Please complete this form below or visit us at www.siemens.com/magnetom-world for online registration.
If several people from your institution will be participating, please complete this form for each attendee.
Forms must be received before May 28, 2004.

You may either fax or mail this registration form.

Fax: +49 (0)9131 84-2142 Mailing address on the back page.

Title/First Name

Last Name

Institution

Mailing address
(Include country)

Telephone
(Include country code)

E-mail address

I will attend the ☐ 3rd MAGNETOM World Summit, June 23 – 25
☐ Cardiac MR Ambassador Meeting, June 25 – 27

Hotel Reservation ☐ Yes ☐ No

Arrival Date Departure Date

☐ Single Occupancy ☐ Double Occupancy (Shared with)

Preferred Hotel* ☐ Dorint Seehotel Überfahrt
☐ Hotel Bachmair am See

Please indicate specific issues that you would like to see addressed
by Siemens during this session.

Please verify the visa requirements by contacting your local consulate.
All changes/amendments have to be made to
christina.spiller@siemens.com.

*Hotel reservation changes are always subject to availability.

6
87

EDITORIAL IMPRESSUM

EVENTS

2

3rd MAGNETOM World Summit 2004
Cardiac MR Ambassador Meeting 2004

PRODUCT NEWS

8

MR Spectroscopy with *syngo* MR 2004 A/V:
Automation with Flexibility SVS, 2D CSI, and 3D CSI,
with Long and Short TE

CLINICAL

14

Clinical MR Spectroscopy:
A Primer

16

Metabolite Ratios in Clinical MR Spectroscopy

22

Perfusion MRI and MRS for Brain Tumors

32

MR Spectroscopy Precision and Repeatability:
Evaluation of Brain CSI Data

36

¹H-MRSI Guided Surgery of Brain Tumors

40

Case Report:
Gliomatosis Cerebri

42

Spectroscopy in Differential Diagnosis of an Intracranial Mass Lesion

46

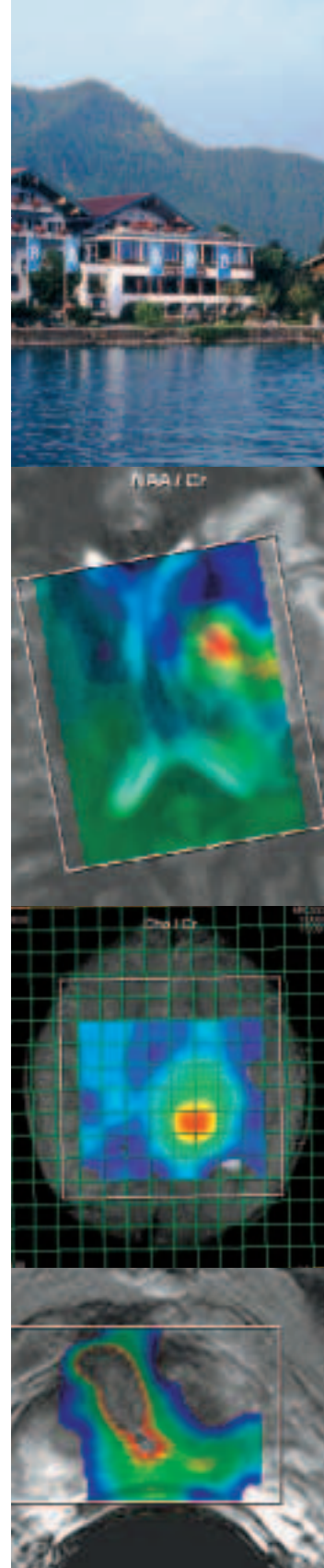
Proton Magnetic Resonance Spectroscopy (MRS) in Primary Pediatric
Brain Tumors

48

Case Report 3T:
Sjögren-Larsson Syndrome

50

Localized Proton Spectroscopy in Hepatic Encephalopathy:
Advantage of 3T-High-Field for Discrimination of
Glutamine and Glutamate



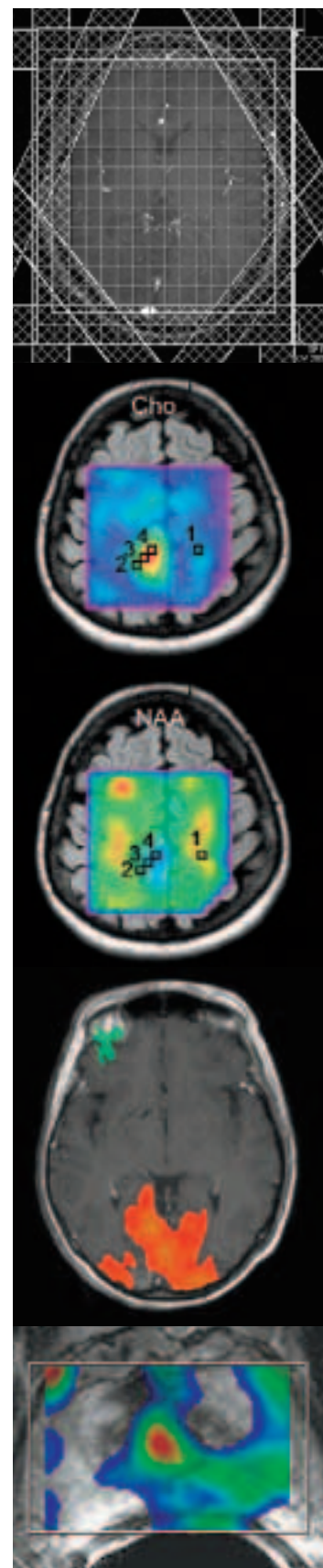
54	Proton MR Spectroscopic Imaging in the Clinical Evaluation of Prostate Cancer
56	Results from IMAPS Study
58	Case Report: Prostate Carcinoma Stage T3b
60	Prostate Carcinoma Detected with Single Voxel Spectroscopy
62	¹ H-MR Spectroscopic Imaging of the Human Prostate: from 1.5 to 3T
64	The Potential of ¹ H MRS of the Breast
66	³¹ P-MR Spectroscopy of the Heart – Current Status and Future Potential
74	³¹ P-Chemical Shift Imaging for Myocardial Infarction
76	Functional investigation of exercising muscle: a non-invasive Magnetic Resonance Spectroscopy – Magnetic Resonance Imaging approach
84	FAQs

LIFE

86	Life
----	------

The information presented in MAGNETOM Flash is for illustration only and is not intended to be relied upon by the reader for instruction as to the practice of medicine. Any health care practitioner reading this information is reminded that they must use their own learning, training and expertise in dealing with their individual patients. This material does not substitute for that duty and is not intended by Siemens Medical Solutions to be used for any purpose in that regard.

The drugs and doses mentioned in MAGNETOM Flash are consistent with the approval labeling for uses and/or indications of the drug. The treating physician bears the sole responsibility for the diagnosis and treatment of patients, including drugs and doses prescribed in connection with such use. The Operating Instructions must always be strictly followed when operating the MR System. The source for the technical data is the corresponding data sheets.



"Life is complex. It has real and imaginary components"


Happily ignoring any deeper meaning for the moment, spectroscopists like myself may regard the mentioned complexity as only the top of the iceberg of MRS complexity. Nevertheless, despite of all its complexity, life goes on: Researchers continue to discover the rich world of MRS techniques and applications, medical doctors find it worthwhile to cope with the extra bit of complexity of clinical MRS to establish new applications. And Siemens Medical Solutions continues to invest in it. Why is that so?

Based on the experience of decades, we have developed new MRS products and WIP packages and we have optimized workflow for clinical practice. The contributions of this issue show how our 1H MRS packages can add value to clinical MR exams, and how multinuclear capabilities can be used to answer questions of basic or clinical research.

New technical developments such as CSI acquisition weighting, Matrix Spectroscopy and display functionality such as transparent metabolite images translate immediately into user benefits. This technical development is on-going: Supporting new MR systems and especially higher field-strength systems, new sequences for making the most out of precious measurement time, and new post-processing concepts designed for extracting the relevant information are on our list. And since at the end of the day the user determines the value of our product, supporting you continues to remain the essential last step to success.

Our research, development and customer support activities thus serve a common goal: making your life with respect to MRS less complex.

Enjoy reading!



Stefan Roell

On behalf of the MR application development MRS team and many product managers and application specialists supporting MRS

Spectroscopy Team





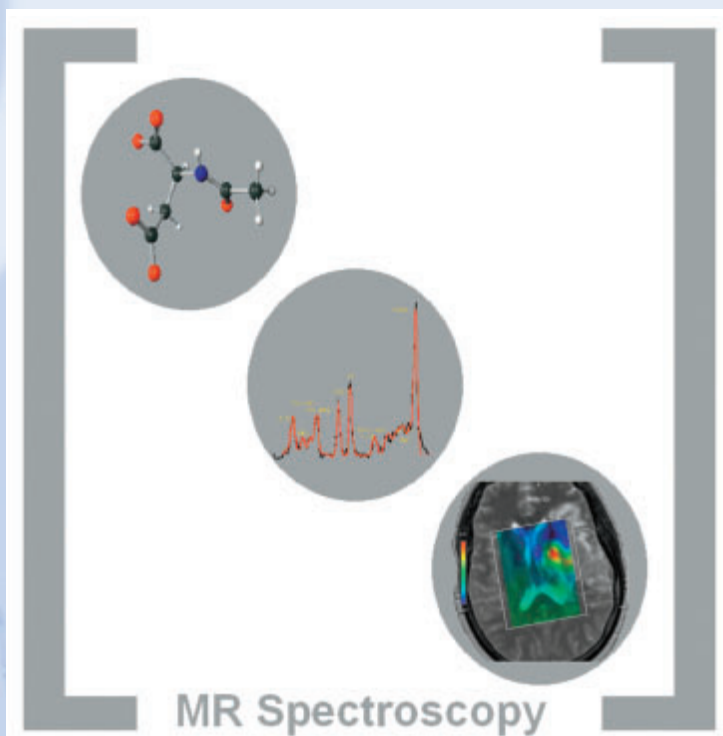
*S. Roell, Ph.D.
MR Application Development
Spectroscopy Team*



*E. Weiland, Ph.D.
MR Application Development
Spectroscopy Team*



*G. Heder, Ph.D.
MR Application Development
Spectroscopy Team*



*J. Ruff, Ph.D.
MR Application Development
Spectroscopy Team*



*N. Salibi, Ph.D.
R&D Collaborations, USA*



*U. Boettcher, Ph.D.
MR Application Development
Spectroscopy Team*



*M. Vorbuchner, R.T.
MR Application Development
Spectroscopy Team*

MR Spectroscopy with syngo MR 2004 A/V: Automation with Flexibility SVS, 2D CSI, and 3D CSI, with Long and Short TE

Nouha Salibi¹, Ph.D.
Stein Roell², Ph.D.

¹ Siemens Medical Solutions,
R&D Collaborations,
Malvern, PA, USA

² Siemens Medical Solutions,
MREA, Erlangen, Germany

Over the last few years, MR Spectroscopy (MRS) has become a routine component of clinical MRI examinations at many imaging centers around the world. The latest release of Siemens' syngo MR software is designed to offer unprecedented versatility and ease of use, allowing you to maximize the clinical usefulness of MRS at your institution.

MRS Techniques with syngo MR 2004 A/V: More Versatility than Ever Before

Proton MR spectroscopy* with syngo MR 2004 A/V includes single-voxel spectroscopy (SVS), as well as multi-voxel 2D and 3D chemical shift imaging (2D CSI and 3D CSI), with VOI (volume of interest) positioning

* The multinuclear option is available for MAGNETOM Symphony and Sonata systems (including upgrades) with syngo MR 2002B and above, for MAGNETOM Trio and Allegra with 2004A. For the MAGNETOM Avanto system it will be available with the upcoming SW release.

WIP: The information about this product is preliminary. The product is under development and is not commercially available in the US and its future availability cannot be ensured.

on 3 reference images (Fig. 3), free angulation capability, automated measurement adjustment software, and automated post-processing software. Both SVS and CSI sequences have volume-selective schemes that are based on either the SE (Spin Echo) technique or the STEAM (STimulated Echo Acquisition Mode) technique. All sequences have built-in variable TEs (echo times), with a minimum TE value of 30 ms for the SE-based sequences and 20 ms for STEAM. In MR spectroscopy, variable TE values provide the ability to control the T2 contrast of spectral peaks in the same way tissue T2 contrast is controlled in MR imaging. Short TE measurements are important for detection of metabolite signals that have a short T2 decay and are not visible on long TE spectra [1].

Matrix Spectroscopy

Matrix Spectroscopy supports MRS exams using Tim matrix coils or any other multiple element receive coil. This unique feature is available with syngo MR 2004V for the first time. By using matrix coils, greater SNR is gained than with single channel coils – SNR is something we can never have enough of in MRS. This SNR gain can be invested in, for example, reducing acquisition time or in increasing spatial resolution. Furthermore, due to its complete integration within Tim technology, Matrix Spectroscopy ensures that spectroscopy exams are part of the optimized Tim

workflow, so that no coil changes are required for MRS exams and reconstruction times are hardly noticeable. Hence, we minimize not only acquisition times, but also the entire exam time.

Matrix Spectroscopy supports all types of sequences: CSI, SVS and FID acquisitions. CSI datasets of a size of e.g. 32x32x16x1024 complex samples can be simultaneously received from four channels. When, for example, 16 receive channels are used, there are still no restrictions on other acquisition parameters such as TR or spectral resolution. Furthermore, a prime development goal has been the robustness of the method: phase coherent signal combination ensures maximum SNR. Due to the self-weighting property of the algorithm, the combined data is largely independent of the choice of coil elements made by the user. Robustness and accuracy has been proven by extensive in vivo testing. Finally, homogenization of CSI data is obtained either by normalizing the signals (i) to the very homogeneous sensitivity profile of the body-coil using pre-scan data, or (ii) to the least-squares norm well known for image normalization.

Lipid Contamination and Outer Volume Saturation

Lipid signals in the range of 0 ppm to 2 ppm are more prominent on short TE spectra. They may appear in brain spectra from inside the volume of interest (VOI) as a result of pathology,

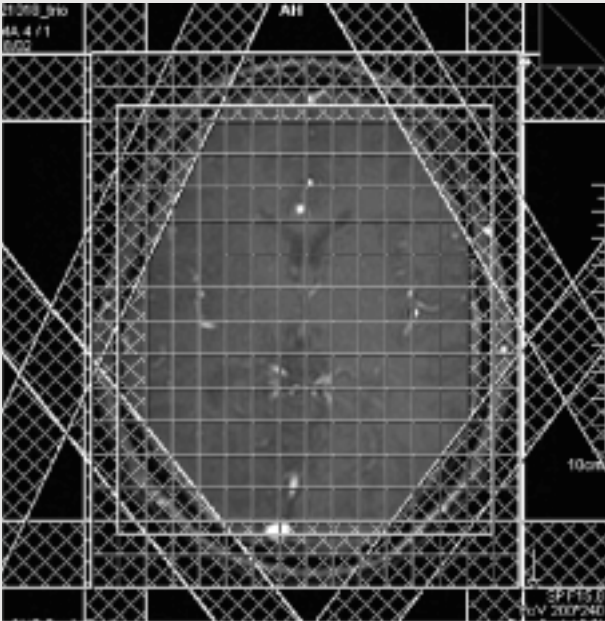


Figure 1 Outer volume saturation (OVS) slabs placed on a transverse brain image to suppress lipid signal from the scalp.

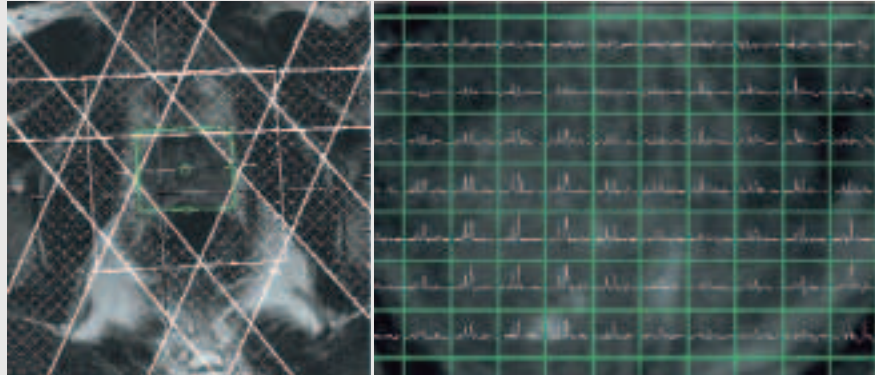


Figure 2a Positioning of outer volume saturation (OVS) slabs around a 3D CSI VOI of a proton MRS examination in prostate cancer (left). OVS, along with spectral lipid suppression, eliminate lipid contamination inside the VOI. This is clearly demonstrated in the spectral map (right) and on the spectra shown in Fig. 2b.

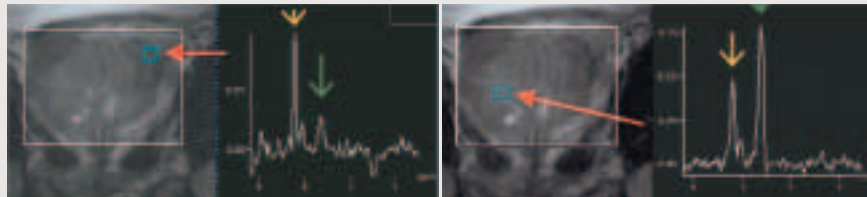


Figure 2b The image on the left shows a spectrum from a voxel in the lesion (indicated by the short red arrow). It has a high choline peak at 3.2 ppm (yellow arrow) and a reduced citrate signal at 2.6 ppm (green arrow) compared to the spectrum from a voxel in normal tissue (indicated by the long red arrow in the image on the right). The result shows an excellent lipid suppression.

or from outside the VOI as a result of contamination when a VOI is positioned very close to lipid-containing structures. Such contamination is also seen in prostate spectra, and can be eliminated by carefully placing outer volume saturation (OVS) slabs outside the volume of interest (Figs. 1 and 2a). In addition to OVS, prostate MRS sequences include spectral lipid suppression. A total of 12 OVS slabs can be positioned. 8 can be placed interactively by the user and 4 invisible slabs using the "fully excited VOI" feature.

MRS Data Presentation: Easy to Use

The automated syngo MR 2004 A/V post-processing software offers a number of new features for easy presentation of MRS data. Metabolite ratios for a single-voxel spectrum are automatically calculated and presented in a "table of results" format. CSI data can be displayed as single spectra, spectral maps, metabolite images, or images of metabolite ratios (Figs. 4, 5, and 6). Integral values of metabolite peaks (or their ratios) for individual voxels can be overlaid as a matrix onto an appropriate MR image or onto a "metabolite image".

2D CSI with syngo MR 2002 A/V

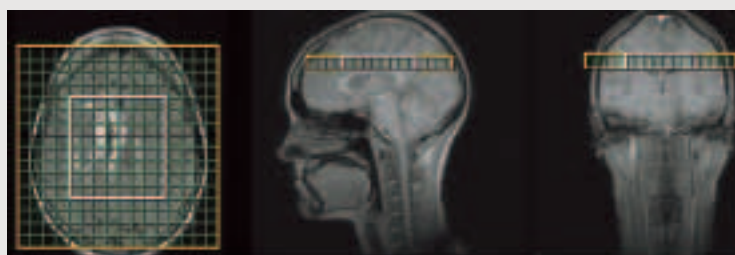


Figure 3 Positioning of a 2D CSI slice including presumably healthy brain tissue, as well as most of a lesion diagnosed as infiltrating anaplastic astrocytoma; the patient had undergone a resection of this neoplasm 12 months prior to this MRS follow-up examination.

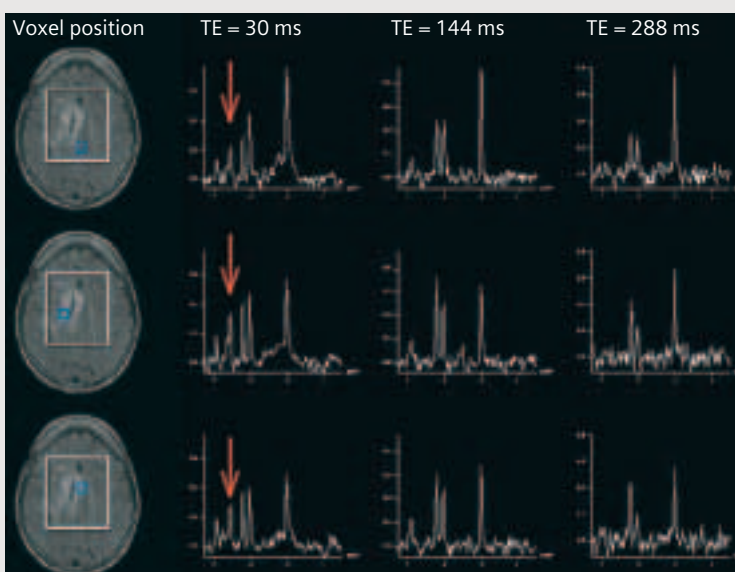


Figure 4 Spectra from the 2D CSI slice in Fig. 3. A 4 min 39 sec 2D CSI measurement was performed on the same slice at three different TEs. The last three columns show spectra from the same voxel (shown in the first column of each row) at the TEs indicated along the top of the figure. The first row represents control spectra. The last two rows are from the lesion. Spectra from the lesion have a reduced NAA/Cr ratio and an elevated Cho/Cr ratio. Short TE spectra from the lesion (second column, last two rows) have elevated myo-inositol (ml) (arrow) compared to the control spectrum (second column, first row).

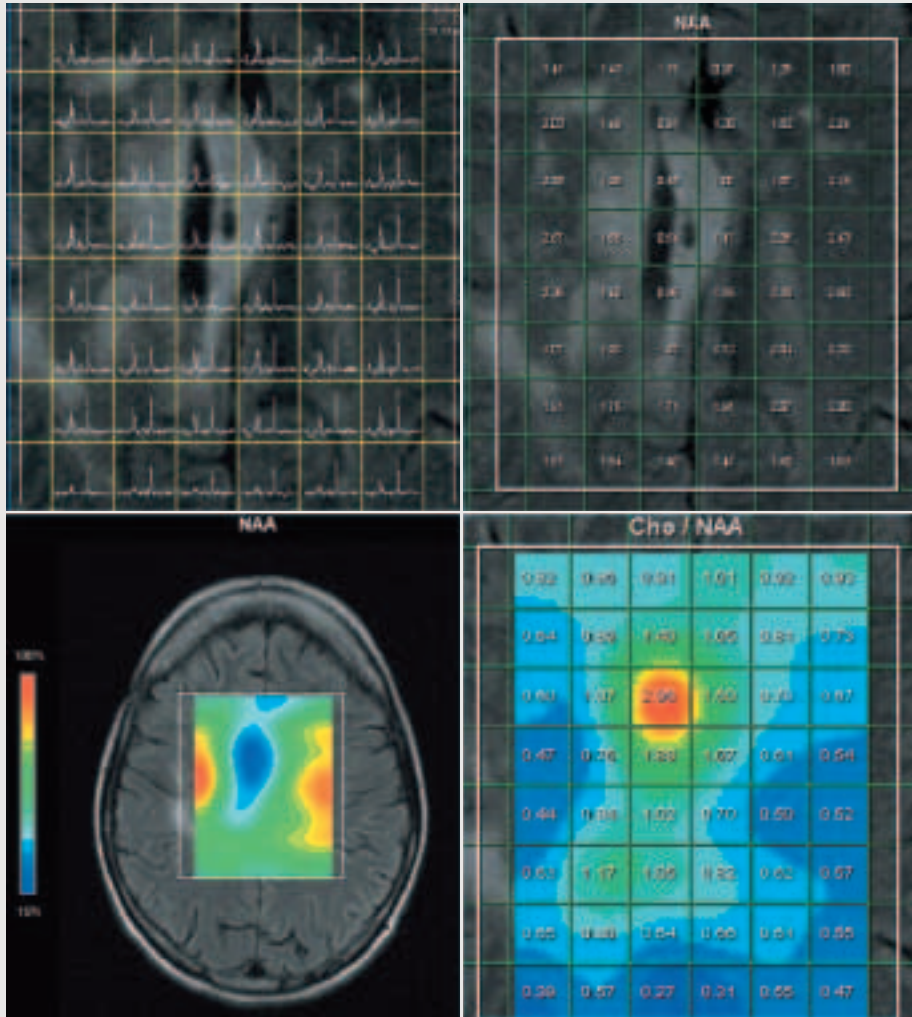


Figure 5 Top row: spectral map (left) and matrix of NAA integral values (right) generated from the 2D CSI data set (TE = 144 ms) demonstrate distribution of metabolites over the region of interest. Bottom row: map of the Cho/NAA ratio overlaid onto the corresponding metabolite image (right), and the NAA peak integral map overlaid onto the corresponding transverse image (left). It is clearly shown that NAA is considerably reduced within the lesion and in the immediately surrounding areas. The MRS results, along with other findings, suggest presence of residual tumor.

Oblique 3D CSI with syngo MR 2004 A/V

TE = 30 ms. Measurement time:
7 min 46 sec

Conclusion

MR Spectroscopy with the latest release of the syngo MR software offers unprecedented clinical utility through automation and flexibility. The full range of MRS techniques (SVS, 2D CSI, and 3D CSI) can be performed, with both long and short TEs. The MRS data can be displayed in several user-friendly formats, making it easier than ever to integrate MRS into your clinical MR imaging routine.

Acknowledgements:

Special thanks to Dr. A. Heerschap, Dr. T. Scheenen, Dr. D. Klomp et al., University Hospital Nijmegen, St. Radboud, NL, for the MRS data of Figure 2, and to Dr. E. Knopp and Dr. M. Law, NYU Medical Center, for the MRS data of Figures 3, 4, and 5.

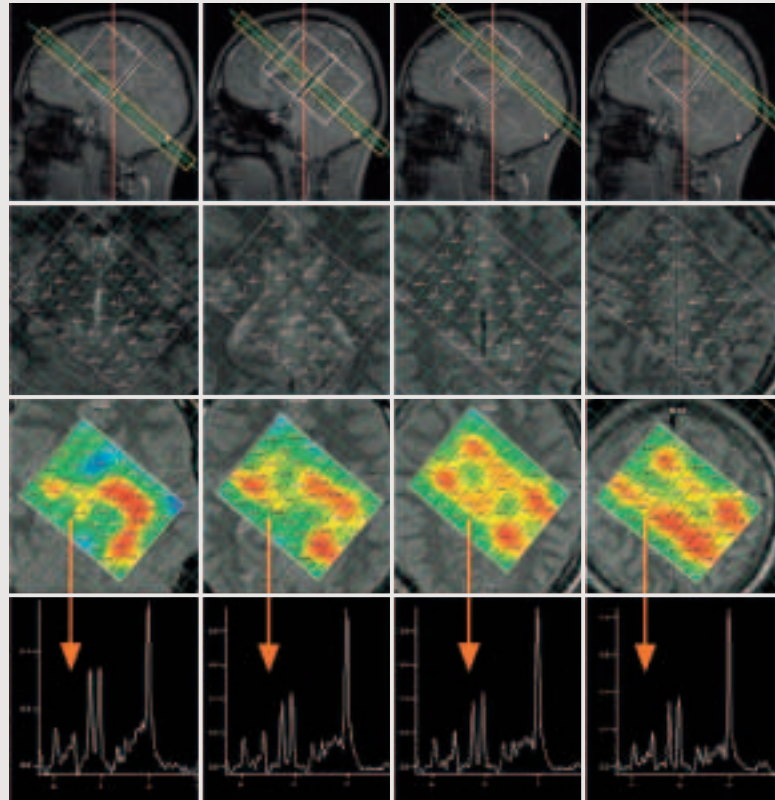


Figure 6 This figure illustrates some features of the syngo MR 2002A/V 3D CSI technique, including coverage, resolution, short TE acquisition, reduced measurement time, and a variety of ways to display the corresponding MRS data. This 3D CSI data set was acquired on the brain of a healthy volunteer with TR = 1500 ms, TE = 30 ms, and a measurement time of 7 min 46 sec, using weighted k-space sampling. The volume of interest (60 mm x 80 mm x 60 mm) is angled by 40 degrees from the transverse to the coronal orientation. Of the eight 3D partitions measured, four are within the volume of interest as demonstrated above. Each partition has a thickness of 15 mm and an in-plane resolution of 10 mm x 10 mm. The first row indicates the position of each of the four partitions that corresponds to the data shown in the same column. The second row shows spectral maps corresponding to each partition. The third row illustrates the display of the NAA integral values over the corresponding NAA metabolite images. The fourth row displays high quality short TE spectra from voxels in the third row (indicated by arrows).



Tim

will change MR forever.

It's a whole new way to think about MR. Going beyond incremental enhancements in magnet technology and gradient power to something radically different. A transforming technology that shifts the spotlight onto a new and tremendously innovative RF system and matrix coil design. Tim technology is a unique combination of features that will launch the next era in powerful MR advances. From revolutionary acquisition quality to breakthrough applications and remarkable profitability. It's opening up new worlds of possibility.

- Tim is a revolutionary. **Select exams, not coils.** [76 x 32] Up to 76 seamlessly integrated matrix coil elements and up to 32 RF channels combined to create one Total imaging matrix.
- Tim sees all. **Local becomes total.** True 205 cm (6' 9") seamless, whole-body anatomical coverage with no coil reconfiguration or patient repositioning.
- Tim knows no boundaries. **Parallel in all directions.** Head to toe, front to back, and side to side for unlimited Parallel Imaging.

Clinical MR Spectroscopy: A Primer

Nouha Salibi, Ph.D.

Siemens Medical Solutions USA,
R&D Collaborations,
Malvern, PA, USA

MR Spectroscopy as a Clinical Tool

Over the last few years, MR spectroscopy (MRS) has migrated beyond research laboratories to become an integral part of the clinical diagnostic routine. Although its main current application consists of proton MRS in the brain, there is a growing interest in using MRS for understanding pathology in the prostate, liver, muscle, breast, and heart. Multi-nuclear spectroscopy* promises to extend the clinical applications of MRS even further. MR images are based on MR signals from water and fat, which are the two most abundant metabolites in the body and generate strong MR signals that dominate those from other metabolites. Apart from water and fat, MRS can detect metabolites that are indicative of diseases, and can help in evaluating the effectiveness of certain therapeutic approaches. In many instances, MRS is an attractive, noninvasive approach for resolving ambiguous findings seen on MR images and for monitoring the recovery of tissue under various therapeutic approaches.

** The multinuclear option is available for MAGNETOM Symphony and Sonata systems (including upgrades) with syngo MR 2002B and above, for MAGNETOM Trio and Allegra with 2004A. For the MAGNETOM Avanto system it will be available with the upcoming SW release.*

WIP: The information about this product is preliminary. The product is under development and is not commercially available in the US and its future availability cannot be ensured.

MRS Techniques

Clinical proton MRS techniques include single-voxel spectroscopy (SVS) and multi-voxel 2D and 3D chemical shift imaging (2D CSI and 3D CSI). SVS and some CSI sequences use volume-selective schemes that are based on either the SE (Spin Echo) technique or the STEAM (Stimulated Echo Acquisition Mode) technique. Both SE and STEAM have three selective radiofrequency (RF) pulses to excite three orthogonal planes. A spectrum is collected from the volume defined by the intersection of the three excited planes. The SE sequence has one 90° pulse followed by two 180° pulses, whereas STEAM has three 90° pulses. While both sequences yield the same metabolic information, SE has twice as much signal. Single voxel spectroscopy produces a single spectrum from a single voxel (Fig. 2) that is typically 8 cm³ in volume, whereas CSI measures spectra from multiple voxels that are typically 1 cm³-1.5 cm³ in volume. CSI data may be presented in a variety of displays including individual spectra, spectral maps, or colored metabolite images overlaid on anatomical images (Figs. 3, 4). The two techniques are illustrated in Figures 2-4, where the same lesion has been examined with SVS (Fig. 2) and CSI (Figs. 3, 4). The two measurements yield comparable metabolic differences between spectra from the lesion and from the surrounding tissue. However, the relative changes among peaks are slightly different due to the difference in the relative amount of healthy tissue contained in the SVS (8 cm³) and the CSI (1.5 cm³) voxels.

Which Technique When?

The choice of MRS technique should be tailored to each particular clinical

case. In certain instances, SVS is a straightforward approach to collecting the desired MRS information (especially with metabolic brain disorders); it produces a single spectrum from a single volume of 2 cm³ to 8 cm³ in size. In other instances, however, SVS may not be optimal for investigating a lesion that is too large to be fully contained within the voxel, or a lesion that is too small to affect spectral peaks from a 2 cm³ voxel. 2D or 3D CSI multi-voxel techniques allow better coverage of one large lesion or multiple lesions, and allow higher spatial resolution than SVS, which is needed for the investigation of regional variations within the VOI. Moreover, CSI measurement times are currently comparable to SVS measurement times. In the examples shown in Figures 3-4, the CSI approach allows examination of the lesion, as well as of the tissue surrounding the lesion, from the same CSI data set.

MRS at Various TEs

In MR spectroscopy, variable TE values provide the ability to control the "T2 contrast" of spectral peaks in the same way tissue T2 contrast is controlled in MR imaging. Short T2 metabolite signals decay faster, and the corresponding spectral peaks are not seen on long TE spectra. As illustrated in Figure 5, detection of such metabolites requires short TE measurements. The major healthy brain metabolite peaks that are seen on long TE spectra include N-acetyl aspartate (NAA) at 2.02 ppm and 2.6 ppm, total choline (Cho) at 3.20 ppm, and total creatine (Cr) at 3.02 ppm and 3.9 ppm. Short TE spectra contain additional peaks, which include glutamine and glutamate (Glx) between 2.05-2.5 ppm and 3.65-3.8 ppm, scyllo-inositol (SI) at 3.36 ppm, glucose at 3.43 ppm and

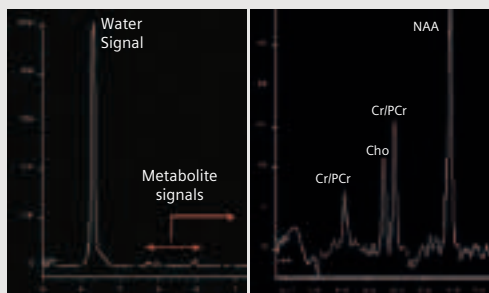


Figure 1 Spectra from normal brain tissue. Small metabolite peaks are not visible in the presence of a large water peak (left spectrum). A water-suppressed spectrum on the right clearly displays the major brain metabolite peaks at TE = 144 ms, namely N-acetyl aspartate (NAA), choline (Cho), and creatine/phosphocreatine (Cr/PCr).

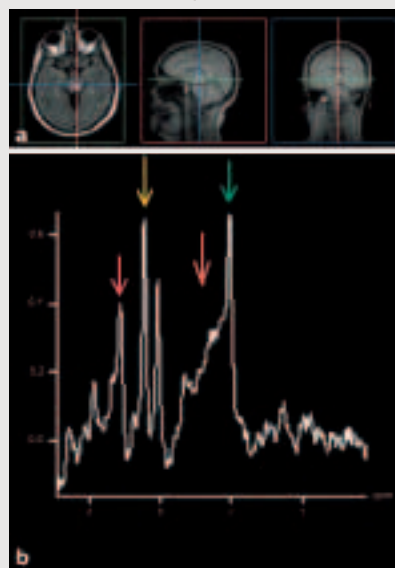


Figure 2 (a), a single voxel is positioned to enclose a low-grade brain stem glioma. The voxel is 8 cm³. The corresponding spectrum (b) is acquired with the SE sequence (TR = 1500 ms and TE = 30 ms). The spectrum shows reduced NAA (green arrow) with elevated choline (yellow arrow) and elevated myo-inositol (red arrow) and Glx (orange arrow).

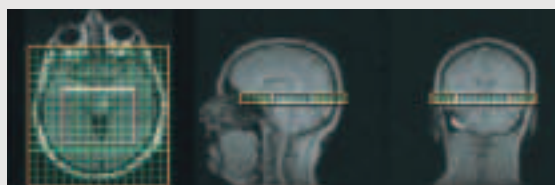


Figure 3 Positioning of a 2D CSI slice including the low-grade brain stem glioma, as well as healthy brain tissue. Some CSI results are shown in Fig. 4.



Figure 4 2D CSI data set acquired with TR = 1500 ms, TE = 30 ms, and a spatial resolution of 1.5 cm³. CSI results are shown as a spectral map (b), as spectra from the voxels indicated by red arrows (a), and as a choline metabolite image (c) generated from integral peak values. Elevated choline within the lesion is seen in the spectral map (b) and in the metabolite image (c) (red area). The upper spectrum in (a) is from the lesion and shows reduced NAA (green arrow), and elevated Cho (yellow arrow), ml (red arrow), and Glx, as compared to the lower spectrum in (a) which is from surrounding tissue.

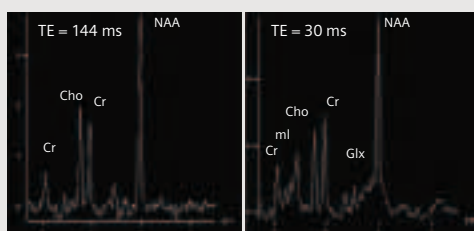


Figure 5 Spectra from the same 8 cm³ single voxel in healthy brain tissue, acquired with the SE sequence at TE = 144 ms (left) and TE = 30 ms (right). Additional metabolite peaks are seen on the short TE spectrum. (Not all peaks are labeled for clarity).

3.8 ppm, and myo-inositol (ml) at 3.56 ppm and 4.06 ppm. Figure 5 also illustrates the dependence of peak metabolite ratios on TE. At TE = 144 ms, the choline peak is higher than creatine, whereas at TE = 30 ms, choline is lower than creatine due to the fact that creatine has a shorter T2 and decays faster than choline.

MRS and Magnetic Field Strength

MR spectroscopy is currently performed on clinical and research scanners at magnetic field strengths of 1 Tesla, 1.5 Tesla, and 3 Tesla. Spectroscopy at fields higher than 1.5T has been driven by the demand for improved sensitivity and better spectral resolution (i.e. chemical shift dispersion), which in turn allow for more reliable quantitation of MRS spectra. However, clinical MRS at higher fields presents new challenges, including increased chemical shift misregistration, and increased magnetic susceptibility effects that reduce resolution and sensitivity. New technical developments to overcome such challenges are currently being investigated and implemented in order to optimize the advantages of higher field MRS.

Conclusion

In recent years, considerable technological advances in MR scanner hardware and software have allowed the development of new and sophisticated approaches to MR spectroscopy. The currently available SVS and CSI techniques offer flexibility, automation, and a variety of features that can be tailored to specific clinical MR examinations in order to make MR spectroscopy an integral part of your clinical MRI routine.

Metabolite Ratios in Clinical MR Spectroscopy

Nouha Salibi, Ph.D.

Siemens Medical Solutions USA,
R&D Collaborations,
Malvern, PA, USA

1-Quantification in Clinical MR Spectroscopy

MR spectroscopy (MRS) is an established and accurate analytical tool in chemistry and biochemistry where it is used under optimized and controlled experimental conditions. The ability of MRS to provide reliable absolute quantification has not materialized with clinical MR Spectroscopy because it is not currently practical to incorporate absolute quantification into routine clinical practice. Time and effort are necessary to meet technical and clinical challenges, which include relatively noisy spectra and poorly separated peaks at 1T and 1.5T, the use of an internal or external reference, and the need for correcting many parameters that affect spectral peak intensities such as coil loading, partial volume effects, regional susceptibility effects and relaxation times. Of these challenges, only those related to S/N and peak separation may benefit from MRS at higher field strength.

Many approaches to clinical interpretation of spectra have been proposed as an alternative to absolute quantification. In certain instances, visual inspection of spectra or qualitative interpretation may provide the clinical answer. A more common practice is the comparison of metabolite ratios from pathological tissue to those from identical normal brain tissue of healthy volunteers. Metabolite ratios are readily provided by the scanner software and do not

require additional correction. Although this method is practical to use clinically, its success depends on the consistent use of the same measurement technique, same parameters and identical voxel position on all subjects. As demonstrated below, metabolite ratios vary with measurement parameters such as TR (Fig. 1) and TE (Fig. 5, table 1) and with regions of the brain (Figs. 1 and 2). Additionally, ratios are typically taken with respect to creatine (Cr), which is the most stable metabolite in the brain. However certain diseases do affect creatine levels in the brain, as demonstrated in the case study presented below.

2-Regional Variations of Metabolite Ratios

Figures 1 and 2 demonstrate variations in spectral patterns with voxel position and with TE. Data were obtained at 1.5T from the brain of a healthy volunteer with TR = 1500 ms, TE = 30 ms (Fig. 1) and TE = 144 ms (Fig. 2) in white matter, gray matter, cerebellum and pons. The observed variations imply that metabolite ratios from a voxel containing pathology should be compared to metabolite ratios measured with the same parameters at a similar voxel position in healthy volunteers or in an unaffected contra-lateral area of the brain, if possible.

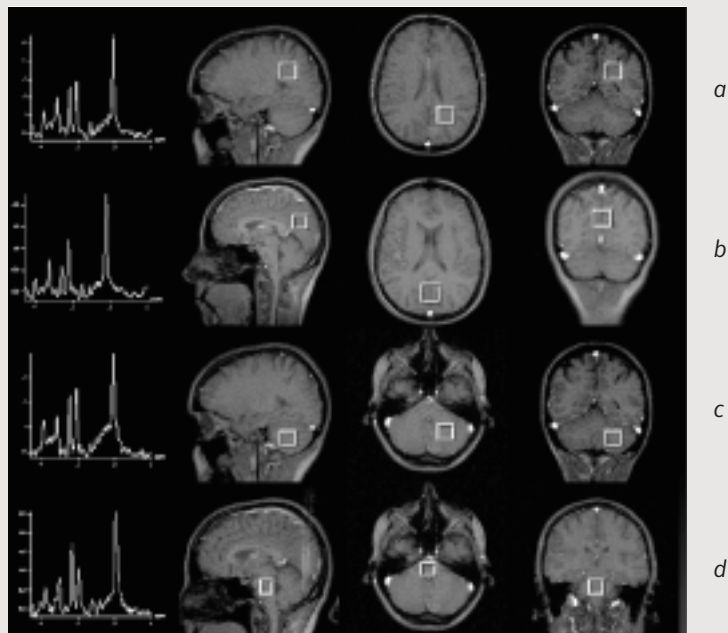


Figure 1 Spectra from an 8 cm³ single voxel measurements in various regions of the brain at 1.5T: Parietal white matter (a), midline gray matter (b), cerebellum (c) and pons (d). All spectra were acquired with the SE sequence at TE = 30 ms, TR = 1500 ms and 128 averages. Visual inspection of these spectra clearly demonstrates variations in the relative peak amplitudes. Similar variations are reflected in the calculated peak integral values and metabolite ratios.

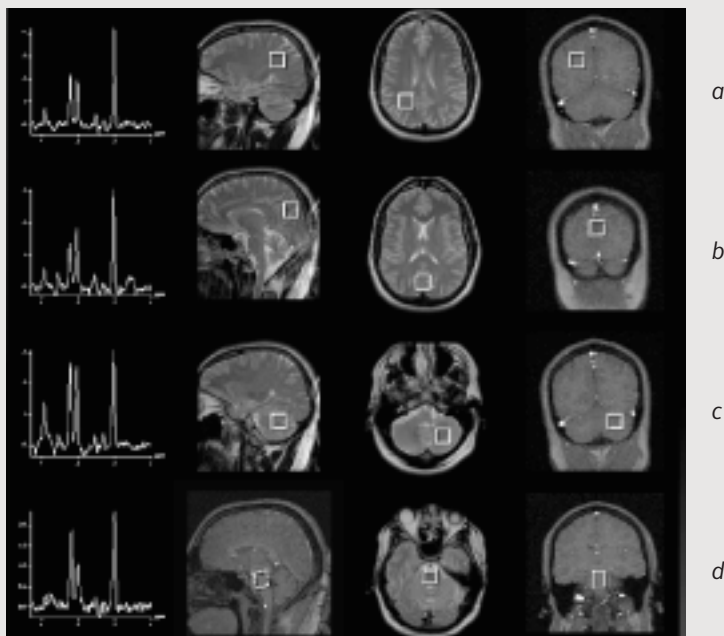


Figure 2 Spectra from 8 cm³ single voxel measurements in various regions of the brain at 1.5T: Parietal white matter (a), midline grey matter (b), cerebellum (c) and pons (d). All spectra were acquired with the SE sequence at TE = 144 ms, TR = 1500 ms and 128 averages. Visual inspection of these spectra clearly demonstrates variations in the relative peak amplitudes. Similar variations are reflected in the calculated peak integral values and metabolite ratios.

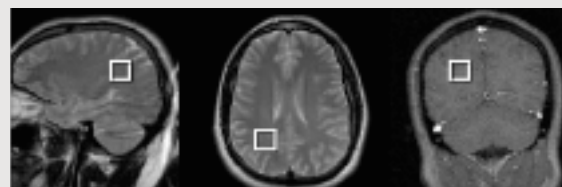


Figure 3 An 8 cm³ voxel is positioned mostly in white matter to measure the spectra in figure 4.

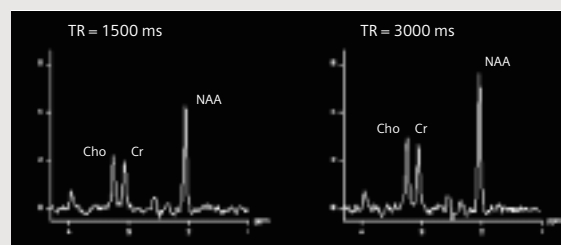


Figure 4 Spectra from the voxel shown in figure 3, acquired with the SE sequence at TR = 1500 ms, and 3000 ms (TE = 144 ms) are displayed on the same scale. The longer TR spectrum has higher metabolite peaks due to the longer time available for T1 recovery of the magnetization.

3-Metabolite Ratios at Various TR

For optimum S/N per unit time, clinical MR spectra are typically measured with a TR of 1500 ms to 3000 ms for both single voxel spectroscopy (SVS) and chemical shift imaging (CSI). Figure 4 shows spectra obtained at these TR values with a TE of 144 ms from the voxel defined in Figure 3. The metabolite ratios derived from peak integral values of these spectra are NAA/Cr = 2.21 and 2.0, and

Cho/Cr = 1.20 and 1.08 at TR = 1500 ms and 3000 ms respectively. The longer TR spectrum has higher metabolite peaks due to the longer time available for T1 recovery of the magnetization. The decrease in metabolite ratios with TR is due to the fact that T1 of creatine (Cr) is longer than T1 of Choline (Cho) and NAA (N-acetyl aspartate). Hence, for accurate interpretation and comparison of spectra, it is best to perform routine MRS exams with the same repetition time.

4-Metabolite Ratios at Various TE's

N. Salibi¹, Ph.D.; Glenn Foster², RT, RMR and Richard Nagel², RT, RMR
¹ Siemens Medical Solutions USA, Inc, Malvern, PA, USA
² Washington University School of Medicine, St. Louis, MO, USA

Although clinical brain spectra are routinely measured at the same TR value, it is now common practice to measure the same SVS or CSI volume

at more than one TE value. Multiple TE measurements yield added metabolic information and increased confidence in the interpretation of spectra. The experiment described in this section illustrates the effect of TE on metabolite ratios.

MR spectroscopy measurements were performed on a 1.5T MAGNETOM Sonata and on the brain of a healthy adult volunteer. A 20 mm x 20 mm x 20 mm voxel was placed in parietal white matter (Fig. 5); the spin echo (SE) sequence was used with TE = 30 ms, 60 ms, 100 ms, 144 ms, 200 ms, 250 ms and 288 ms. TR (2000 ms) and all other parameters including the shim were kept constant. Spectra in Figure 6 were evaluated with the Siemens post-processing software.

Peak integral values from Figure 6 were used to calculate the metabolite ratios listed in Table 1. The ratios indicate increasing values of NAA/Cr and Cho/Cr at longer echo times. The increase is due to the fact that creatine has the shortest T2 relaxation time and decays faster than NAA and choline (Fig. 7). This difference in the T2 decay of metabolites also explains the fact that shorter TE (30 ms) spectra* contain more metabolite peaks (i.e. short T2 metabolites) than longer TE (144 ms and 288 ms) spectra (Fig. 6). In spectroscopy, as in imaging, TE may be used to manipulate relative signal intensities or contrast. Hence interpretation of clinical spectra and metabolite ratios, like the interpretation of MR images, has to take into account the measurement echo time.

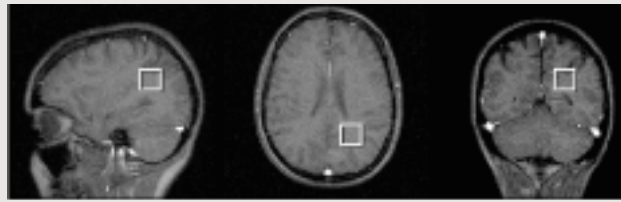


Figure 5 Position of the voxel used to measure metabolite ratios at various TEs.

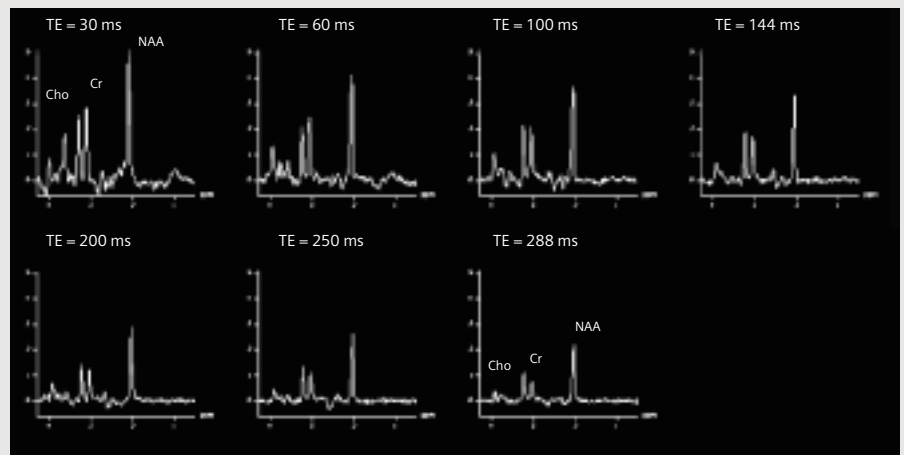


Figure 6 Spectra from parietal white matter of adult brain obtained at 1.5T with the SE sequence at various TEs. All other parameters including the shim were the same. The effect of TE on metabolite ratios is easily seen by comparing relative amplitudes of choline and creatine peaks at various TEs.

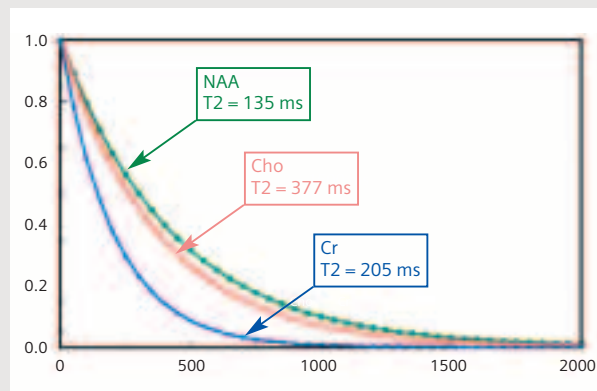


Figure 7 This figure shows the signal decay of NAA, choline (cho) and creatine (Cr). T2 values were derived from a semi logarithmic plot of peak integral values of the spectra in figure 6 as a function of TE.

TE(ms)	NAA/Cr	Cho/Cr
30	1.70	0.84
144	2.13	1.14
288	3.49	1.60

Table 1 metabolite ratios at different values of TE from the voxel in figure 3.

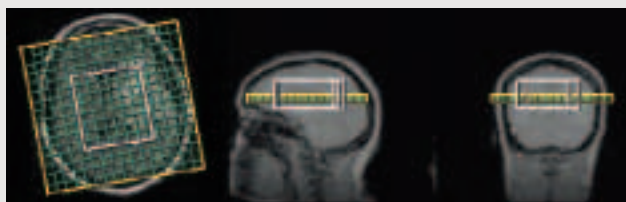


Figure 8 Positioning of a 3D CSI slab with a display of the slice used to generate the metabolite images in the following figures.

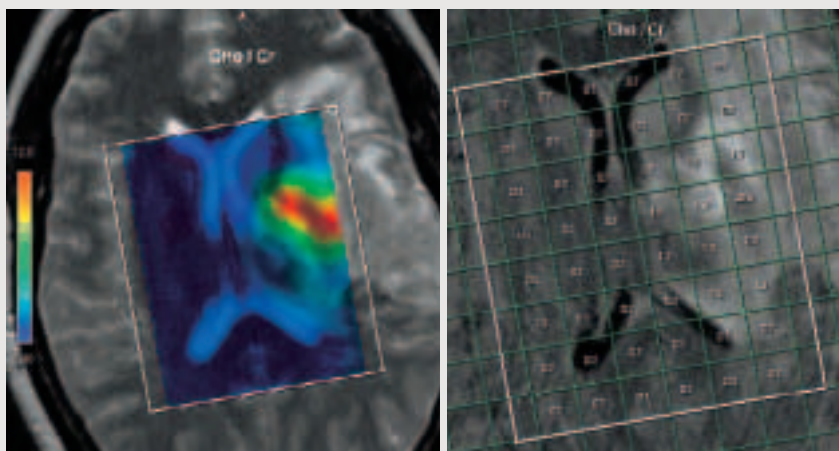


Figure 9 A Color metabolite image** of Cho/Cr (left), and a map of the numerical values of Cho/Cr (right). Both indicate higher Cho/Cr on the affected left side of the brain compared to healthy tissue on the right side of the brain.

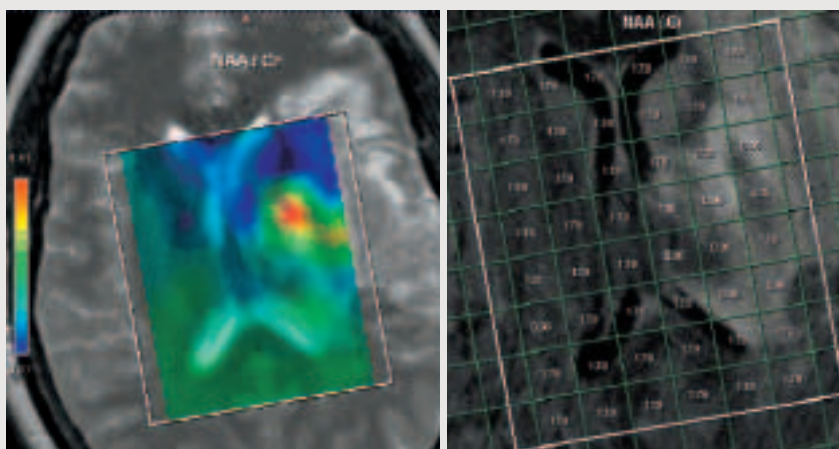


Figure 10 A color metabolite image** of NAA/Cr (left), and a map of the numerical values of NAA/Cr (right). Both indicate elevated NAA/Cr on the affected left side of the brain compared to healthy tissue on the right side of the brain.

5-Clinical Interpretation of Metabolite Ratios: A Case Study

N. Salibi¹, Ph.D., E.A. Knopp², M.D., Meng Law², M.D.,

¹ Siemens Medical Solutions USA, Inc, Malvern, PA, USA

² New York University school of Medicine, New York, NY, USA

A 3D CSI data set was obtained on a 45 year-old woman with a 10-day history of right arm and leg weakness, diagnosed with a stroke affecting the left middle cerebral artery vascular territory. Spectra were obtained at 1.5 T from a 3D volume measuring 80 mm x 70 mm x 40 mm. The CSI spin echo sequence was used with a TE of 144 ms, TR of 1500 ms, a spatial resolution of 10 mm x 10 mm x 10 mm and a measurement time of 8 min 20 sec. MRS data were processed with the Siemens post-processing software.

Figure 8 shows the selected 3D VOI (volume of interest) positioned over the affected area of the brain as seen on the MR images. Data from the slice indicated in the graph are representative of the complete 3D data set. Transparent** color images of Cho/Cr (Fig. 9) and NAA/Cr (Fig. 10) along with maps of numerical values of metabolite ratios show elevated Cho/Cr and NAA/Cr ratios on the affected left side of the brain compared to the normal contra-lateral side.

* For description of MRS techniques and their applications in the brain, the reader is referred to page 14 of this issue:
Clinical MR Spectroscopy: A Primer.

** Transparent metabolite images are available with syngo MR 2004.

This however does not imply an elevation in the NAA and Cho levels. Indeed NAA and choline metabolite images (Fig. 11) indicate a reduction of NAA and choline in that area. Furthermore inspection of the spectral map (Fig. 12) and of individual spectra (Fig. 13) confirms the fact that all metabolites are reduced on the left side of the brain; and the higher Cho/Cr and NAA/Cr ratios are a result of creatine being reduced the most in the setting of ischemia. Figures 13 and 14 demonstrate the importance of displaying spectra on the same scale for accurate comparison and interpretation.

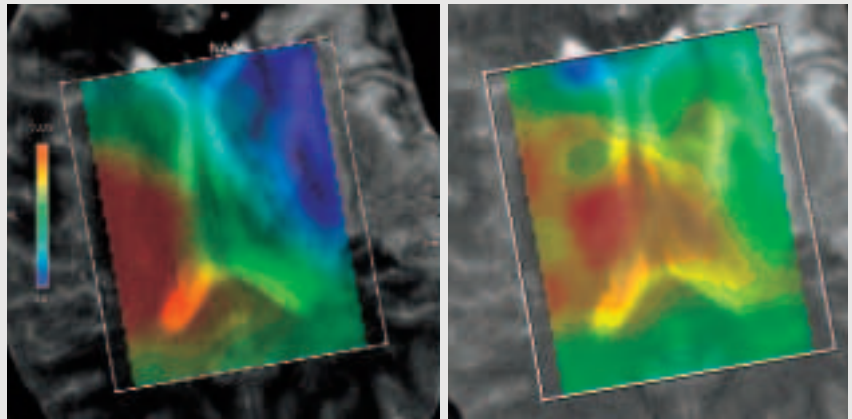


Figure 11 Metabolite images** of NAA (left) and choline (right) indicate reduced metabolite levels on the affected left side of the brain compared to healthy tissue on the right side of the brain.

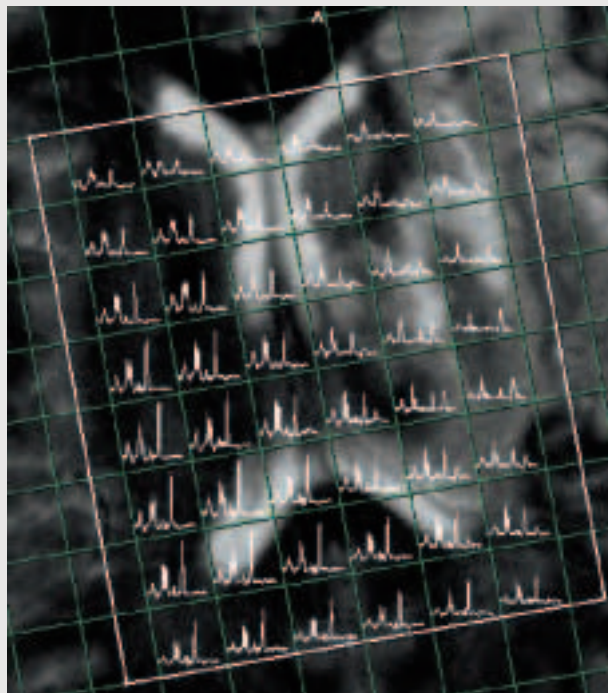


Figure 12 Spectral map shows overall reduced level of all metabolites on the affected left side compared to the right side of the brain.

** Transparent metabolite images are available with syngo MR 2004.

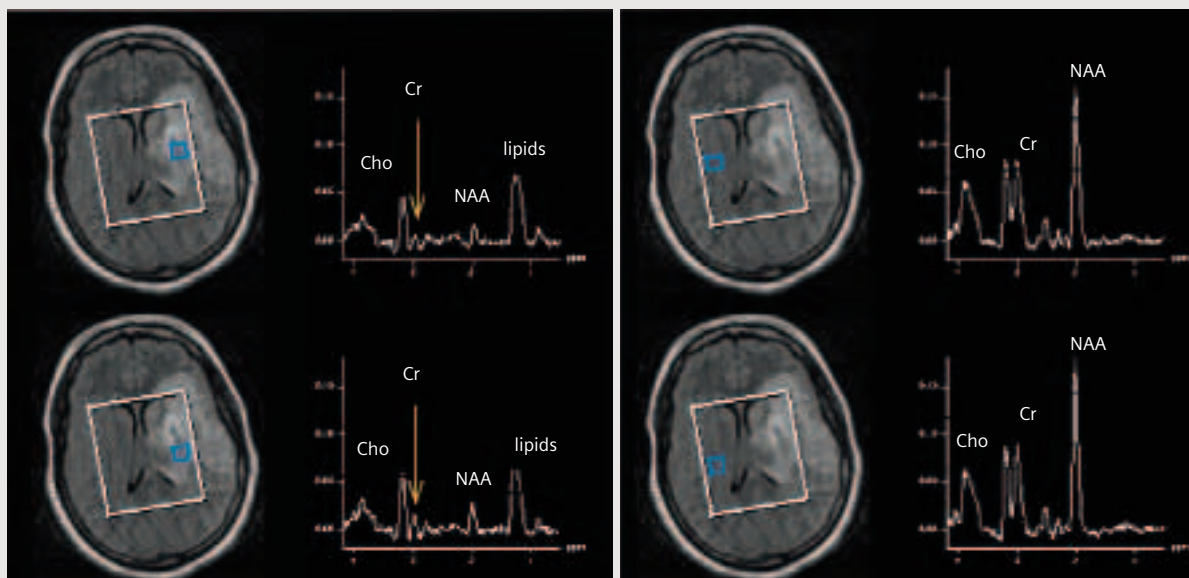


Figure 13 Spectra from indicated voxels within the affected side of the brain (left) and from contralateral normal voxels (right) are displayed on the same scale. Spectra from the affected side show overall reduction in metabolites and the presence of lipids, an indication of membrane breakdown. Reduction of creatine and NAA is more pronounced than that of choline. The absence of lactate suggests that this is probably a subacute stroke.

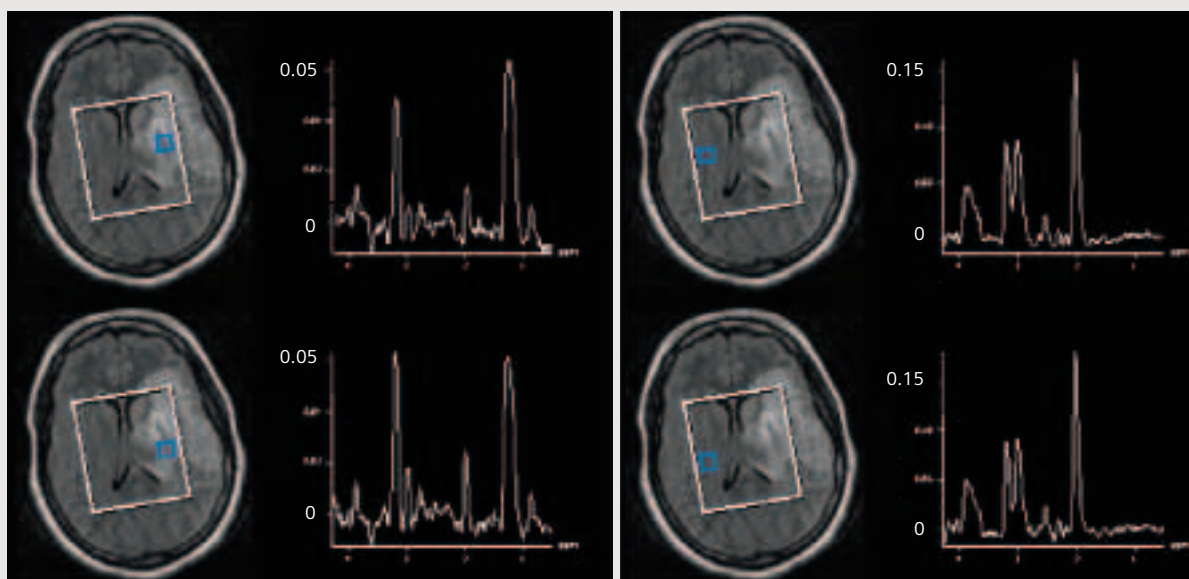


Figure 14 The same spectra as in figure 13 are displayed on different vertical scales defined by the highest peak in each spectrum. Without taking into consideration differences in vertical scales this display suggests that the spectra on the left show an elevation in choline levels with reduced NAA and creatine levels, and presence of lipids. The spectra may then be misinterpreted as tumor spectra.

Perfusion MRI and MRS for Brain Tumors

Meng Law¹, M.D.; N. Salibi², Ph.D.;
E.A. Knopp¹, M.D.

¹ New York University School of
Medicine, New York, NY, USA

² Siemens Medical Solutions USA,
Inc, Malvern, PA, USA

Introduction

Advanced MRI techniques, such as MR spectroscopy, diffusion and perfusion MR imaging can give important *in vivo* physiological and metabolic information, complementing morphologic findings from conventional MRI in the clinical setting. Combining perfusion MRI and MR spectroscopy will help in solving difficult cases and increase confidence in making a diagnosis.

Techniques

Brain tumor MR Imaging protocol: typical parameters for brain tumor imaging at 1.5 Tesla are shown in Table 1. Perfusion MRI exams are performed with TR/TE = 1,000 ms/54 ms; field of view 210 mm x 210 mm; section thickness 3-8 mm (typically 5 mm); matrix 128 x 128; in-plane voxel size 1.8 x 1.8 mm; intersection gap 0%-30%; flip angle 30°; signal bandwidth 1,470 Hz/pixel. Ten slices are usually obtained to cover the entire lesion volume as identified on T2-weighted images. A series of 60 multi-slice acquisitions are acquired at 1-second intervals. The combination of a 1,000-msec repetition time and a 30° flip angle ensures that T1 effects are minimized. The first 10 acquisitions are performed prior to the contrast agent injection to establish a pre-contrast baseline. At the 10th acquisition, gadopentetate dimeglumine (0.1 mmol/kg) is injected with a

power injector at a flow rate of 3-5 ml/sec through the intravenous catheter (18-22 gauge), the contrast agent injection is immediately followed by a bolus injection of saline (total of 20 ml at the same rate).

Proton MRSI protocol

The volume of interest is confirmed with scout HASTE (Half-Fourier Acquisition Single-Shot Turbo-Spin-Echo) images (TR/TE/excitations = 15 ms/6 ms/1; inversion time of 500 ms). Ten 5 mm sections are obtained with a 1 minute 15 seconds scan in the axial, coronal, and sagittal planes. Depending on lesion size, a volume selective 2D or 3D CSI sequence with TR/TE = 1,500 ms/144 ms (or 1500ms/30ms) is used for MRSI. A measurement at TE = 288 ms was initially included in the protocol and dropped later. As demonstrated in the examples below, this measurement provided no additional clinical information, although it contributed to a better understanding of the behavior of metabolite signals at various TEs. The hybrid multivoxel CSI technique uses a PRESS double spin echo scheme for pre-selection of a volume of interest (VOI) that is usually defined to include the abnormality as well as normal-appearing brain tissue when possible. To prevent strong contribution to the spectra from subcutaneous fat signals, the VOI is completely enclosed within the brain and positioned at the center of the phase-encoded field of view (FOV), which is large enough to prevent wraparound artifact. For lesions that are cortically based or near the skull base, the VOI can be rotated, and up to 8 outer volume saturation (OVS) slabs can be placed over the skull (Fig. 1). A typical VOI consists of an 80 mm x 80 mm region placed within a 160 mm x 160 mm FOV on a 10 mm to 20 mm slice.

A 16 x 16 phase-encoding matrix gives an 8 x 8 array of spectra in the VOI with an in plane resolution of 10 mm x 10 mm. Although the acquired 2D or 3D CSI data set can be measured with a higher spatial resolution, to save time interpolation is sometimes used to reduce the effective voxel size. Spatial resolution is set by adjusting the FOV and matrix size while keeping the measurement time at 8 minutes or less. A second 3D (or 2D) CSI sequence is also obtained (time permitting) with TR/TE = 1500 ms/30 ms (Table 1).

Clinical Applications of Perfusion MR and MR Spectroscopy in Brain Tumors

Assessment of Glioma Grade

Combined Perfusion MRI and MR Spectroscopy in the clinical setting provide complementary information that can be used for prospective grading of gliomas. This has important clinical utility to the neurosurgeon and neuro-oncologist (Figs. 2-5). For example, high-grade gliomas generally have higher relative cerebral blood volume rCBV* measurements and Cho levels than low grade gliomas [1].

Gliomatosis Cerebri

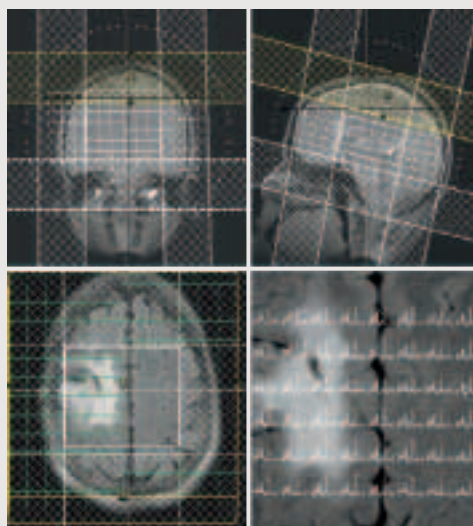
Gliomatosis cerebri is characterized by involvement of at least two lobes of the brain by a glial cell tumor of neuroepithelial origin with relative preservation of neuronal architecture [2]. Gliomatosis cerebri, which refers to the contiguous involvement of different regions of the brain, must be differentiated from multi-centric glioma, which is defined as multiple foci of tumor in different sites. Histopathologically, there is a lack of vascular hyperplasia in gliomatosis cerebri; this accounts for the relatively low rCBV* measurements, mean

Table 1 Brain tumor imaging protocol.

Sequence	TR (ms)	TE (ms)	Flip Angle /TI	Acq/NEX	Thickness (mm)	No. Slices	Matrix	FOV (mm)	Acq. time (min.sec)
Scout/Localizer	15	6	NA	1	8	3	256	280	0.19
Axial T1	600	14	90	2	5	20	256	210	3.36
Axial FLAIR	9000	110	180/2500	1	5	20	256	210	3.56
Axial T2	3400	119	180	1	5	20	256	210	1.36
1. Dual Echo/PD	3400	16	180	1	5	26	256	256	7.59#
Diffusion/ADC	3400	95	NA	3	5	20	128	210	1.15
2. DTI*	4000	95	NA	4	5	20	128	210	1.56
PERFUSION MRI	1000	54	30 degrees	60 (1/s)	3 to 8	10	128	210	1
Post Gd T1	600	14	90	1	5	20	256	210	3.36
MRSI	1500	144	90 2D CSI	3	10	1	16 x 16	160	6.05
		30	90 3D CSI	1	10	8	12 x 12	160	7.53
3. MP Rage	1100	4.38	15	1	0.9	192	256	230	3.33

Note: Total imaging time is approximately 30 mins. The optional sequences are:

1. Dual echo T2 – Proton density for patients in a stereotactic headframe, acquired instead of the FLAIR. Larger field of view (FOV) and square FOV (256x256) are used to match the software in the operating room for stereotactic biopsy or resection. No angulation.
2. Diffusion Tensor Imaging (DTI in 12 directions).
3. MPRage – reconstructed in the axial, coronal and sagittal planes. TI denotes Inversion Time.

**Figure 1**

*WIP: The information about this product is preliminary. The product is under development and is not commercially available in the US and its future availability cannot be ensured.

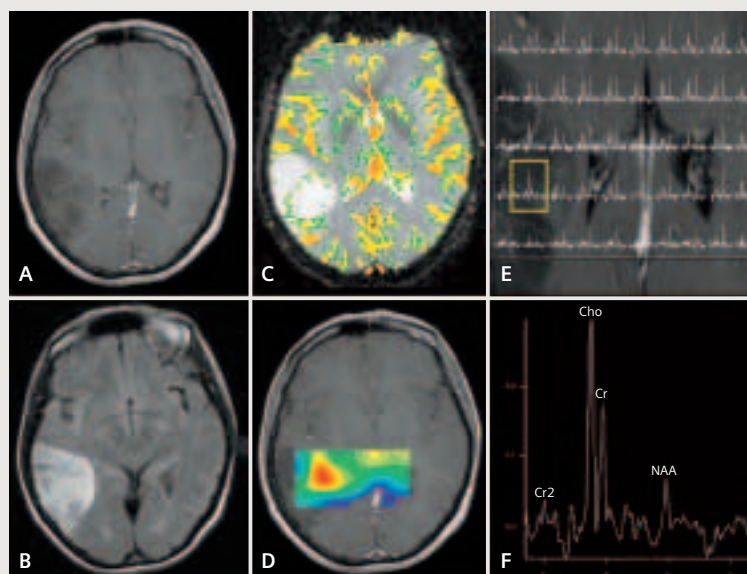


Figure 2 A 52-year-old woman with a histologically confirmed grade II/IV glioma. A: Axial T1-weighted image post-gadolinium shows a lesion in the right temporo-parietal region with low signal and minimal enhancement. B: Axial FLAIR image shows increase in T2 signal within the lesion with minimal edema. C: Gradient-echo axial perfusion MRI with rCBV* color overlay map, shows a low rCBV* of 1.70 in keeping with a low-grade glioma. There is a thin rim of slightly increased perfusion at the margin of the lesion. D: Cho color overlay metabolite map showing the region of increased Cho, which sometimes does not correspond to the region of highest rCBV* seen on the perfusion MRI study in C. This may be due to the fact that MRSI and perfusion MRI are measuring different parameters of tumoral activity. E: Spectral map shows regions of Cho elevation only within the region of abnormal signal indicating a lack of tumor infiltration in the peritumoral region in this grade II lesion. F: Spectrum (TE 144 ms) showing Cho elevation with respect to Cr and NAA within the tumor. Data were acquired on a 1.5T MAGNETOM Symphony.

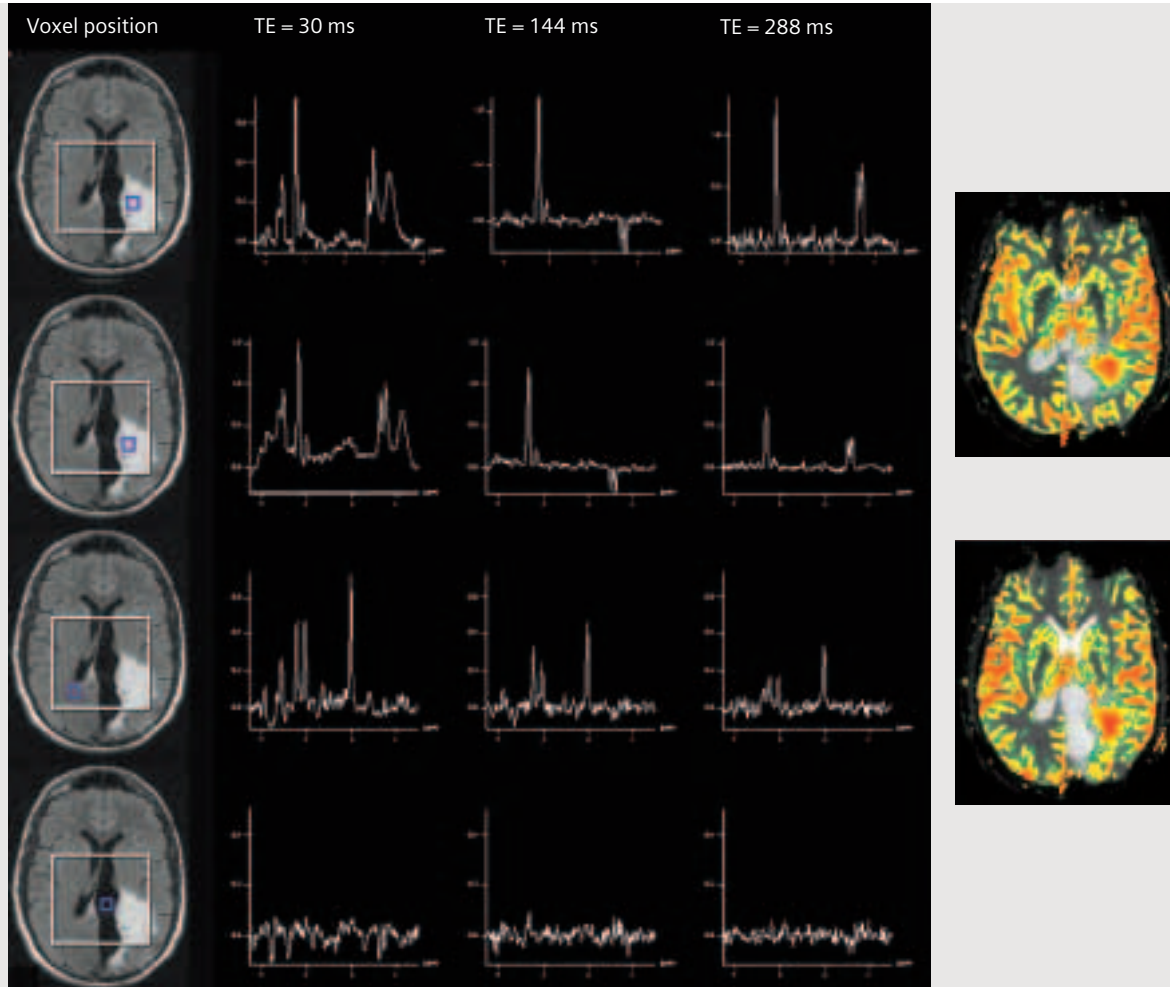


Figure 3 MRSI and perfusion MRI images from a patient demonstrating recurrent high-grade glioma within the left parietal region. Images illustrate typical features of spectra at different echo times (TE). A: The first column of images shows axial FLAIR images with the voxel position corresponding to the spectra in the same row. Short TE (30 ms), intermediate TE (144 ms), and long TE (288 ms) spectra are displayed in the second, third, and fourth column respectively. In the fifth column corresponding rCBV* color overlay maps, (B), and (C), of the recurrent glioma demonstrate evidence of increased rCBV* in regions of significant Cho elevation. The 1st and 2nd rows of (A) represent spectra from a voxel within the recurrent tumor demonstrating marked elevation in Cho relative to Cr and NAA. There is also a lactate peak that is inverted at the intermediate TE of 144 ms and upright at TEs of 30 and 288 ms. Note that myo-inositol, Glx (Glutamine/Glutamate) and lipid peaks are more readily appreciated at the short TE (2nd row, 30 ms). There is an elevated Glx complex of peaks (2.05-2.5 ppm). (In addition to the Glx, there may be a very small NAA peak that disappears at long TE because of T2 decay). The 3rd row displays spectra from a voxel within normal appearing contralateral brain. Note the decrease in signal (from metabolites) relative to baseline noise at longer echo time (288 ms) due to the T2 decay of signal from metabolites at longer echo time. The 4th row displays a voxel in the ventricles, where the lack of metabolites within CSF results in a noisy spectrum, seen at all echo times (30, 144 and 288 ms). Data were acquired on a 1.5T MAGNETOM Symphony.

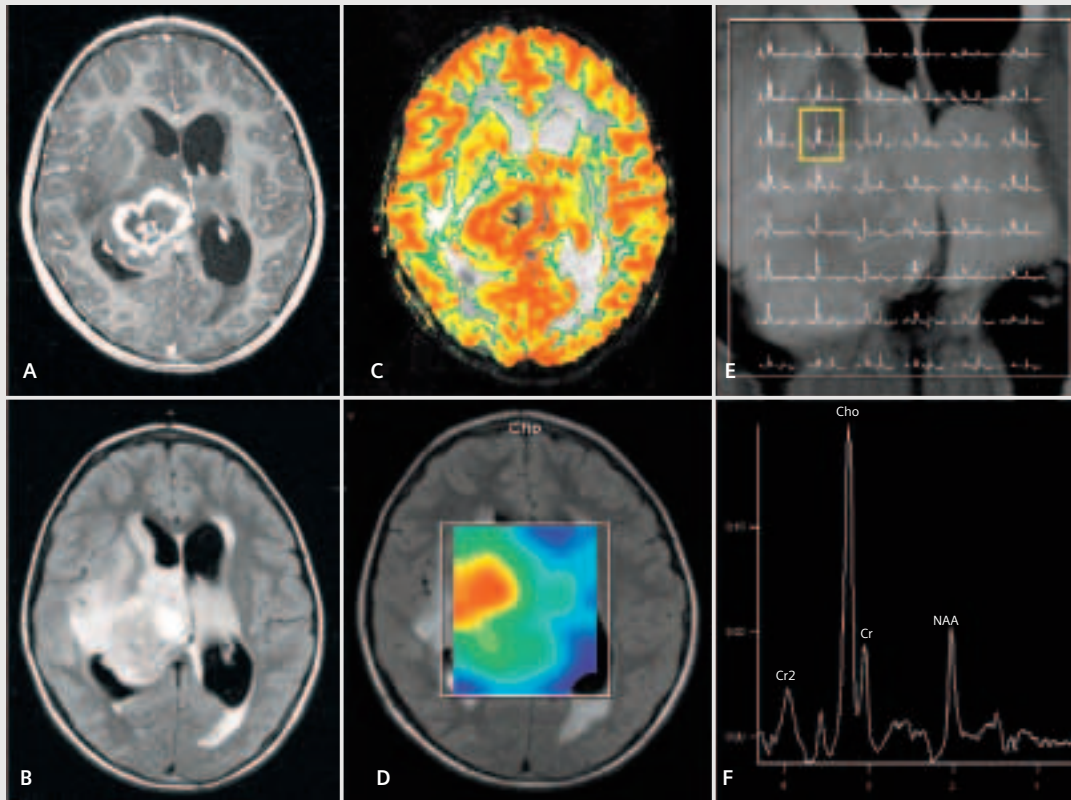


Figure 4 A 70-year-old woman with a histologically confirmed grade III/IV glioma. A: Post-gadolinium Axial T1-weighted image shows a lesion in the right thalamic region with heterogeneous peripheral contrast enhancement and a central cystic/necrotic region. B: Axial FLAIR image shows increase in T2 signal within the lesion with moderate surrounding edema. The patient also has hydrocephalus and transpendymal edema around the ventricles. C: Gradient-echo axial perfusion MRI with rCBV* color overlay map, shows a high rCBV* of 3.70 in keeping with a high-grade glioma. There is a thick rind of marked increased perfusion. D: Cho color overlay metabolite map showing the region of increased Cho, which again does not correspond exactly to the region of highest rCBV* seen on the perfusion MRI study in C. E: Spectral map shows regions of Cho elevation within the region of abnormal signal as well as tumor infiltration beyond the region of enhancement, anteriorly and potentially across the midline into the left thalamus. The central areas do not demonstrate substantial amount of lipids/lactate as compared to a grade IV lesion. F: Spectrum (TE 144 ms) from the peritumoral region showing marked Cho elevation with respect to Cr and NAA indicating tumor infiltration. Data were acquired on a 1.5T MAGNETOM Symphony.

*WIP: The information about this product is preliminary. The product is under development and is not commercially available in the US and its future availability cannot be ensured.

1.02±0.42 [3], in (Fig. 6). Normal Cho, elevated myo-Inositol, and decreased NAA have been demonstrated with MRS in gliomatosis cerebri [4] (Fig. 6). The combination of these spectroscopy findings and reduced perfusion suggest that gliomatosis cerebri can be differentiated from high-grade multicentric glioma.

Metastatic Neoplasms

A solitary brain metastases may be indistinguishable from a primary glioma by conventional MRI imaging. The pathophysiology of the peri-tumoral region of gliomas and metastases is well known by neurosurgeons and neuro-pathologists. High-grade gliomas are known to be infiltrating tumors, with tumoral tissue infiltrating along vascular channels, whereas in metastases, the peri-tumoral region contains no infiltrating tumor cells or vascular endothelial proliferation and is almost purely vasogenic edema [5-7]. In the differentiation of glioma from metastases, finding high Cho and high rCBV* in the peri-tumoral region of a lesion (Figs. 7-8) is more likely to represent glioma rather than metastases [7].

Non-Neoplastic Mimics – Cerebrovascular Injury

The clinical differentiation between a cerebral infarct and glioma is usually straightforward, with acute cerebrovascular events presenting with notable neurologic symptoms and signs. Diffusion-weighted imaging is also extremely sensitive and time efficient in demonstrating ischemia and infarction. However, in some clinical instances where the clinical history and diffusion-weighted imaging is somewhat confusing (Fig. 9), MRSI and perfusion MRI can be used to differentiate a surgical lesion (tumor) from a non-surgical lesion

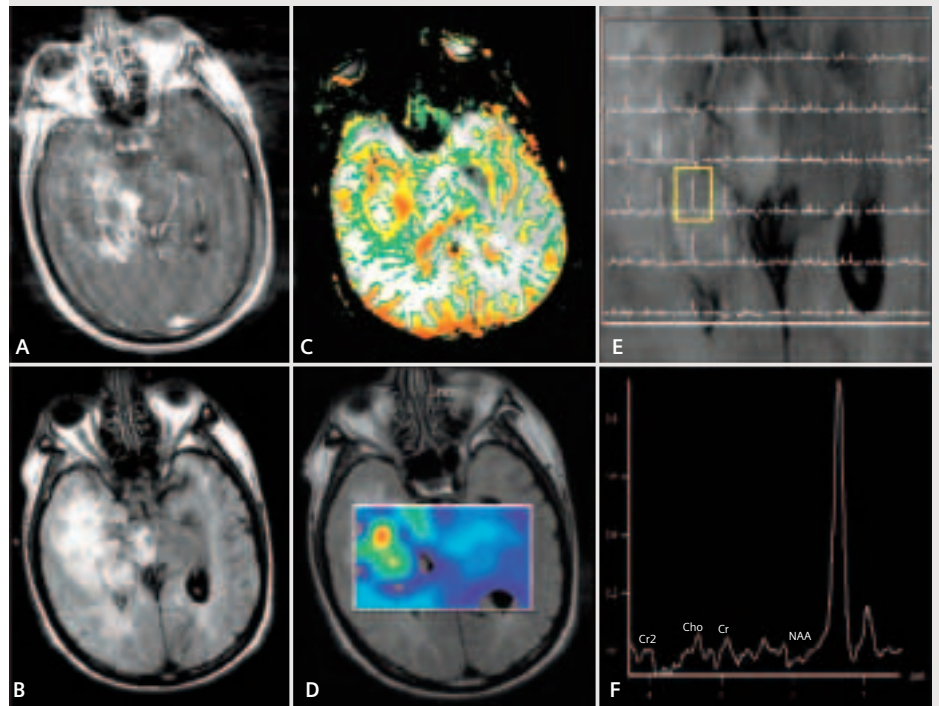


Figure 5 A 60-year-old man with a histologically confirmed grade IV glioma. A: Post-gadolinium axial T1-weighted image (motion degraded) shows a lesion in the right temporal region with heterogeneous peripheral contrast enhancement and central necrosis. B: Axial FLAIR image shows increase in T2 signal within the lesion with marked surrounding edema/tumor infiltration. There is also infiltration into the right occipital region and right midbrain. C: Gradient-echo axial perfusion MRI with rCBV* color overlay map, shows a high rCBV* of 8.90 in keeping with a grade IV glioma. There is increased perfusion around the periphery of the lesion with decreased perfusion within the necrotic center. D: Cho color overlay metabolite map showing the region of increased Cho which corresponds to the regions of high rCBV* seen on the perfusion MRI study in C. E: Spectral map shows regions of lipid within the region of abnormal signal indicating necrosis in a glioblastoma multiforme. F: Spectrum (TE 30 ms) showing marked lipids elevation (primarily aliphatic methylene groups [-CH₂-] of fatty acids at 1.2-1.4 ppm). Data were acquired on a 1.5T MAGNETOM Symphony.

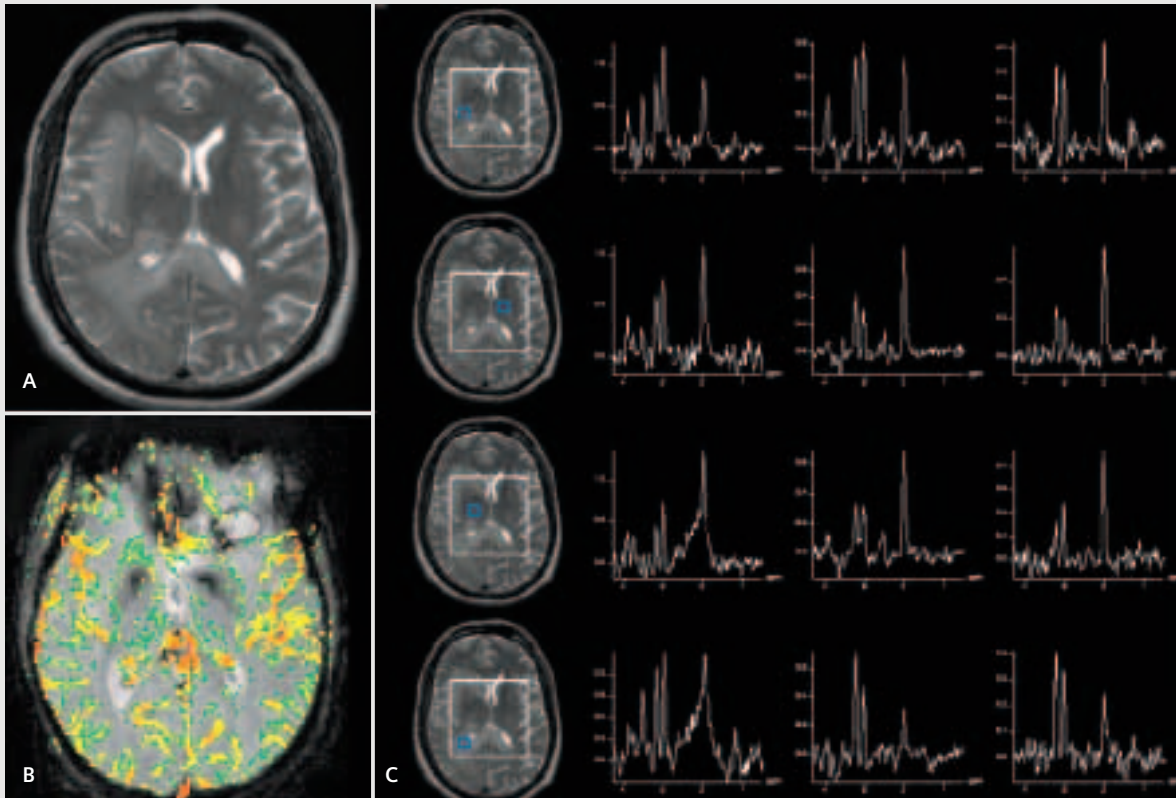


Figure 6 A: Axial T2-weighted image shows extensive hyperintensity involving the right hemispheric white matter. Contiguous involvement of at least two lobes of the brain is characteristic of gliomatosis cerebri. B: Gradient echo perfusion MRI with rCBV* color overlay demonstrating reduced perfusion. Mean rCBV* was 1.02. C: Multi-TE MRSI of gliomatosis cerebri. The first column shows axial T2-weighted images with the voxel position corresponding to the spectra in the same row. Short TE (30 ms), intermediate TE (144 ms), and long TE (288 ms) spectra are displayed in the second, third, and fourth columns respectively. The 1st row demonstrates spectra from within the tumor, at short TE, there is elevation in myo-inositol and decrease in NAA without appreciable increase in Cho seen at all echo times (30, 144 and 288 ms). The 2nd and 3rd row demonstrate normal spectra from within the normal appearing contralateral brain and the relatively unaffected right thalamus respectively. The 4th row demonstrates elevation in myo-inositol at short TE (30 ms) and some elevation in Cho within the tumor. Myo-inositol elevation in the setting of normal Cho has been described in gliomatosis cerebri (4). Increased Cho/Cr and Cho/NAA have also been described with longer TE's (3). Data were acquired on a 1.5T MAGNETOM Symphony.

*WIP: The information about this product is preliminary. The product is under development and is not commercially available in the US and its future availability cannot be ensured.

(stroke). Strokes generally demonstrate increased mean transit time (MTT), and decreased CBF [8-13]. Strokes may demonstrate elevated or decreased rCBV*. In contrast, tumors generally demonstrate increased rCBV* and CBF*. Review of the MTT, CBF* and rCBV* measurements and color overlay maps will not only demonstrate substantial reduction in perfusion in a stroke compared with a tumor but it will conform to a vascular territory (Fig. 9).

An initial inspection of spectroscopy data obtained in a stroke will demonstrate Cho/Cr elevation due to cell membrane destruction and demyelination, as well as decrease in NAA from neuronal and axonal damage. Lactate is also demonstrated for up to 6 weeks and sometimes beyond, initially from anaerobic glycolysis, then later from macrophage activity and persistent ischemia [14]. However, the major difference between a stroke and tumor can best be appreciated by comparing a spectrum from within the stroke to a spectrum from contralateral healthy tissue, which can be done with a multi-voxel MRSI acquisition. The primary difference is a reduction in all metabolites in stroke compared with the contralateral normal brain. Cr, as an energy marker, is particularly reduced in stroke. Even though there may be Cho/Cr elevation and NAA/Cr decrease, when comparing the Cho to normal contralateral Cho(n), there will be a reduction in the Cho/Cho(n) ratio. This demonstrates the value of directly comparing abnormal with normal metabolite levels and measuring Cho/Cho(n) Cho/Cr(n) and NAA/NAA(n) ratios which may increase the specificity somewhat in characterizing mass lesions in the clinical setting when absolute quantification, relative to an external standard cannot be made.

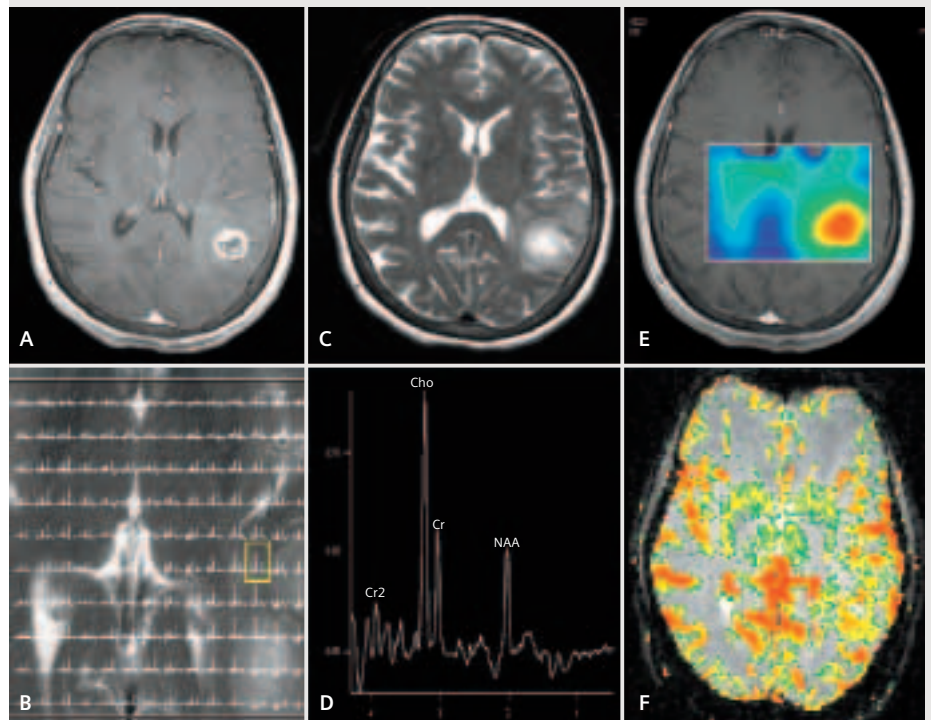


Figure 7 A glioblastoma multiforme. A: Axial T1-weighted image post-gadolinium shows a peripherally enhancing mass with heterogeneous signal intensity and central necrosis in the left parietal region. B: Axial T2-weighted image demonstrates moderate surrounding T2 signal abnormality, which is likely to represent infiltrating tumor and edema. C: Cho metabolite color overlay demonstrates elevation in Cho in and around the region of enhancement and T2 signal abnormality. D: MRSI (TE 144 ms) spectral map confirms the increase in Cho within the lesion as well as within the abnormal T2 signal anteriorly. E: Spectrum (TE 144 ms) from within the anterior peri-tumoral region demonstrating increase in Cho/Cr and in Cho/NAA from tumoral infiltration of adjacent peri-tumoral tissues. F: Gradient-echo axial perfusion MRI with rCBV* color overlay show increase in vascularity within the enhancing tumor as well as in the peritumoral region anteriorly. These MRSI and perfusion MRI findings in the peritumoral region help to differentiate an infiltrating primary high-grade glioma from a metastasis. Data were acquired on a 3T MAGNETOM Allegra.

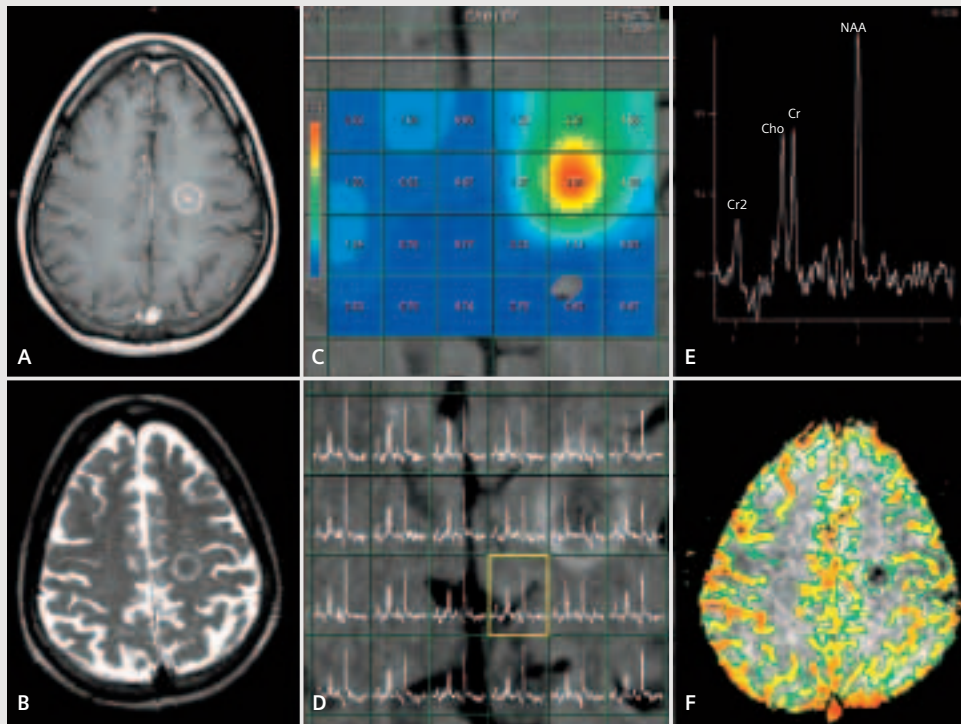


Figure 8 60 year-old-woman with a metastasis from breast carcinoma. *A: Axial T1-weighted image post-gadolinium shows a well defined mass in the left frontal region. B: Axial T2-weighted image demonstrates negligible edema surrounding this lesion. C: Cho metabolite color overlay demonstrates Cho/Cr elevation within the tumor and in voxels where there is partial volume averaging with the tumor. D: MRSI (TE 144 ms) spectral map demonstrates no elevation in Cho within voxels in the peri-tumoral region of the lesion, indicating a non-infiltrating lesion like a metastasis. E: Spectrum (TE 144 ms) from a voxel in the peri-tumoral region with normal metabolite peaks. F: Gradient-echo axial perfusion MRI with rCBV* color overlay may demonstrate increase in tumor vascularity confined to the enhancing tumor but not within the peri-tumoral region. Data were acquired on a 1.5T MAGNETOM Symphony.*

**WIP: The information about this product is preliminary. The product is under development and is not commercially available in the US and its future availability cannot be ensured.*

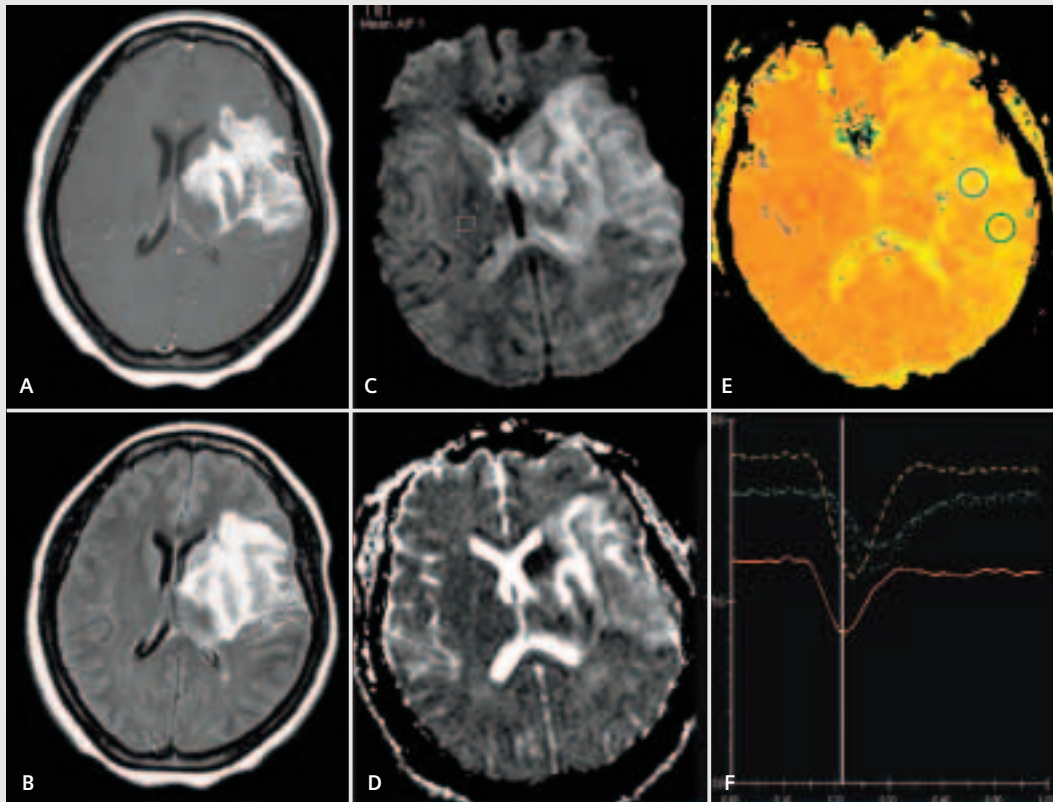


Figure 9 45-year-old-woman presenting with a 10-day history of right arm and leg weakness: The clinical and final diagnosis was a left middle cerebral artery territory stroke, however conventional MRI, including diffusion weighted imaging was inconclusive. A: Axial T1-weighted image post-gadolinium demonstrates abnormal enhancement in the left hemisphere involving gray and white matter. B: Axial FLAIR image demonstrates abnormal T2 signal as well as some mass effect. There is a small amount of edema. C: Diffusion-weighted image ($B = 1000$) demonstrating some increase in signal. D: The ADC map also shows areas of increased signal, which may represent "T2-shine-through effect" as well as some areas of decrease signal, which may represent true diffusion restriction. These findings on diffusion are sometimes also seen in very heterogeneous high-grade gliomas. E: Gradient-echo axial perfusion MRI with mean transit time (MTT) color overlay demonstrating prolongation in the MTT throughout the entire middle cerebral artery (MCA) territory in keeping with left MCA ischemia. F: Signal intensity versus time curves color coded to the 4 ROIs placed on the MTT maps, demonstrating prolongation in MTT in the green, blue and to a lesser extent the yellow ROIs. The red ROI indicates normal MTT in the contralateral hemisphere. The delay in MTT and reduced CBF^* in the MCA distribution is in keeping with a stroke. Data were acquired on a 1.5T MAGNETOM Symphony.

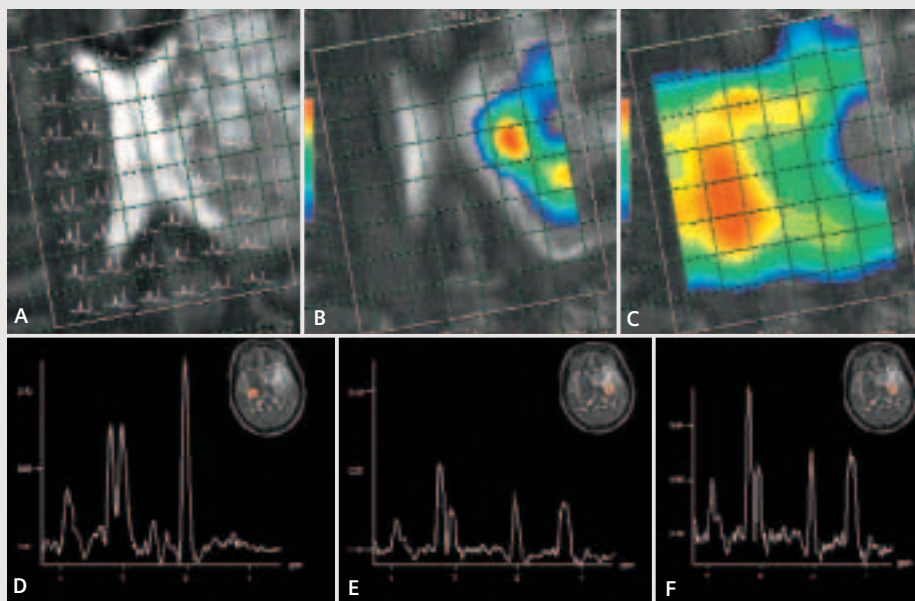


Figure 10 45-year-old-woman with a left MCA stroke. A: MRSI (TE 144 ms) spectral map demonstrating an increase in Cho/Cr within the abnormal voxels in the left hemisphere, however, there is an overall decrease in metabolites when compared with the right hemisphere. B: The Cho/Cr metabolite ratio color overlay map shows increase in Cho/Cr, which can be misinterpreted for a neoplastic process. C: The Cho metabolite color overlay demonstrates a decrease in Cho (but NOT Cho/Cr) when compared with the right hemisphere. D: MRSI (TE 144 ms) showing a spectrum from the normal right hemisphere. Note is made of the vertical scale and the normal Cho level [Cho (n)], which is used as a control for comparing the abnormal side. E: A spectrum from the abnormal left side displayed on the same scale as the spectrum in D. It shows a decrease in all metabolites including choline, which indicates an ischemic rather than neoplastic process. F: The same spectrum from E scaled to the highest peak in the spectrum i.e choline may be misinterpreted as a neoplastic process. This display illustrates the pitfall of reading a spectrum without a contralateral control. Finding substantial reduction in Cr, Cho and NAA by comparing a spectrum with the normal contralateral control can increase the specificity and exclude a neoplastic process in favor of infarct in this case. Data were acquired on a 1.5T MAGNETOM Symphony.

*WIP: The information about this product is preliminary. The product is under development and is not commercially available in the US and its future availability cannot be ensured.

References

- [1] Law M, Yang S, Wang H, et al. Glioma Grading: Sensitivity, Specificity and Predictive Value of Perfusion MRI and Proton Spectroscopic Imaging compared with Conventional MR Imaging. *AJNR* 2003 24: 1989-1998.
- [2] Kleihues P, Cavaneer P. WHO Classification of Tumors: Pathology and Genetic of Tumours of the Nervous System. Lyon: IARC Press, 2000.
- [3] Yang S, Wetzel S, Law M, et al. Dynamic contrast-enhanced T2*-weighted MR imaging of gliomatosis cerebri. *AJNR Am J Neuroradiol* 2002; 23:350-355.
- [4] Saraf-Lavi E, Bowen BC, Pattany PM, et al. Proton MR Spectroscopy of Gliomatosis Cerebri: Case Report of Elevated Myoinositol with Normal Choline Levels. *AJNR* 2003; 24:946-951.
- [5] Burger PC. Classification, grading, and patterns of spread of malignant gliomas. *Neurosurgical topics: malignant cerebral glioma*. American Association of Neurological Surgeons. Park Ridge, Ill, 1990; 3-17.
- [6] Burger PC, Vogel FS, Green SB, et al. Glioblastoma multiforme and anaplastic astrocytoma: Pathologic criteria and prognostic implications. *Cancer* 1985; 56:1106-1111.
- [7] Law M, Cha S, Knapp EA, et al. High-Grade Gliomas and Solitary Metastases: Differentiation by Using Perfusion and Proton Spectroscopic MR Imaging. *Radiology* 2002; 222:715-721.
- [8] Karonen J, Liu Y, Vanninen R, et al. Combined Perfusion- and Diffusion-weighted MR Imaging in Acute Ischemic Stroke during the 1st Week: A Longitudinal Study. *Radiology* 2000; 217:886-894.
- [9] Sorensen AG, Copen WA, Ostergaard L, et al. Hyperacute stroke: simultaneous measurement of relative cerebral blood volume, relative cerebral blood flow, and mean transit time. *Radiology* 1999; 210:519-527.
- [10] Sorensen AG, Buonanno FS, Gonzalez RG, et al. Hyperacute stroke: evaluation with combined multisection diffusion-weighted and hemodynamically weighted echo-planar MR imaging. *Radiology* 1996; 199:391-401.
- [11] Hatazawa J, Shimosegawa E, Toyoshima H, et al. Cerebral blood volume in acute brain infarction: A combined study with dynamic susceptibility contrast MRI and 99 mTc-HMPAO-SPECT. *Stroke* 1999; 30:800-806.
- [12] Crosby D, Simonson T, Fisher D, et al. Echo-planar MR Imaging: correlation of intracranial perfusion-sensitive imaging with cerebral angiography. *Society of Magnetic Resonance* 1994; 277.
- [13] Saunders DE. MR spectroscopy in stroke. *Br Med Bull* 2000; 56:334-345.

MR Spectroscopy Precision and Repeatability: Evaluation of Brain CSI Data

Jiani Hu, Yimin Shen,
Yang Xuan and E. Mark Haacke

Wayne State University,
Magnetic Resonance Research
Facility

Abstract

Our goal in this study was to determine the precision of the CSI (Chemical shift Imaging) measurements offered by the Sonata and our ability to reproduce these results when the data are re-acquired on separate days and separate imaging scenarios. Variations of the CSI measurements within the brain are also reported. Results of this work suggest that the precision of the integral values for a given voxel is on the order of 6% for NAA, 10% for Cre and 11% for Cho. The reproducibility is found to be almost identical implying that the results from one day to the next are in good agreement with each other statistically. Variation in metabolite content throughout the brain gives voxel variability on the order of 10% for NAA, 12% for Cre and 16% for Cho. The ratios of these metabolites will, of course, have appropriately larger errors.

Introduction

With the introduction of any new system, the question of hardware and software performance comes into play. Our goal in this study was to determine the precision of the CSI measurements offered by the Sonata and our ability to reproduce these results when the data are re-acquired on separate days and separate imaging scenarios.

CSI is used for monitoring the effect of therapy on certain pathologies such as tumor and multiple sclerosis. A knowledge of the various sources of error that affect CSI results is critical for drawing conclusions from repeated measurements on the same subject in a longitudinal study. Similarly, the natural variability in different voxels in the brain may be very different from the noise levels apparent within a given voxel. Therefore to draw conclusions as to what is normal and what is not within a given voxel requires knowledge of this variation.

Methods

A young healthy 22 year old male volunteer was scanned first in the spring of 2003. A special foam head constraint was used in order to keep the head fairly still. This eliminates errors from head motion that may otherwise obscure statistical errors inherent to the sequence and software associated with CSI. While in the magnet, the subject was scanned 8 consecutive times with no pause between scans. A month later, the same subject was positioned in the magnet without the foam headholder. Using an anatomical landmark on the forehead an attempt was made to reproduce the same head positioning used earlier. A CSI measurement was acquired at the same anatomical slice position and with

the same parameters, and repeated once without a pause. The subject was then brought out of the magnet for a short break, after which he was repositioned in the magnet and scanned again. This process was repeated 3 times yielding a total 6 scans.

The 2D CSI parameters were: (sequence CSI_se_135), FOV = 160x160x15 mm³, number of voxels 16x16x1, resolution per voxel = 10x10x15 mm³, TR=1500, TE=135, NA=4, and TA=7°06". Other settings included a Hamming filter, number of sampling points NP=1024, BW = 1kHz, preparatory scans = 4, phase encoding = weighted, WS BW = 35Hz, delta frequency = -2.7ppm.

Results

The slice of interest used for the data evaluations reported here is shown in Figure 1. The region of interest with 6 x 6 voxels is shown in Figure 1a along with the coronal and sagittal views. A single voxel spectrum is shown in Figure 1b and a CSI example for each voxel is shown in Figure 1c. Integral values of metabolite peaks in each voxel were used in the evaluation.

Average standard deviation over all voxels: Assuming that the standard deviation over the 8 measurements is the same for all voxels, it is reasonable to quote the mean standard deviation over all 36 voxels (column 1 of table 1). A histogram of the standard deviations shows that this is in fact reasonable.

Precision of the mean of all voxels from scan to scan: The next step was to compare the variation in the means over the 8 repetitions. Ideally, one could compare the values in each voxel but that would require perfect spatial match of the 36 voxels. Since the voxel to voxel variation is seen to be rather large, a

Metabolite or ratio of metabolites	μ_{vs} Mean of all the Sd of all 36 single voxels	μ_g Mean over all 36 voxels	$100 \mu_{vs}/\mu_g$	Sd of the global mean over 8 scans	μ_{spat} Spatial Sd of the means over all 36 voxels	$100 \mu_{spat}/\mu_g$
naa	0.18	3.12	6%	0.02	0.31	10%
cr	0.17	1.64	10%	0.04	0.20	12%
cho	0.18	1.67	11%	0.07	0.26	16%
naa/cr	0.24	1.93	12%	0.06	0.33	17%
cho/cr	0.16	1.04	15%	0.05	0.23	22%

Table 1 An estimate of the error in the means from 8 scans.

Metabolite or ratio of metabolites	μ_{vr} Mean of all the Sd of all 36 single voxels	μ_g Mean of integral 36 voxels value over all 36 voxels	$100 \mu_{vr}/\mu_g$	Sd of the global mean over 6 scans	μ_{spat} Spatial Sd of the means over all 36 voxels	$100 \mu_{spat}/\mu_g$
naa	0.21	3.16	7%	0.07	0.32	10%
cr	0.19	1.68	11%	0.03	0.22	13%
cho	0.21	1.74	12%	0.10	0.26	15%
naa/cr	0.25	1.92	13%	0.03	0.35	18%
cho/cr	0.17	1.05	16%	0.05	0.21	20%

Table 2 An estimate of the error in the means from 6 scans.

small offset or change in partial volume effect could make a big difference in this test of reproducibility. To avoid this problem, we compared only the means over all 36 voxels. The global mean (μ_g column 2 of table 1) of each metabolite was then found over all 36 voxels. As might be expected, the global mean had a very low standard deviation (column 4 of table 1).

Variance from voxel to voxel within the brain: Finally, a comparison of the spatial variation in metabolite concentration was made over

the 36 voxels in this particular slice. This of course could vary from location to location in the brain. The spatial variance is much larger than the precision (μ_{spat} column 5 of table 1).

Precision of the mean over different sittings: All 6 cases were included in the analysis. Despite the fact that these scans were acquired on different days, the spatial and tissue variations were only slightly larger than in the single sitting case (see table 2).

Discussion and Conclusions

We have tested the same day precision (data set 1, table 1) and reproducibility from day to day (data set 2, table 2) of the 2D CSI approach currently available on the Siemens Sonata scanner. It is encouraging that both the means and standard deviations are statistically consistent with each other. In order to be able to have the confidence in the lower standard deviations, it is critical to very carefully reposition the subject. In this case, variations will fall within the expected precision values quoted

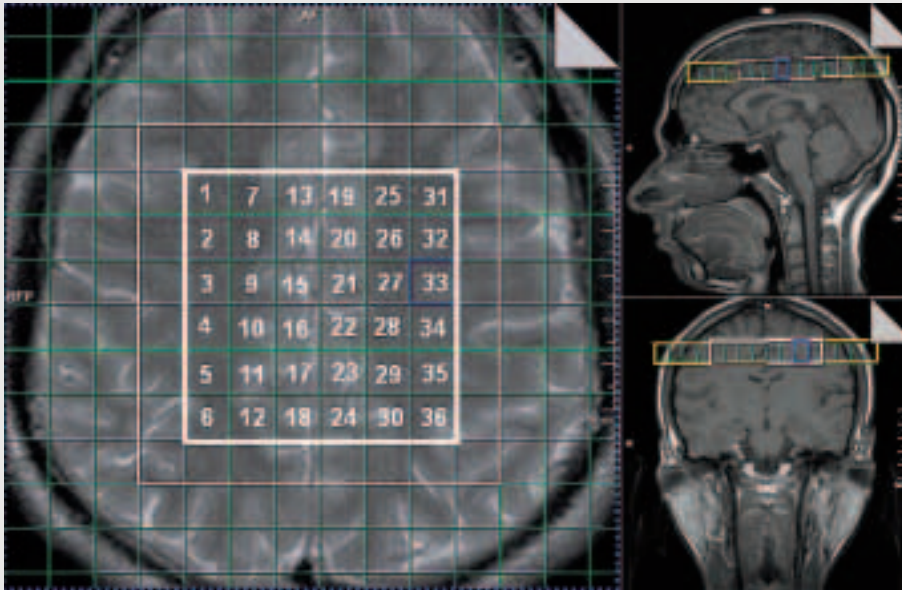


Figure 1a

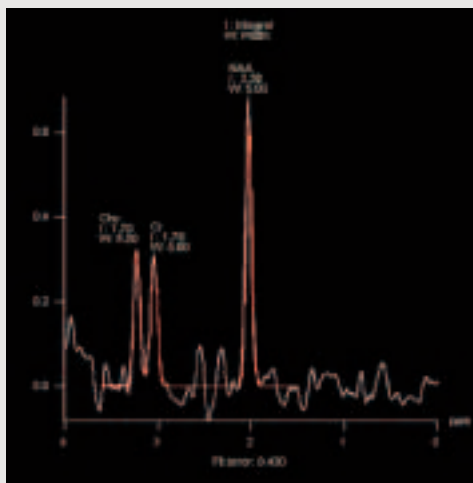
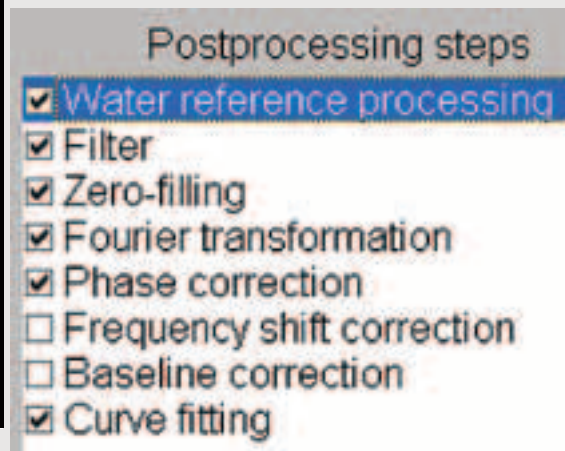


Figure 1b



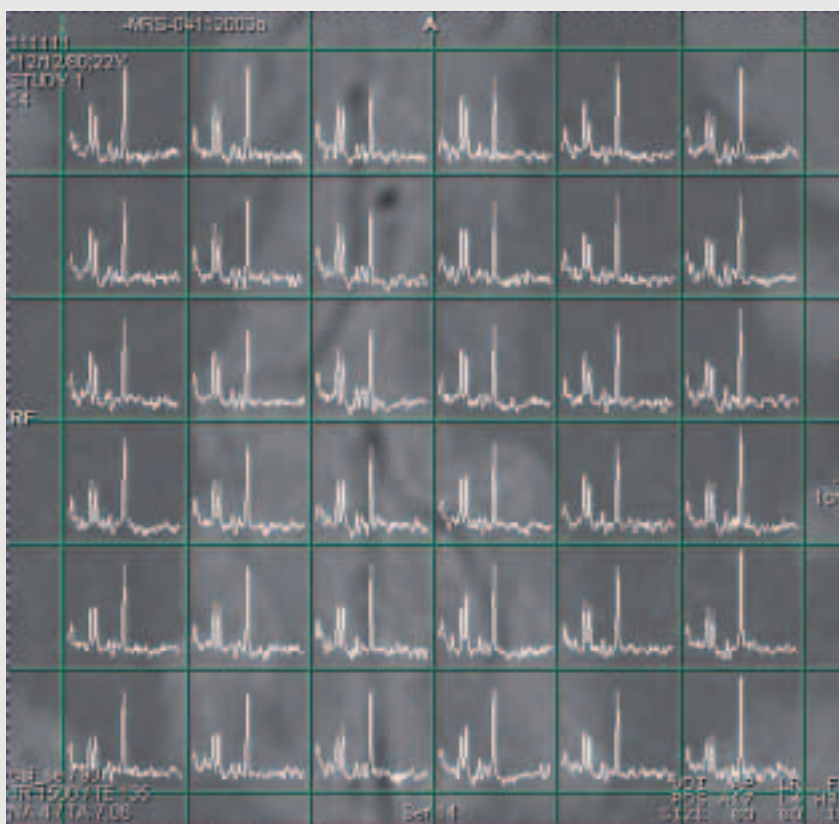


Figure 1c

in table 1. In these tables we quote the standard deviation. However, since we used 8 scans in table 1, the standard error of the mean will be the quoted standard error divided by $\sqrt{7}$.

Clearly, to determine that an appreciable change has occurred over time in a disease or after treatment one would look for changes of at least two standard deviations. Unfortunately, reducing the noise levels to less than 3% for NAA and 5% for Cho and Cr requires 4 scans or roughly 30 minutes. This is certainly not impossible, but the need for it should be determined based on the size of the change being sought. However, if this is done, it is recommended that the scans be run separately as we did above so that if motion does occur for a given scan that at least one of the scans remains usable.

In conclusion, with a 7 minute scan, it is possible to obtain estimates for NAA, Cr and Cho with errors on the order of 6%, 10% and 11%, respectively (see column 3 in table 1 and 2). With careful patient positioning, this precision can be replicated even when imaging the same person on another day.

Editor's note:

Please note that the new features Phoenix supporting MRS protocols, and auto-align, both available with syngo MR 2004A/V, will further support you to increase the reproducibility of your results.

¹H-MRSI Guided Surgery of Brain Tumors

^{1,2}Andreas Stadlbauer, MSc,
Erlangen

²Stephan Gruber, Ph.D.

²Ewald Moser, Ph.D., Vienna

¹Christopher Nimsy, M.D.,
Erlangen

¹Peter Grummich, Ph.D.

¹Rudolf Fahlbusch, M.D., Erlangen

¹Oliver Ganslandt, M.D.

¹Department of Neurosurgery,
Neurocenter,
University of Erlangen-Nuernberg,
Erlangen, Germany

²Centre of Excellence for High-Field
MR, Medical University of Vienna,
Vienna, Austria

Abstract

Proton magnetic resonance spectroscopic imaging (¹H-MRSI) is a non-invasive tool to measure the spatial distribution of brain metabolites. This technique may therefore provide biochemical information in vivo, useful in distinguishing pathologic from normal brain areas. However, it is often difficult to delineate the tumor borders of high and low grade gliomas in conventional T1- and T2-weighted magnetic resonance imaging (MRI). We have developed a method to intraoperatively investigate pathologic changes in the spatial distribution of choline-containing compounds (Cho), total creatine (Cr) and N-acetyl-aspartate (NAA) in brain tumors combining ¹H-MRSI with frameless stereotaxy. Metabolic maps were calculated and segmentation of the tumors was performed. Spectroscopic images of the segmented tumor were matched onto an anatomical 3D-MRI set and used subsequently for neurosurgical planning. Display of spectroscopic information in the navigation microscope was performed during surgery leading to ¹H-MRSI guided neuronavigation. We conclude that our method may present another step towards intraoperative identification of tumor border zones based on the metabolic changes due to tumor infiltration.

Introduction

The main goal in neurosurgery of lesions is to achieve tumor resection as complete as possible while preserving normal brain tissue and function. Information about the localization and spatial extent of the lesion should be available before and during the surgical procedure. Frameless stereotactic methods in neurosurgery (neuronavigation) have been used as a platform to integrate

functional information in the operating room, leading to so-called functional neuronavigation. In conventional MRI it is often difficult to delineate the heterogeneous structure of lesions, especially of gliomas. Even the current method of choice, contrast-enhanced MRI as a technique for visualizing regions where the blood-brain barrier is damaged, is not tumor specific and can result in ambiguous or misleading results [1, 2]. Establishing the position and the size of the border zone between tumor and normal brain tissue is one of the major problems in therapy planning. Proton magnetic resonance spectroscopic imaging (¹H-MRSI) allows noninvasive measurements of the concentration and spatial distribution of brain metabolites and therefore may provide biochemical information in vivo, useful in distinguishing pathologic from normal brain areas [3]. Brain tumors show increased levels of choline-containing compounds (Cho) and a reduction in N-acetyl-aspartate (NAA) and creatine (Cr). Cho is thought to be a marker for increased membrane turnover or higher cellular density [4]. NAA is mainly contained within neurons [5] and Cr is a marker for energy metabolism [6]. The range of Cho increase and NAA decrease is compatible with the range of tumor infiltration [1, 7]. Metabolite maps of NAA and Cho allow the differentiation of areas of necrosis, solid tumor and varying degrees of tumor infiltration and tissue edema.

Materials and Methods

3D-MRI and ¹H-MRSI:

All MR studies were performed on a MAGNETOM Sonata 1.5 Tesla (Siemens Medical Solutions, Erlangen, Germany) equipped with the standard head coil. Tumor patients – all with supratentorial gliomas (WHO

grade II to IV) – were examined using high-resolution ^1H -MRSI. In each MRSI session a localization scan and an axial spin echo (SE) sequence (T1-weighted) were acquired for MRSI excitation volume location. The SE sequence was used for matching spectroscopic images to an anatomic three-dimensional magnetic resonance image set. The parameters were TR/TE 500/15 ms, 256x256 matrix size, 16x16 cm FOV, 20 slices with a distance factor of 0% and a slice thickness of 2 mm. The MRSI sequence, which used PRESS (Point-RESolved Spectroscopy) volume preselection, was performed immediately afterwards. Water suppression was achieved using three CHESS (CHEMical Shift Selective) pulses prior to the PRESS excitation. The MRSI parameters were TR/TE 1600/135 ms, 24x24 circular phase-encoding scheme across a 16x16 cm FOV, slice thickness 10 mm, 50% Hamming-filter and 2 NEX, spectral width 1000 Hz and 1024 complex points acquisition size. The total spectroscopic data acquisition time was less than 13 minutes.

The MRSI slab was aligned precisely to a selected SE slice by copy and paste of the image position. Due to the same FOV of the SE and the MRSI experiment, and with the assumption of negligible head motion between the time of the MRI and MRSI acquisition, direct correlation of the data of the MRSI slab (10 mm thick) with five slices (each 2 mm thick) of the anatomical MRI was achieved. Immobilization of the patients' heads was achieved by fixation in a head-rest.

In a single session a three-dimensional anatomic magnetization prepared rapid acquisition gradient echo (MPRAGE) sequence was performed with the following parameters: TR/TE 2020/4.38 ms, 25x25 cm FOV, 1 mm isotropic and 160 slices. For registra-

tion in the neuronavigation system between 6 and 8 adhesive skin fiducials were placed in a scattered pattern on the head surface prior to imaging.

MRSI Data Analysis:

The peak areas for Cho, Cr and NAA were calculated by integration over the frequency range of 3.34-3.14 ppm, 3.14-2.94 ppm and 2.22-1.82 ppm, respectively (see spectra #1 to #4 in Fig. 1). Smooth linear interpolation to a 256x256 matrix resulted in metabolic maps. Cho and NAA images (Figs. 1a and b) were used to calculate a map of Cho/NAA ratios (Fig. 1c). Tumor segmentation procedure was developed on the assumptions that (i) the values for

Cho/NAA in normal brain follow a Gaussian distribution, and (ii) those for the tumor, including the border zone, are significantly increased. For segmentation we determined a 'healthy region', unaffected by predominantly white matter on the contralateral side and at sufficient distance from the lesion according to the Cho/NAA ratio map (red rectangle in Fig. 1c). The mean and the standard deviation (SD) of the Cho/NAA ratios were calculated for this selected region and all Cho/NAA values in the whole map less than the mean+3SD were set to zero. This leads to the elimination of all normal brain areas in the Cho/NAA map and hence to the segmentation of the tumor (Fig. 1d) [8].

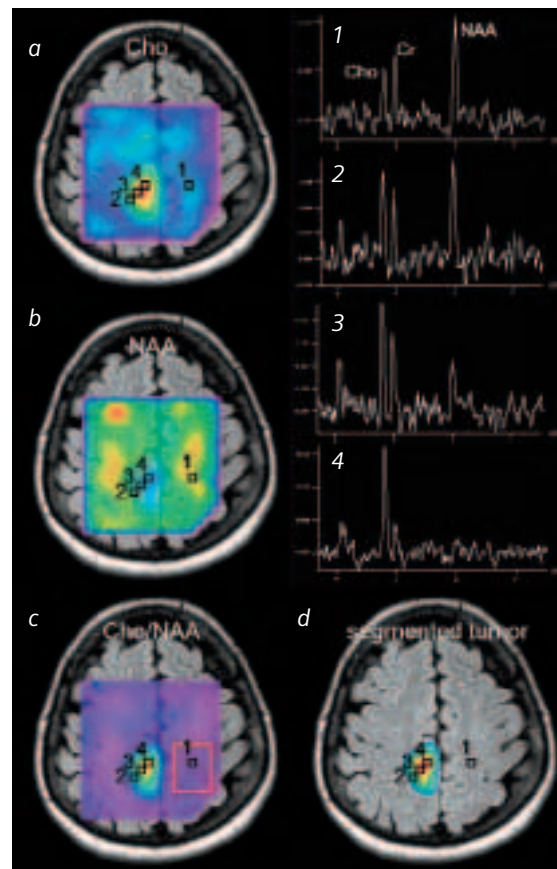


Figure 1 Anatomical images (T2-weighted) overlaid with metabolic maps of a patient with a glioblastoma multiforme (GBM). a: Cho map; b: NAA map; c: map of the Cho/NAA ratios with selected "healthy region" (red rectangle); and d: map of the segmented tumor. Spectra of (1) contralateral normal brain, (2) the tumor border, (3) the transition to tumor center, and (4) the tumor center according to the marked positions in a to d.

MRI/MRSI hybrid dataset and frameless stereotaxy:

A so-called MRI/MRSI hybrid dataset consists of both anatomical and metabolic information. Replacing of raw images of the five correlated anatomical slices in the SE data set by the corresponding Cho/NAA ratio map of the segmented tumor results in this hybrid data set [9]. It was transferred to a frameless stereotactic system (VectorVisionSky, BrainLab, Heimstetten, Germany) via fast ethernet by using the DICOM 3 protocol (Digital Imaging and Communications in Medicine) and image fusion to a 3D MRI dataset was performed (Fig. 2a to c). Regions of interest (ROIs) were drawn with the help of MRSI (Figs. 3a and b). The navigation microscope (NC4-Multi-vision, Zeiss, Oberkochen, Germany) in combination with the ceiling mounted navigation system, enables MRSI guided surgery of brain tumors.

Results

MRSI data analysis, including the calculation of metabolic maps and segmentation, as well as the integration of these spectroscopic results in functional neuronavigation was successfully performed in neurosurgical treatment planning. Fig. 1 shows the characteristic change in spectral patterns, representing biochemical information, starting from normal (white matter) tissue (spectrum #1: NAA > Cr and Cho, Cr > Cho) via tumor border (spectrum #2: NAA approx. Cho or Cr, Cho > Cr), tumor (spectrum #3: NAA < Cr or Cho) and tumor center (spectrum #4: NAA approx. 0, Cho >> Cr). Metabolic maps, in particular for Cho/NAA (Fig. 1c and d), clearly allows visualization and segmentation of tumor as well as identification of tumor center and border zones.

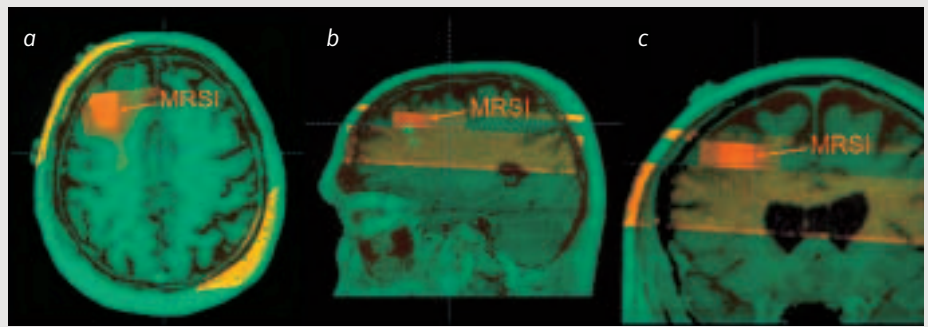


Figure 2 Image fusion of metabolic maps (MRI/MRSI hybrid data set, in orange) to a 3D-MRI dataset (in green) of a patient with an oligodendrogliom (WHO grade III). The result is a 3D-MRI consisting of anatomical and metabolic information for surgical planning. A: Axial, B: sagittal and C: coronal reconstruction of the 3D data set after image fusion, respectively. (Note: The small light green rectangles below the MRSI (orange) in (B): are results of a MEG examination (language stimulation).

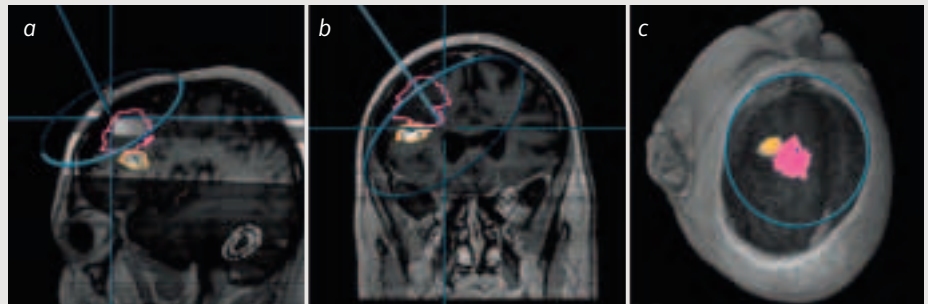


Figure 3 ¹H-MRSI guided neurosurgical planning. A: and B: reconstruction of a sagittal and coronal view from the stereotactic 3D data set (same patient as in Fig. 2). The pink line represents the segmentation of the tumor margin with help of MRSI which was done manually by a neurosurgeon. (Note: The orange line presents the region of interest based on the MEG examination, same as Fig. 2b.) C: 3D reconstructed tumor resection plan. The target volume was the pink volume. (Note: The orange volume is the 3D reconstructed result of the MEG experiment.)

Tumor patients underwent surgery with functional neuronavigation after integration of ¹H-MRSI. The projection of segmented MRSI data into the operating viewing field allowed easy identification of the tumor border based on biochemical information (Fig. 4a to c).

The total time for performing this procedure was about one hour. This was divided into 20 minutes for conventional MRI (SE sequence) and MRSI data acquisition, 30 minutes for MRSI data analysis, and 10 minutes for obtaining the MRI/MRSI hybrid data set.

Discussion

We present a technique for the integration of high-resolution ¹H-MRSI information into the neurosurgical operating room. We used a combined imaging data set consisting of conventional MRI slices and segmented metabolic maps of the MRSI slice, a so called MRI/MRSI hybrid data set, for merging biochemical information in a global anatomical 3D MRI. Drawing ROIs based on high-resolution metabolic images allows intra-operative visualization of the spectroscopic information displayed through

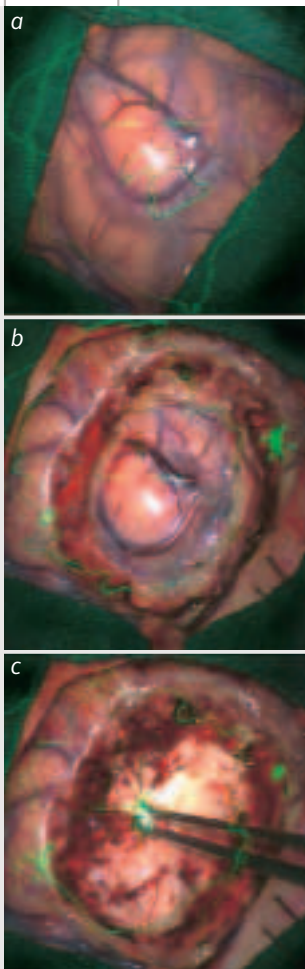


Figure 4 ¹H-MRSI guided brain tumor resection. a to c: View through the eyepieces of the navigation microscope. Regions of interest (tumor border) as drawn by the neurosurgeon on the basis of the spectroscopic information (and MEG information) are outlined in green. The dotted lines represent the maximum tumor dimension as seen from this angle. The green dots are labels for biopsy sampling positions.

the eyepieces of the microscope, leading to MRSI guided tumor resection.

Only few studies so far used MRSI to support biopsy target delineation [1, 7, 10-12] or radiation therapy treatment planning [12, 13]. None of these studies integrated MRSI data in a neuronavigation system and performed intraoperative visualization of MRSI data through image injection. Preul et al. [14] achieved integration of MRSI data (metabolic maps of Cho) of two patients into an image-guided, frameless stereotactic

system by computing a transformation between the MRSI-space and the global MRI-space using the targeting volume acquired immediately prior to MRSI acquisition. By this approach they overcame the fact that MRSI lacks detailed structural information. Our strategy for merging MRSI data to a global 3D MRI dataset was the full accurate integration of metabolic images with co-registered anatomical images (MRI/MRSI hybrid dataset) resulting in a dataset consisting of both, anatomical and biochemical information.

In conclusion, integration of spectroscopic information obtained by high-resolution ¹H-MRSI with frameless stereotaxy may be useful in glioma resection leading to an improved delineation of the tumor infiltration zone.

Acknowledgement

We would like to thank the Magnetic Resonance Spectroscopy Development Department of Siemens Medical Systems and especially Stefan Röhl for his support. This work was supported by a grant of the Deutsche Forschungsgemeinschaft (DFG): GA638/2-1.

References

- [1] Dowling C, Bollen AW, Noworolski SM, McDermott MW, Barbaro NM, Day MR, et al. Preoperative proton MR spectroscopic imaging of brain tumors: correlation with histopathologic analysis of resection specimens. *AJNR Am J Neuroradiol* 2001;22(4):604-12.
- [2] Kondziolka D, Lunsford LD, Martinez AJ. Unreliability of contemporary neurodiagnostic imaging in evaluating suspected adult supratentorial (low-grade) astrocytoma. *J Neurosurg* 1993;79(4):533-6.
- [3] Kamada K, Moller M, Sagner M, Ganslandt O, Kaltenhauser M, Kober H, et al. A combined study of tumor-related brain lesions using MEG and proton MR spectroscopic imaging. *J Neurol Sci* 2001;186(1-2):13-21.
- [4] Michaelis T, Merboldt KD, Bruhn H, Hanicke W, Frahm J. Absolute concentrations of metabolites in the adult human brain in vivo: quantification of localized proton MR spectra. *Radiology* 1993;187(1):219-27.
- [5] Urenjak J, Williams SR, Gadian DG, Noble M. Proton nuclear magnetic resonance spectroscopy unambiguously identifies different neural cell types. *J Neurosci* 1993;13(3):981-9.
- [6] Kemp GJ. Non-invasive methods for studying brain energy metabolism: what they show and what it means. *Dev Neurosci* 2000;22(5-6):418-28.
- [7] Croteau D, Scarpace L, Hearshen D, Gutierrez J, Fisher JL, Rock JP, et al. Correlation between magnetic resonance spectroscopy imaging and image-guided biopsies: semiquantitative and qualitative histopathological analyses of patients with untreated glioma. *Neurosurgery* 2001;49(4):823-9.
- [8] Stadlbauer A, Ganslandt O, Gruber S, Nimsky C, Fahlbusch R, Moser E. Metabolic tumor imaging and absolute quantification of metabolic changes in gliomas. *ESMRMB*. 2003. Rotterdam. P.194
- [9] Stadlbauer A, Ganslandt O, Gruber S, Nimsky C, Fahlbusch R, Moser E. MR spectroscopy guided brain tumor resection: Integration of MRSI in functional neuro-navigation using a MRI/MRSI hybrid dataset. *J Neurosurg*. 2003. Rotterdam. P.196
- [10] Hall WA, Martin A, Liu H, Truwit CL. Improving diagnostic yield in brain biopsy: coupling spectroscopic targeting with real-time needle placement. *J Magn Reson Imaging* 2001;13(1):12-5.
- [11] Rock JP, Hearshen D, Scarpace L, Croteau D, Gutierrez J, Fisher JL, et al. Correlations between magnetic resonance spectroscopy and image-guided histopathology, with special attention to radiation necrosis. *Neurosurgery* 2002;51(4):912-9; discussion 919-20.
- [12] McKnight TR, von dem Bussche MH, Vigneron DB, Lu Y, Berger MS, McDermott MW, et al. Histopathological validation of a three-dimensional magnetic resonance spectroscopy index as a predictor of tumor presence. *J Neurosurg* 2002;97(4):794-802.
- [13] Pirzkall A, McKnight TR, Graves EE, Carol MP, Sneed PK, Wara WW, et al. MR-spectroscopy guided target delineation for high-grade gliomas. *Int J Radiat Oncol Biol Phys* 2001;50(4):915-28.
- [14] Preul MC, Leblanc R, Caramanos Z, Kasrai R, Narayanan S, Arnold DL. Magnetic resonance spectroscopy guided brain tumor resection: differentiation between recurrent glioma and radiation change in two diagnostically difficult cases. *Can J Neurol Sci* 1998;25(1):13-22.

Case Report: Gliomatosis Cerebri

Damien Galanaud Ph.D.
O.Chinot, F. Nicoli, S. Confort-Gouny,
Y. Le Fur, M. Barrie-Attarian,
J.P. Ranjeva, S. Fuentes, P. Viout,
D. Figarella-Branger, P.J. Cozzone

Centre d'Exploration Métabolique
par Résonance Magnétique
(CIMEREM)
Marseilles, France

Patient History

A 70-year-old man was referred to the Neurology Department of La Timone Hospital in Marseilles exhibiting a mental deterioration of one month duration. Magnetic resonance imaging and spectroscopy (including both single voxel and spectroscopic imaging) was performed. Based on these radiological and metabolic data, gliomatosis cerebri was suspected. A stereotactic biopsy yielded glial tumor cells, confirming this diagnosis. Chemotherapy was instituted, but the patient's condition rapidly worsened and he died within a month.

Images and sequence details

Figure 1

Chemical Shift Imaging (CSI) of the patient (A) and of a control subject with low grade glioma (B). The sequence used was an acquisition weighted apodized sequence developed in our institution (D. Galanaud et al., MAGMA, 2001, 13:127-33). TR = 1500 ms, TE = 136 ms, 15 mm slice thickness, 6 outer volume suppression slices are used. Spectra are processed using a proprietary software. NAA: N-Acetyl Aspartate. Cho: Choline containing compounds. Cr: Creatine/phosphocreatine. The CSI map showing the Cho/Cr ratio is overlaid on a FLAIR image to allow better metabolic/anatomic correlation.

Discussion

Gliomatosis cerebri (GC) is a diffuse infiltration of brain parenchyma by tumor cells of glial origin. It is important to differentiate primitive gliomatosis cerebri (which has a very poor prognosis) from infiltrating low grade gliomas (LGG), sometimes called secondary gliomatosis, which carry a much better prognosis and often respond to chemotherapy and radiotherapy. Conventional pathology does not discriminate between these two diseases since it is most commonly based on small stereotactic biopsy samples and thus does not provide a global picture of the lesion. Conventional MR imaging contributes to this differential diagnosis: it has been shown by many authors that GC tends to (i) predominate on the white matter and relatively spare the cortex (ii) often invade the basal ganglia and/or the brainstem (iii) lack significant focal mass effect and contrast enhancement at the initial

examination. These findings are, however, inconstant and in atypical cases it is difficult to differentiate between GC and LGG by conventional imaging alone. Chemical shift imaging (CSI), also called 2D proton MR spectroscopy, studies the metabolic properties of brain tissue. We have shown that the metabolic patterns of GC and LGG differ strikingly (D Galanaud et al., J Neurosurg, 2003, 98: 269-76). On the one hand, LGG has a classical glial tumor metabolism, associating elevated Cho and ml, reduced NAA and Cr. On the other hand, GC shows markedly elevated Cr and ml and moderately elevated Cho and reduced NAA. These metabolic differences provide the ability to make a clear-cut differentiation between GC and LGG, even in individual patients.

This data, which is included in our database of more than 200 tumors, emphasizes the ability of MR spectroscopy and CSI to provide diagnostic and prognostic information for brain tumor patients, even when conventional MRI and biopsy based pathology are taken in default.

Scanner Model used:

Siemens MAGNETOM Vision plus

Coil used:

Head coil

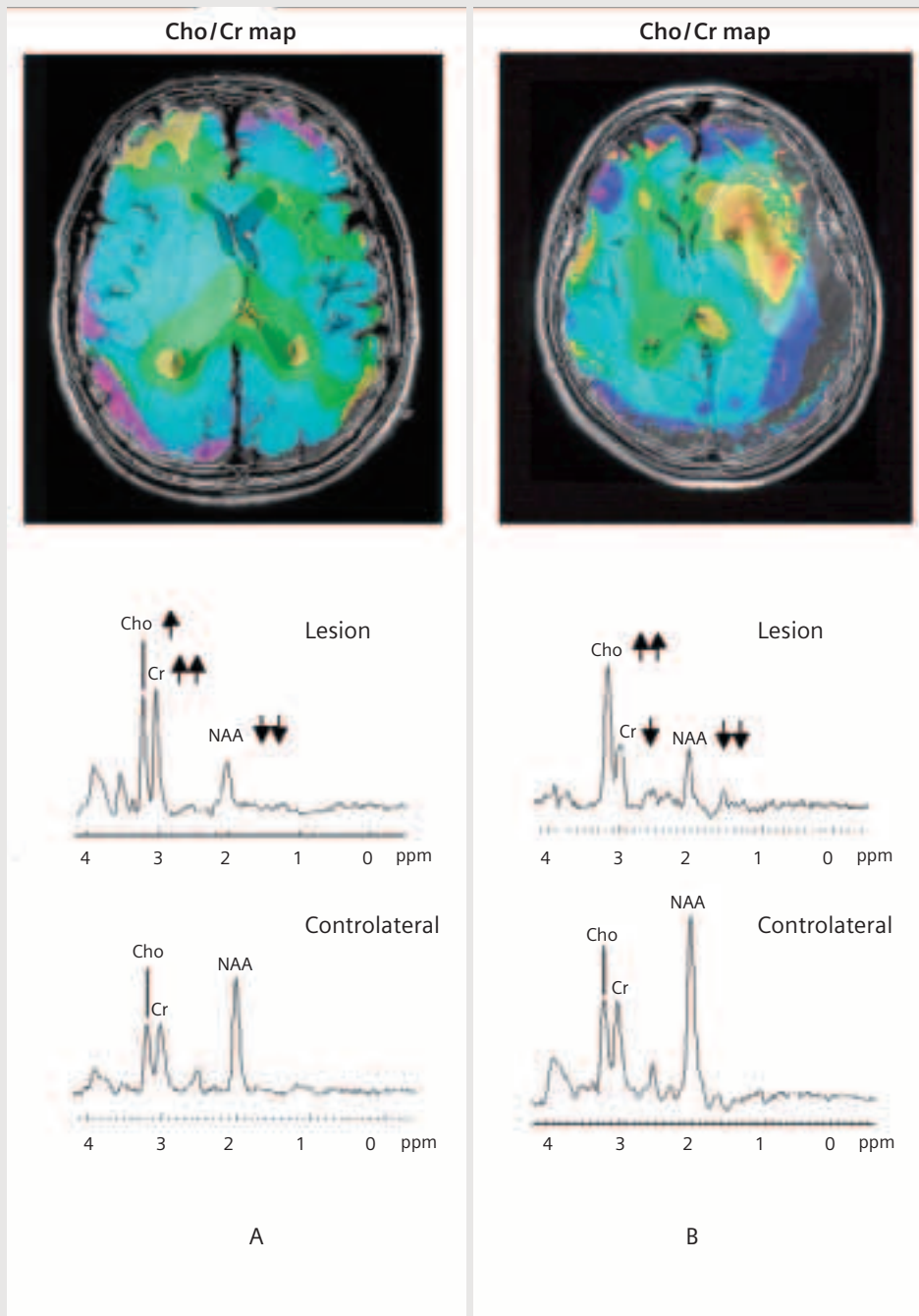


Figure 1

Spectroscopy in Differential Diagnosis of an Intracranial Mass Lesion

Priv. Doz. Dr. med. F. Fellner
Dr. rer. biol. hum. C. Fellner

Radiologisches Institut
Oberösterreichische Landes-
nervenklinik Wagner-Jauregg
Linz

Until recently, differentiating between inflammatory and neoplastic mass lesions has been difficult. Nowadays, however, the complementary information received from MR spectroscopy and diffusion weighted imaging has helped to improve and even alter the diagnosis of an intracranial mass lesion.

History

The patient was sent to MR with peripheral facial paralysis. MR revealed fluid in the mastoid cells and contrast enhancement in the anatomical area where the peripheral part of the facial nerve crosses. These findings supported the diagnosis of infection in the mastoid cells. The right occipital lobe also revealed a mass lesion of 1.5 cm. MR spectroscopy was advised for further evaluation of the lesion.

Image Findings

The examination was carried out using a MAGNETOM Symphony with standard CP Head Array coil. For spectroscopy examination, the SE (PRESS) single voxel sequence with echo times of 30, 135 and 270 ms was used. Short echo time examination lasted 3.12 mins, the longer TE measurements lasted 6.24 mins each. The voxel sizes were 15x15x15 mm³ and 18x16x20 mm³ respectively. MR spectroscopy was also performed in the presumably normal left occipital lobe for comparison purposes. In measurements with echo-times of 30 ms and 135 ms, the integral value of NAA and creatine peaks were lower than normal. All spectra showed an increase in choline. At 1.3 ppm, which represents lactate/lipid, inversion of the peak was seen at TE of 135 ms. At 30 ms, lipid peak had significantly increased. At 270 ms, no significant peak at this location was seen. The NAA/Cho ratio at 135 ms echo-time was lower than for normal brain tissue. Additional diffusion weighted sequences with $b = 1000 \text{ s/mm}^2$ showed the lesion to be hypo-intense which was also an indication that it could be tumor rather than abscess.

Results and Discussion

Further examinations revealed mass lesions in the breast with multiple lesions in the lung, which could be metastasis with primary lesion in the breast. Before resection of the lesion with neuro-navigation, functional imaging with a simple optical paradigm was also performed. The patient was asked to close and open her eyes 3 times. Each phase – rest and activation – was scanned 10 times with an EPI sequence, 36 slices, with a slice thickness of 3 mm. The resulting BOLD images were fused with T1 weighted images. These images were also used in the neuro-navigation system applied during the operation.

The histological analysis of the resected lesion indicated metastasis of papillary cancer such as breast or ovarian cancer.

The diagnosis of brain abscesses is generally based on clinical findings and image findings from CT and MR. Great care is required with image findings due to the fact that abscesses and cystic-necrotic tumors can look very similar and differential diagnosis is not always easy. As in this case, MR spectroscopy and diffusion weighted images can bring complementary information. Cystic tumors and abscesses show increased lactate peak. Lactate is a non-specific metabolite that results from anaerobic glycolysis. The spectra from cystic, necrotic brain tumors differ from abscesses. Abscesses show an increase of acetate and succinate, amino acids and lactate due to increased glycolysis. Amino acids like valine and leucine are end products from enzymes that are released from neutrophils in the abscess. It is very important to differentiate amino acids (valine, leucine and isoleucine at 0.9 ppm) and lipids (0.8-1.2 ppm). Lipids can be seen in tumors and abscesses whereas, on the other hand, in vivo

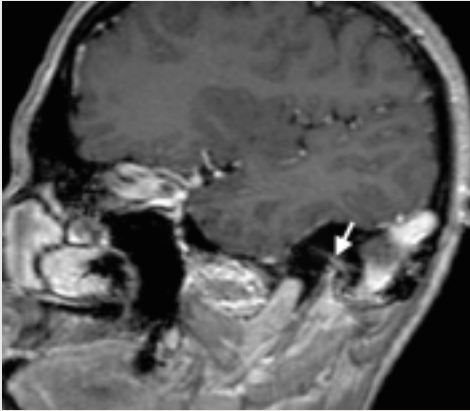


Figure 1a

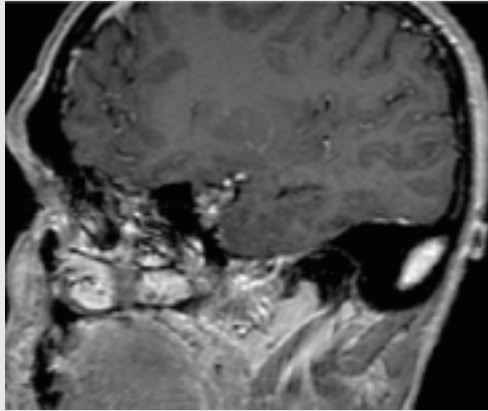


Figure 1b

Figure 1 Pathologic enhancement of the left facial nerve due to inflammatory changes in the petrous bone. 1b shows normal appearance of the right facial nerve. Oblique coronal views from 3D MP-RAGE data set.

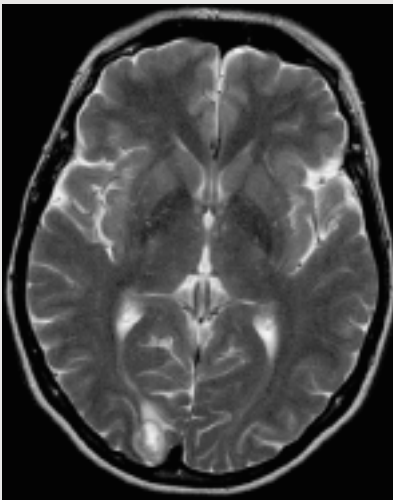


Figure 2a

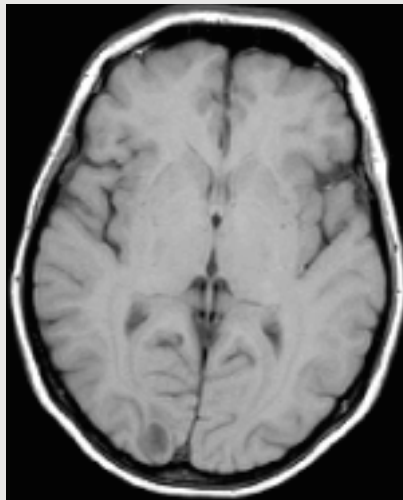


Figure 2b

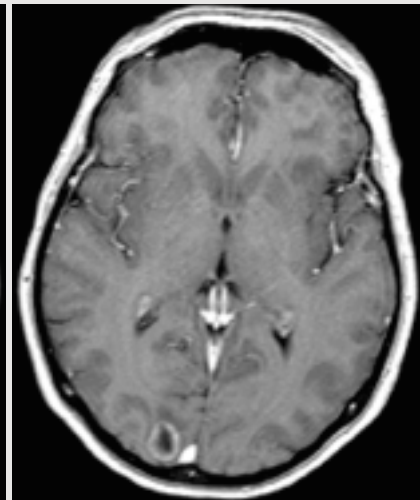


Figure 2c

Figure 2 Mass lesion in the occipital lobe with peripheral enhancement and central liquid part. Differential diagnosis included abscess or tumor. (a) T2 weighted TurboSE sequence; (b) T1 weighted spin echo sequence before contrast; (c) transverse reconstruction from gadolinium-enhanced 3D MP-RAGE data set.

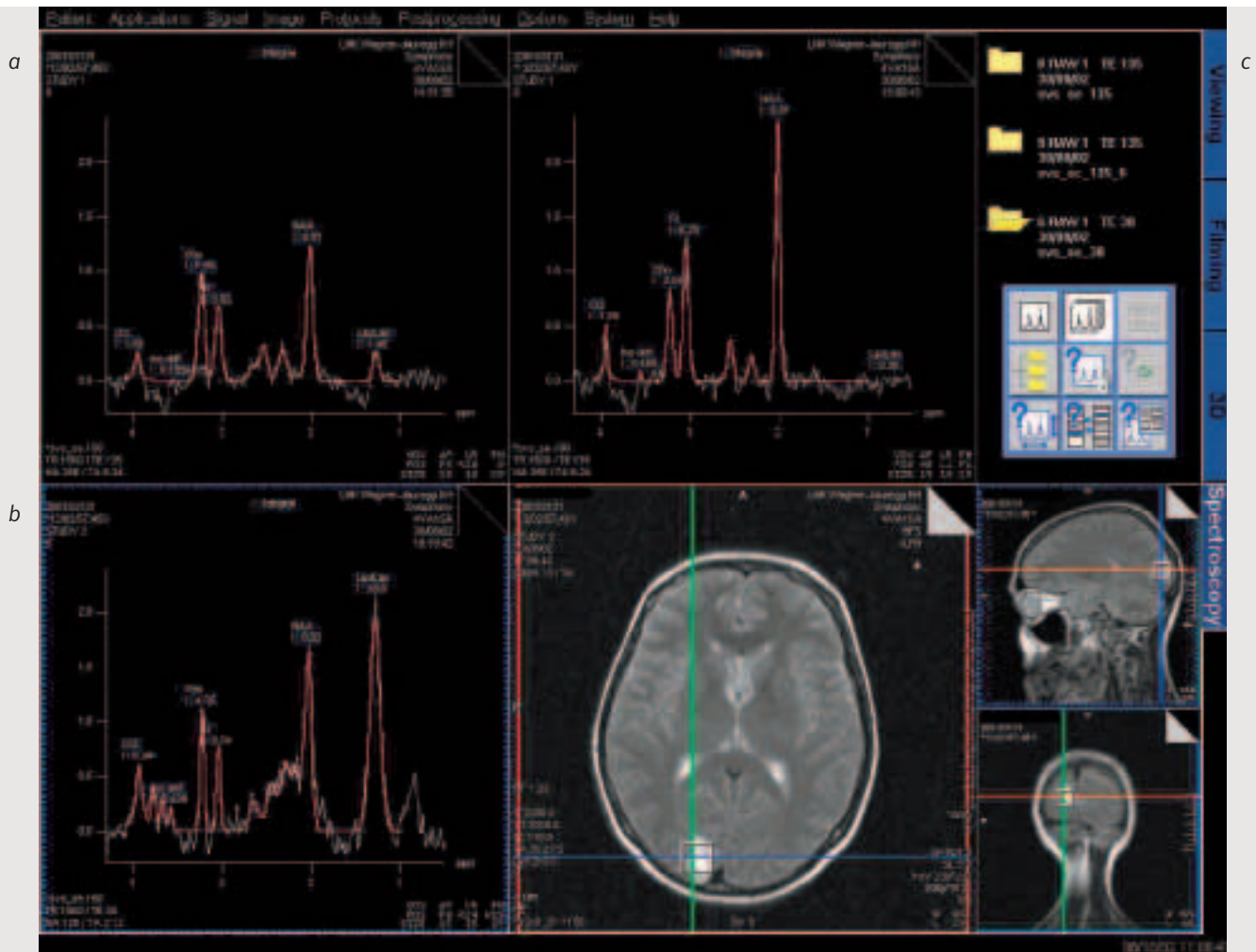


Figure 3 Single voxel MR spectroscopy. Shown are three measurements with echo times of 135 ms, 30 ms. B shows the spectrum from the normal left side. In the metastatic lesion one can see decreased NAA and increased choline, as well as increased lipid peaks.

analysis of tumors will not show any amino acids except in in vitro conditions. At an echo time of 135 ms, the lactate doublet and the amino acid multiplets are inverted due to the j-coupling effect. This inversion is not to be found with lipids. This is an additional helpful finding along with the lack of acetate and succinate in tumors. Care must be taken that these findings of an abscess are accurate before giving antibiotic therapy as there seems to be a decrease in acetate and succinate following antibiotic therapy. For differentiation of cystic-necrotic tumors and brain abscesses, diffusion weighted images are also very useful. The pus in brain abscesses is hyperintense in contrast to the cystic or necrotic parts of tumors. This finding is not 100% reliable, however, as there have been some reports in the literature showing hyperintense tumor lesions. In the occipital lesion of the patient there was an increased lipid peak, which indicated a metastatic lesion. (In metastatic lesions, a higher contrast of lipid may be found in comparison to glioblastomas, anaplastic astrocytomas, abscesses or other intracranial mass lesions.)

The use of MR spectroscopy and diffusion weighted imaging will improve the diagnostic certainty of imaging techniques, which in turn will decrease the number of interventional approaches such as surgery and biopsy.

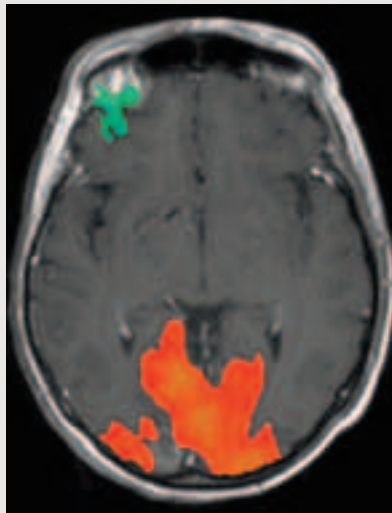


Figure 4 Preoperative fMRI with an easy paradigm (eye closing and opening). The images show activation in the visual areas in both occipital lobes, which will help during the operation in sparing these important anatomical landmarks.

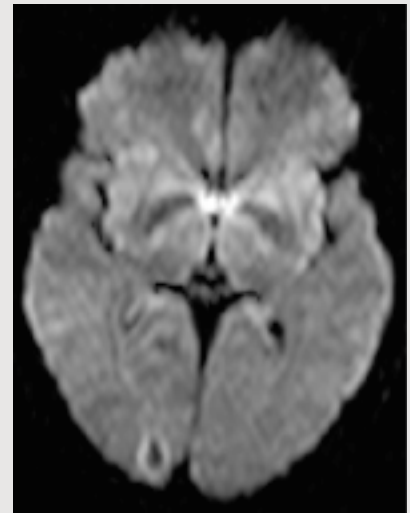


Figure 5 Diffusion weighted image shows central part of the lesion as hypointense, which is an indicator of metastatic or tumor lesion.

Proton Magnetic Resonance Spectroscopy (MRS) in Primary Pediatric Brain Tumors

Richard Jones, Ph.D.
Susan Palasis, M.D.

Dept. of Radiology,
Children's Healthcare of Atlanta,
Atlanta, GA, USA

Evaluation of intracranial pathology is optimally performed with MR imaging. Based on conventional imaging features alone, it is often possible to differentially diagnose between intracranial masses. MR spectroscopy has shown itself to be a useful adjunctive tool in further characterization of pathology. Characteristic spectral patterns have the ability to differentiate between intracranial neoplasms and other mass lesions. With the advent of more advanced MRS techniques, such as chemical shift imaging, we now have the ability to more completely evaluate the chemical make-up of the tumor. Combining the information we receive from both long and short TE proton MRS, tumor grade can be inferred.

History

This is a seven-year-old male with a recent history of headaches. The child developed a new onset seizure and was sent for neuroimaging evaluation. A non-enhanced CT scan of the head demonstrated a mass lesion in the left medial occipital lobe. A plain and contrast enhanced MRI of the brain was performed which confirmed the presence of a brain tumor. MR spectroscopy was performed for further tumor characterization.

Technique

The data was acquired on a 1.5 Tesla MAGNETOM Symphony scanner using the standard head coil. The CSI was acquired using TR/TE = 1700/270 and a 16x16 matrix, with four averages and elliptical sampling the total scan time was 8 minutes and three seconds. Suppression bands on all sides of the volume were used to suppress signal outside of the region of interest.

Results and Discussion

The diagnosis of tumor with MRS is often straightforward with a typical spectrum of low N-acetyl-aspartate (NAA) and high choline (Cho) observed on long TE evaluation. This is useful adjunctive information to conventional imaging based diagnosis. A major benefit of spectroscopy, however, is its ability to further analyze tumor physiology. Low grade and high grade tumors can have a similar MRI appearance, but often have a very different MRS appearance. MRS has moved beyond the single voxel long TE examination. Chemical shift imaging (CSI) allows us to look at the entire extent of the tumor and the surrounding tissues. Metabolite maps allow us to readily appreciate

the inherent heterogeneity of these lesions which can be useful for biopsy guidance and for tumor extension past obvious gross anatomic boundaries on MRI.

In the case being presented, conventional MR images (Figs. 1a and b) demonstrate a solid and cystic mass with heterogeneous enhancement and mild peritumoral edema. Metabolite maps obtained with long TE CSI (Figs. 2a, 2b, 2c) show a very high Cho:NAA ratio consistent with viable solid tumor, low creatine (Cr) and high lactate. The metabolite abnormalities closely correlate to the anatomic boundaries of the mass. The single voxel short TE MRS (Figs. 3a and b) demonstrates moderate myoinositol (ml) elevation and very high lipids. This combination of metabolite patterns on short and long TE MRS has been observed in tumors of high grade. MRS offers us a level of specificity that could not be achieved with conventional MRI alone.



Figure 1a

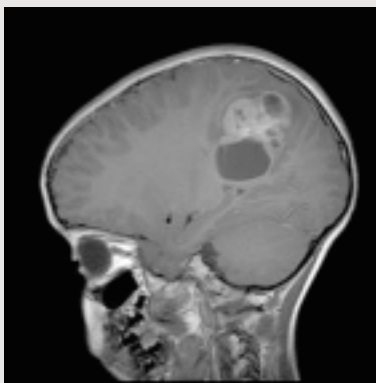


Figure 1b

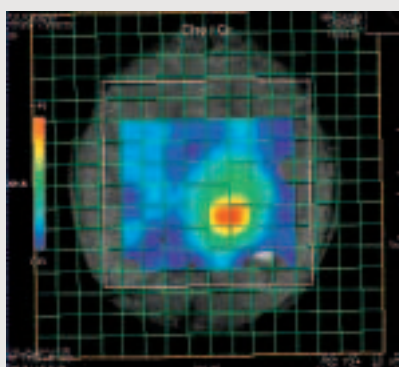


Figure 2a

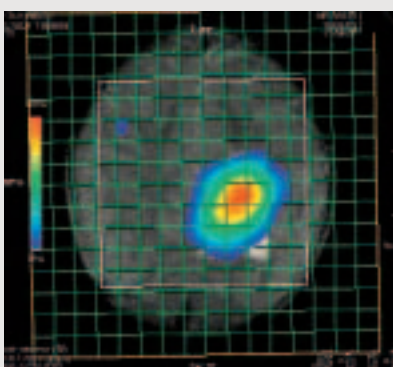


Figure 2b

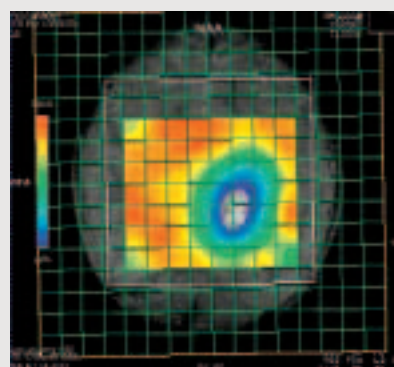


Figure 2c



Figure 3a

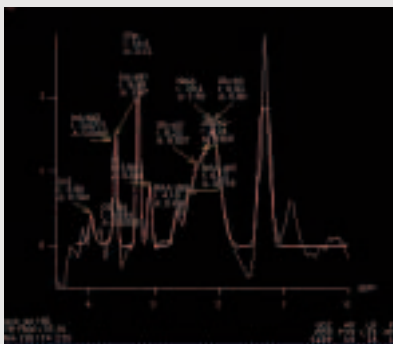


Figure 3b

Case Report: 3T Sjögren-Larsson Syndrome

Marinette van der Graaf, Ph.D.
MR Spectroscopist

Department of Radiology,
University Medical Center
Nijmegen, The Netherlands

Patient History

A 33-year-old man was known to have had a clinical diagnosis of Sjögren-Larsson syndrome (an inborn error of metabolism causing congenital skin disorder, spasticity, and mental retardation) since infancy. Because of genetic counseling in the family, an attempt was made to prove the diagnosis at the molecular level. Unexpectedly, repeated biochemical investigations were negative. Because of the high clinical suspicion, additional investigations were requested, including cerebral MR imaging and spectroscopy.

Image Findings (Figs. 1, 2, 3, 4, 5)

MR images showed only mild signs of cerebral atrophy and subtle white matter involvement with a small periventricular lesion with high signal intensity on a T2-weighted image in the left parieto-occipital region.

The MR spectrum of the gray matter showed a pattern that is normally obtained at 3T using an echo time of 136 ms. However, the MR spectrum of the white matter showed clearly an additional sharp "lipid" signal at 1.3 ppm in addition to a slightly reduced NAA signal.

Discussion

MR imaging hardly showed any abnormality that could be in line with Sjögren-Larsson syndrome. MR spectroscopy of white matter showed a resonance at 1.3 ppm in the white matter spectrum, which was absent in the gray matter spectrum. These findings are highly characteristic for Sjögren-Larsson syndrome (see M.A.A.P. Willemsen et al., Am J Neuro-radiol 25, April 2004, in press). Based upon these results, further molecular studies were requested: these finally proved the diagnosis of Sjögren-Larsson syndrome by demonstration of mutations in the gene involved in this disorder.

Location and Date of Scan:

University Medical Center Nijmegen,
Nijmegen, The Netherlands,
September 2003

Scanner Model used:

Siemens MAGNETOM Trio

Coil used:

CP head coil

Software Version:

NUMARIS 4 syngo MR 2003T (version
VA23A) + spectroscopy option

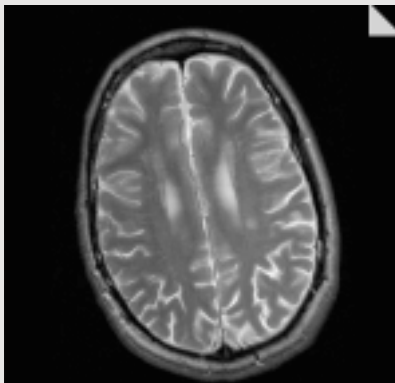


Figure 1 T2 weighted image (TE/TR = 104/4000).

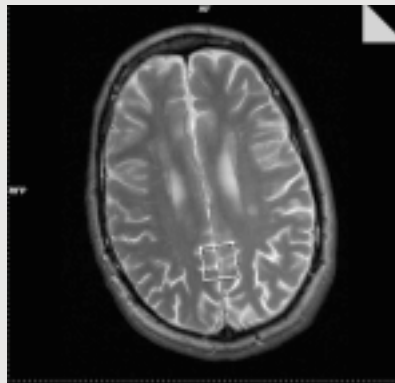


Figure 2 Voxel position gray matter.

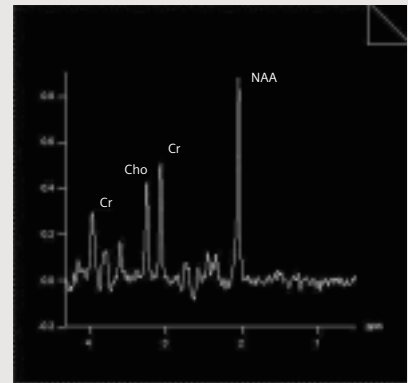


Figure 3 Proton MR spectrum (PRESS, TE/TR = 136/2000) of a 8-ml voxel located in the central occipital gray matter.

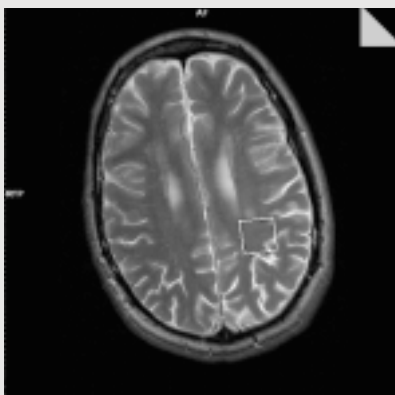


Figure 4 Voxel position white matter.

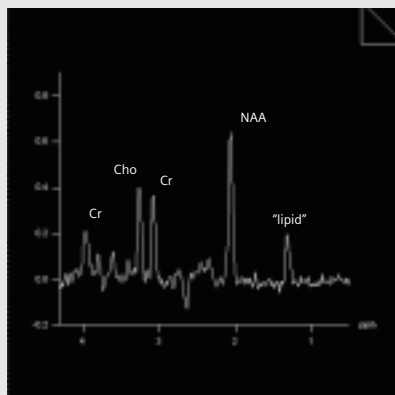


Figure 5 Proton MR spectrum (PRESS, TE/TR = 136/2000) of a 8-ml voxel located mainly in white matter in the occipital trigone.

Localized Proton Spectroscopy in Hepatic Encephalopathy: Advantage of 3T-High-Field for Discrimination of Glutamine and Glutamate

Thomas Nägele¹, Uwe Seeger¹,
Holger Hass², Wilhelm Küker¹,
Stefan Heckl¹, Uwe Klose¹

¹ Department of Neuroradiology,

² Department of Gastroenterology
and Hepatology Medical Clinic,
University of Tübingen

Introduction

In hepatic encephalopathy (HE) – a frequent complication of chronic liver dysfunction – the neuro-psychological impairments range from mild deficits in psychomotor and visio-practic abilities to confusion and finally stupor in higher grades due to decreased hepatocellular detoxification and synthesis functions. In HE, specific changes of brain tissue concentrations of myo-Inositol (ml) (decrease), glutamine/glutamate (Glx) (increase) and Choline (Cho) (decrease) have been reported [1]. For spectroscopic detection of Glx, short echo times and highest possible field strength are preferred. In this study, therefore, we used a short echo time PRESS sequence (TE = 30 ms) to achieve high signal of the J-coupling resonances ml and Glx. Of principal interest is the differentiation of glutamine (Gln) and glutamate (Glu) which is generally very difficult to achieve at the standard field strength of 1.5T. This report shows that this differentiation is possible at a whole body unit of 3T (Siemens Trio), as demonstrated in a patient with chronic liver disease and accom-

panying HE. For comparison, measurements were acquired at 3T and 1.5T (Siemens Sonata) and the spectra were compared with those of a healthy volunteer at 3T and 1.5T.

Patient History and Methods

We examined a 56-year-old man with ethyltoxic liver cirrhosis (Child-Pugh C). The referring hepatologist performed a clinical examination for detection of the HE including a number connection test (NCT) [2] immediately before the MR examinations. Pathological NCT was found with 90 s while the NCT score can be classified as normal provided the time for finishing the test is less than ten times the subjects age in decades [3]. Additionally, the patient suffered from drowsiness as well as elevated ammonia blood levels during the last days in hospital. This made a reliable clinical diagnosis of Hepatic encephalopathy possible.

Two subsequent MRS and MRI examinations of the same patient were performed within one day on a 1.5T whole-body MR System (MAGNETOM Sonata, Siemens AG, Erlangen, Germany) using a conventional circularly polarized head coil and on a 3T whole-body MR System (MAGNETOM Trio, Siemens AG, Erlangen, Germany) using a standard head coil. For the follow-up examination, exact reproducibility of the spectral localization was of special importance. This was achieved by acquiring 3 orthogonal (sagittal,

axial, coronal) gapless heavily T2-weighted (turbo factor 15) turbo spin echo (TSE) data sets within 2 minutes for 3-dimensional positioning of the volume of interest (VOI).

Since it has been shown that occipital gray and white and parietal white matter locations exhibit essentially identical MRS metabolite changes in HE [1], we decided to place the VOI in the medial part of the occipital lobe. This area contains grey and white matter and allows the measurement of a VOI size of 2x2x2 cm³ with good homogeneity of the magnetic field (Fig. 1).

MR imaging consisted of non-enhanced axial T1 weighted (T1w) spin echo (SE) and T2 weighted (T2w) TSE images. Measurement parameters (TR/TE/acquisition time) were 580ms / 12ms / 2min for the T1w and 3000ms / 90ms / 3min for the T2w imaging. Slice thickness SL was 5 mm with a gap of 1 mm.

In chronic liver disease, signal hyperintensities in the basal ganglia on T1w images are found most pronounced in the globus pallidus [4]. They probably represent manganese deposition due to liver dysfunction which is potentially reversible if liver function improves or where there has been a liver transplant [5].

For the detection and quantification of ml and Glx, it is essential to use spectroscopic sequences with a short echo time (TE) to minimize the influence of J-coupling and T2 relaxation (Glx, ml), as both factors lead to a signal decrease.

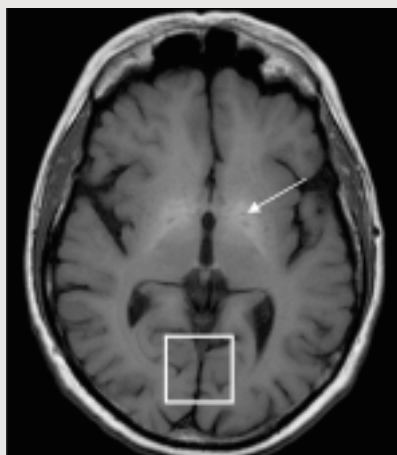


Figure 1 T1w MR image acquired at 1.5T showing the voxel localization (white box) in the occipital gray/white matter. Further signal hyperintensities of the basal ganglia (globus pallidus) are depicted (white arrow) representing manganese deposition due to liver dysfunction which is potentially reversible if liver function improves or where there has been a liver transplant.

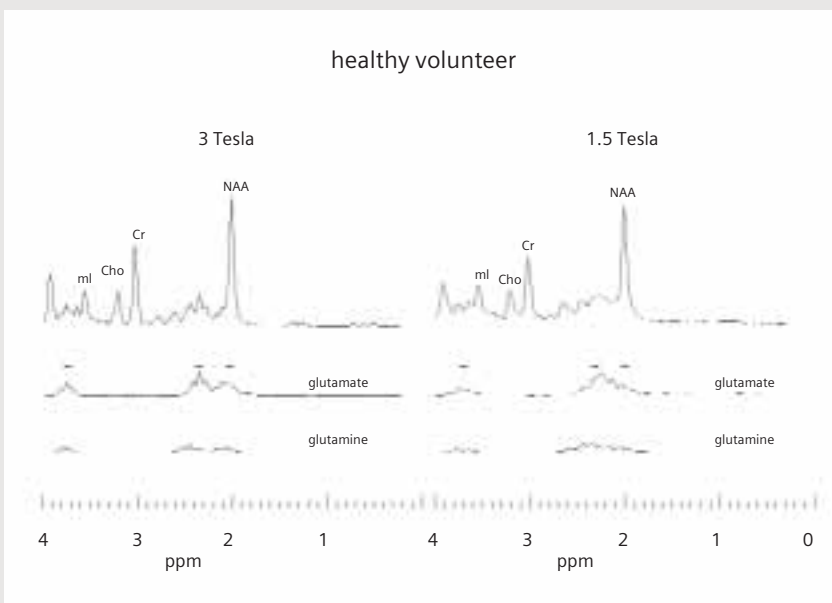


Figure 2 Gray matter short echo time spectra from a healthy volunteer obtained at 1.5T and 3T after evaluation by LCModel. Additionally, the proportions of glutamate and glutamine obtained are shown by scaled model spectra.

Therefore ¹H-MRS was performed using a single voxel double spin echo sequence (PRESS, TR 3000, TE 30, NA = 64) with a measurement time of 3 minutes per voxel. For each voxel a short reference measurement without water suppression was performed for an eddy current correction during postprocessing.

Spectral postprocessing was performed using an optimized LC-model [6] for absolute quantification. In our LC-model, the basis data set was completed by lipid and macromolecule resonances which are especially important in demyelinating and neoplastic lesions [7]. The results of the LC-model evaluation are depicted in Figs. 2 and 3 for both measurements at 1.5 Tesla and 3 Tesla. The left/right column in Fig. 2 shows the results for 3T/1.5T of the healthy volunteer. The upper row depicts the LC-model fit of the spectra, the middle row the glutamate (Glu) and the lower row the glutamine (Gln) signal. It is clearly shown that in normals cerebral concentration of Gln is relatively low [1.9 mMol/l] in comparison to the excitatory neurotransmitter (Glu) [6.5 mMol/l].

Of major importance is the separation of the β- (3.77 ppm) and γ- (2.05-2.45 ppm) resonances of Gln and Glu at 3T due to increased chemical-shift while they are slightly together at 1.5T. This increased chemical-shift allows better separation of Glu and Gln in the LC-model fit at 3T compared to 1.5T.

More prominently, this is depicted in Fig. 3 with the corresponding spectra of the patient with hepatic encephalopathy. The upper row shows again the fit of the LC-model with an HE-typical decrease of choline (Cho) and myo-inositol (ml). Additionally, in comparison with Fig. 2 an elevated glutamine signal can be detected, best seen in the range of the β- and γ-resonances. The elevated

glutamine concentration [5.3 mMol/l] in the patient leads to a similar signal strength of Glu and Gln. Together with the higher chemical-shift at 3T, proper separation and reliable quantification of glutamine and glutamate is possible with the LC-model evaluation (Fig. 4). Usually this is not possible at 1.5T, leading to frequently used combined evaluation of both metabolites as a resonance Glx=Glu+Gln at lower field-strengths.

Discussion

This report shows an example of practical benefit of the theoretically predicted higher chemical shift at 3T compared to 1.5T. Separation of glutamine and glutamate is of major importance for the understanding of HE, which is an important complication of chronic liver dysfunction. 70% of patients with chronic liver dysfunction suffer from HE episodically. The symptoms range from mild deficits in psychomotor and visio-practic abilities to confusion and finally stupor in higher grades due to decreased hepatocellular detoxification and synthesis functions.

High ammonia levels due to reduced detoxification of the liver is thought to be a reason for elevated cerebral glutamine concentrations found in previous spectroscopic studies [5]. These studies were either based on plain peak integration between 3.72 ppm and 3.82 ppm to evaluate a-Glx [1] – as it has been found that the integrated signal corresponds well to the predominant glutamine signal – or on fitting procedures with subsequent peak integral calculations [5].

In principle, none of these vivo studies at 1.5T allow separation of glutamine and glutamate. However, if glutamine and glutamate can be separately quantified, then further interesting insights into the meta-

bolisms of the excitatory neurotransmitter glutamate should be possible. This might be of special interest for detection of the mild and subclinical forms of HE which are characterized by missing clinical symptoms. Nevertheless, these patients are unable to drive a vehicle due to reduced visio-practic abilities [1]. Up to now, subclinical HE is commonly diagnosed by extensive neuropsychological testing. However, all these tests are more or less dependent on the investigator and on the patient's age, sex and education.

References

- [1] Ross B D, Jacobson S, Villamil F, Korula J, Kreis R, Ernst T, et al. Subclinical hepatic encephalopathy: proton MR spectroscopic abnormalities. *Radiology* 1994;193:457-463.
- [2] Parsons-Smith B, Summerskill W, Dawson A, Sherlock S. The electroencephalograph in liver disease. *Lancet* 1957;2:867-871.
- [3] Van Gorp W, Satz P, Mitrushina M. Neuropsychological processes associated with normal aging. *Dev Neuropsychol* 1990;6:279-290.
- [4] Brunberg JA, Kanal E, Hirsch W, Van Thiel DH. Chronic acquired hepatic failure: MR imaging of the brain at 1.5. *AJNR Am J Neuroradiol* 1991;12:909-914.
- [5] Naegel T, Grodd W, Viebahn R, Seeger U, Klose U, Seitz D, Kaiser S, Mader I, Mayer J, Lauchart W, Gregor M, Voigt K. MR imaging and ¹H spectroscopy of brain metabolites in hepatic encephalopathy: time-course of renormalization after liver transplantation. *Radiology* 2000; 216:683 – 691
- [6] Provencher S W: Estimation of metabolite concentrations from localized in vivo proton NMR spectra. *Magn-Reson-Med.* 1993; 30: 672-679
- [7] Seeger U, Klose U, Mader I, Grodd W, Nägele T: Parameterized evaluation of macromolecules and lipids in proton MR spectroscopy of brain diseases. *Magn Reson Med* 2003; 49: 19-28

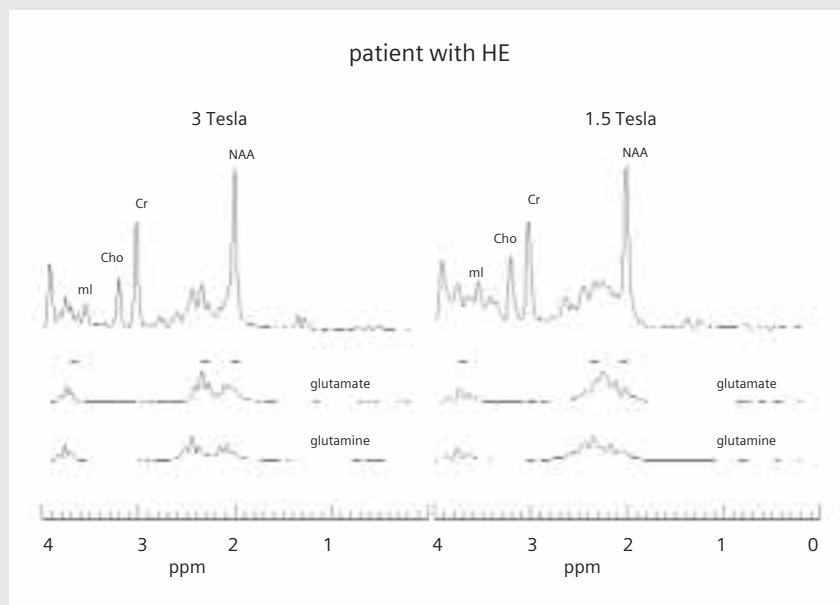


Figure 3 Gray matter short echo time spectra from a patient with HW obtained at 1,5T and 3T after evaluation by LCModel. Additionally, the proportions of glutamate and glutamine obtained are shown by scaled model spectra.

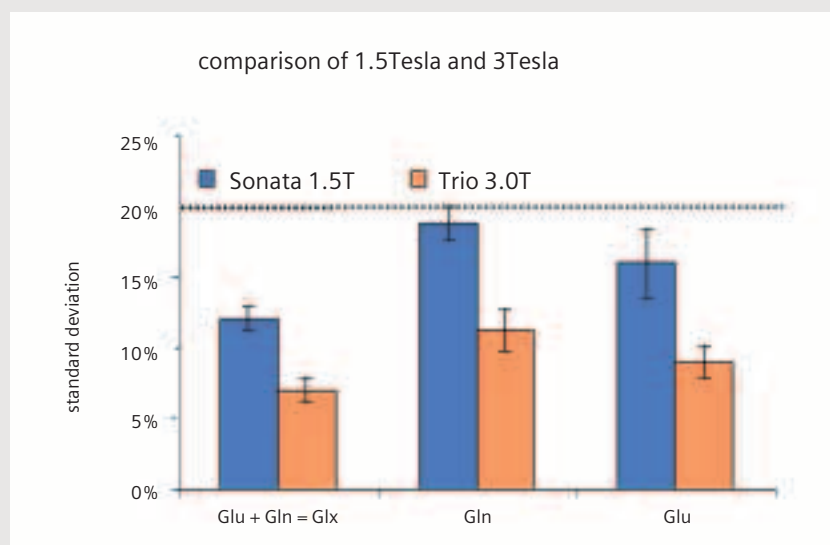


Figure 4 The certainty of the quantification of Gln and Glu is higher at 3T compared to 1.5T. If these two metabolites have to be determined separately, higher field strengths are advantageous, whereas a combined evaluation as Glx is also possible at 1.5T. Especially for Gln, the 20% level that indicates low certitude of the determination in the LC-model is almost reached at 1.5T even in the case of HE when Gln is elevated, which should simplify its determination.

Proton MR Spectroscopic Imaging in the Clinical Evaluation of Prostate Cancer

Heinz-Peter Schlemmer, M.D., Ph.D.

University Hospital Tübingen,
Dept. of Radiology, Tübingen,
Germany

Introduction

Prostate cancer has become a leading cause of morbidity and mortality in men in Western countries. Due to the increasing natural life expectancy, a further increase of the incidence can be expected over the next decades.

Early diagnosis is significantly improved using PSA serum testing. PSA levels have also been shown to correlate with intraprostatic and extraprostatic tumor volume, which are of prognostic importance. The accuracy of mid-range PSA levels of about 4.0 to 10.0 ng/ml in a single patient is limited, however, because much overlap exists in men with prostatic cancer and benign prostatic hyperplasia (BPH). Accordingly, systematic needle biopsy has to be performed in any case to finally confirm the presence of cancer and to assess the tumor grade.

The preferred treatment of early stage cancer confined to the prostate stage is radical prostatectomy. An accurate preoperative identification of extracapsular tumor extension, seminal vesicle invasion and distant tumor spread is important to select surgical candidates and to avert unnecessary surgery. It is important to note, however, that side effects of the treatment adversely affect quality of life, particularly in previously asymptomatic patients with small tumors confined to the gland. Numerous alternative therapeutic approaches have therefore been investigated, which are less invasive and have reduced risk of developing complications such as impotence and incontinence compared to surgery (e.g. stereotactic radiotherapy, androgen deprivation, 'watchful waiting'). Data from randomised clinical trials comparing the cancer control rates are not yet available, however. For individual treatment, planing monitoring and improved methods are necessary to characterize individual tumor aggressiveness particularly in prostate cancer, which is characterized by a high biological variability. Only a small proportion of men with untreated carcinoma will develop serious morbidity or will die from the disease.

For local tumor staging and characterization, the accuracy of most commonly used clinical parameters (digital rectal examination, PSA serum level and Gleason grading) is limited. The role of clinical imaging for local staging and tumor characterization is dramatically evolving. MR imaging with combined endorectal and phased array coil is most challenging for assessing extraprostatic tumour extension and seminal vesicle infiltration with reported accuracies of up to about 80% and 95%, respectively [1] [2]. The accuracy is limited, however, because abnormal signal within the prostate can be

related to both cancer as well as non-malignant abnormalities such as BPH, prostatitis, biopsy-induced intraparenchymal hemorrhage or therapy-induced tissue degeneration.

Beyond morphologic information provided by MR imaging, in vivo proton MR spectroscopy enables to noninvasively detect small mobile biomolecules, which are fingerprints of prostatic metabolism. The whole prostate can be covered with voxel volumes of less than 0.5 ml using 3D MR spectroscopic imaging (MRSI). Combined MRI/MRSI provides high-resolution anatomic and metabolic information enabling better tumor visualization within the prostate. Within each voxel the resonances of citrate (Cit), choline-containing compounds (Cho), and the creatine-phosphocreatine complex (Cr) can be detected and relative signal intensity ratios can easily be determined using software provided by the manufacturer. In prostate cancer increased signal intensities of Cho compared to Cit can be observed. Based on this characteristic metabolic feature of cancer tissue, clinical studies have shown that combined MRI/MRSI enables improved tumor detection and characterization [1]. In particular, increased diagnostic accuracy and decreased inter-observer variability have been found for the diagnosis of extracapsular extension [3] [4]. Moreover, the combined use of MRI/ MRSI increases the overall accuracy of determining prostate cancer volume, which is a proven prognostic factor [5]. Metabolic information of MRSI may also indicate individual tumor aggressiveness, since the increase of Cho and the decrease of Cit signal intensities have been found to correlated with the Gleason score [1].

Diagnostic MRSI as an adjunct to conventional MRI can be indicated in four main categories:

- 1) Evaluation of patients with suspicious PSA-levels but negative prior sextant biopsies: improved tumor localization and support for targeted biopsy [2].
- 2) Pre-operative evaluation of patients with biopsy-proven prostate cancer: assessment of tumor volume and extraprostatic tumor spread [2] for individual therapy planning (e.g. radiotherapy).
- 3) Monitoring effects of minimal invasive treatment strategies.
- 4) Evaluation of patients with rising PSA-levels during follow-up after therapy: Improved detection and localization of local recurrence.

Technical Prerequisites

For successfully monitoring the metabolic state of the prostate, the following prerequisites must be fulfilled:

- 1) Availability of 3D CSI for covering the entire organ.
- 2) A good B0-homogeneity of the area of interest must be reached preferably by an automated shimming procedure. This is the prerequisite for proper function of other technical features such as water and lipid suppression, and signal separation during post-processing.
- 3) Sufficient signal to noise.
- 4) Endorectal Coil.

The metabolic signals of interests are typically 10^4 times weaker than the water signal used for MRI, due to the lower molecular concentrations. Hence it is of paramount importance to collect sufficient signal. The total scan time is usually given by clinical feasibility. Optimal usage of the scan time is achieved by using weighted acquisition, i.e. spending more time on collecting central than peripheral k-space data; e.g. while a $8 \times 8 \times 8$ acquisition of a $TR = 1.5$ s and four averages requires more than 50 minutes using conventional full k-space sampling, the measurement time for acquiring data of the same SNR is reduced to approximately 8 minutes using weighted acquisition. The spatial resolution of weighted acquisition is determined by a filter-function which increases the width of the central lobe of the spatial response function ("effective voxel size"), but which reduces the signal contributions from distant voxels ("voxel bleeding"). For obtaining the latter, this filter function is often applied even to fully sampled k-space data (which leads, however, to a severe loss of SNR). For many clinical questions it is important not to sacrifice further the already low spatial resolution of MRS for increasing SNR. Instead, there is a tendency of using an endorectal coil for receiving close to the prostate the highest signals. Using this setup, effective voxel sizes of approximately 1 cc can be reached for an acquisition time of 10 minutes on a 1.5T scanner.

Future considerations

An ongoing clinical study initiated by Siemens (International Multicenter Assessment of Prostate Spectroscopy, IMAPS) has the goal of proving the value of the described MRS techniques for tumor visualization and localization. Furthermore, larger-

scale clinical trials have to be performed to determine the clinical value of combined MRI/MRSI studies for the management of prostate cancer patients.

Increased spatial and spectral resolution can be expected by using MR scanners with 3 Tesla or even higher magnetic fields. More anatomic details and probably new metabolic markers may further increase the diagnostic accuracy and probably the assessment of individual aggressiveness.

References

- [1] Kurhanewicz J, Swanson MG, Nelson SJ, Vigneron DB. Combined magnetic resonance imaging and spectroscopic imaging approach to molecular imaging of prostate cancer. *J Magn Reson Imaging* 2002; 16(4): 451-63.
- [2] Engelbrecht MR, Jager GJ, Laheij RJ, Verbeek ALM, van Lier HJ, Barentsz JO. Local staging of prostate cancer using magnetic resonance imaging: a meta analysis. *Eur Radiol* 2002; 12: 2294-2302.
- [3] Yu KK, Scheidler J, Hricak H, Vigneron DB, Zaloudek CJ, Males RG, Nelson SJ, Carroll PR, Kurhanewicz J. Prostate cancer: prediction of extracapsular extension with endorectal MR imaging and three-dimensional proton MR spectroscopic imaging. *Radiology* 1999; 213(2): 481-488.
- [4] Scheidler J, Hricak H, Vigneron DB, Yu KK, Sokolov DL, Huang LR, Zaloudek CJ, Nelson SJ, Carroll PR, Kurhanewicz J. Prostate cancer: localization with three-dimensional proton MR spectroscopic imaging-clinicopathologic study. *Radiology* 1999; 213(2): 473-480.
- [5] Coakley FV, Kurhanewicz J, Lu Ying, Jones KD, Swanson MG, Chang SD, Carroll PR, Hricak H. Prostate cancer tumor volume: measurements with endorectal MR and MR spectroscopic imaging. *Radiology* 2002; 223: 91-97.

Results from IMAPS Study

Image Findings (Results)

The localization of the tumor-region in the histopathologic examination of the resected prostate (Fig. 1) is reflected in the MRS data (Fig. 2). Tumor spectra are characterized by high (cholin+creatin)/citrate ratios (Fig. 2b).

Measurement Details

- 3D_CSI_SE_prostate_special sequence with spectral lipid and water saturation (MEGA-pulses)*
- endorectal coil
- automatic adjustments
- acquisition time = 10:41 min
- TR = 650 ms, TE = 120 ms, a = 900, vectorsize = 512 samples, acquisition bandwidth = 1250 Hz, nominal voxel size = 4 x 5 x 5 mm, matrix size = 16 x 16 x 16, weighted acquisition
- Sonata, software MR 2002B

Discussion

This case is an example from the IMAPS study (International Multi-Centre Assessment of Prostate MR Spectroscopy) which investigates the capabilities of ¹H CSI to detect prostate carcinoma in vivo. For this case the MRS-examination confirms the existence and spread of the cancerous tissue. Regarding spectral quality this is a borderline case: data quality is just sufficient for the case to be included. Data quality could be improved by adjusting the

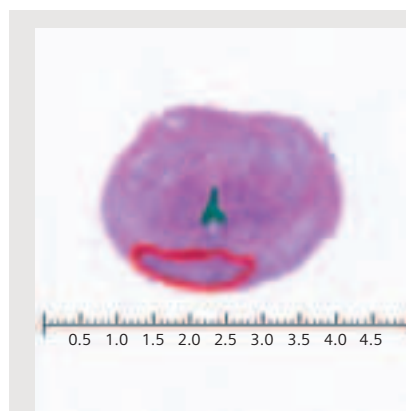


Figure 1 Histopathology result indicated prostate carcinoma. The cancerous region is marked.

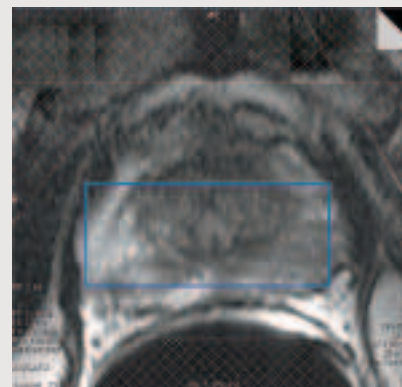


Figure 2 MRS results, which are from the same prostate section as the histopathology slice of Fig. 1.
Figure 2a Axial reference image.

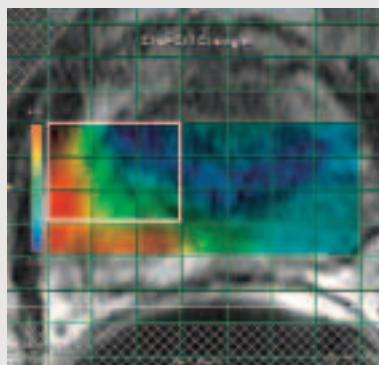


Figure 2b Metabolite map of the ratio (choline+creatine)/citrate. Its expansion is indicated by the blue rectangle in a) Tumor spectra are characterized by high (cholin+creatin)/citrate ratios.

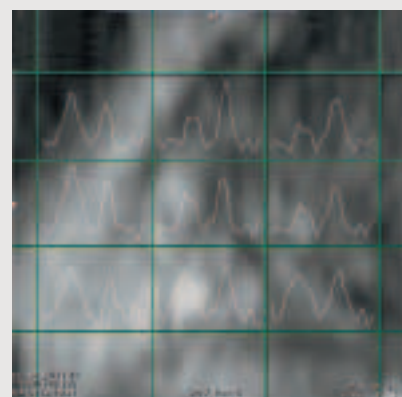


Figure 2c Spectral map, which reflects the alteration of the metabolite composition from suspicious tissue (lower left part with higher choline level) to inconspicuous findings.

saturation slabs more accurately and thereby eliminating lipid contamination.

Courtesy of Dr. Matthias Lichy
Universitätskrankenhaus Tübingen,
Radiologie

* WIP: The information about this product is preliminary. The product is under development and is not commercially available in the US and its future availability cannot be ensured.

Image Findings (Results)

The localization of the tumor-region in the histopathologic examination of the resected prostate (Fig. 1) is reflected in the MRS data (Fig. 2). Tumor spectra are characterized by high (cholin+creatin)/citrate ratios (Fig.2b).

Measurement Details

- 3D_CSI_SE_prostate_special sequence with spectral lipid and water saturation (MEGA-pulses)*
- endorectal coil
- acquisition time = 10:27 min
- TR = 650 ms, TE = 120 ms, $\alpha = 90^\circ$, vectorsize = 512 samples, acquisition bandwidth = 1250 Hz, nominal voxel size = 5 x 5 x 4 mm, matrix size = 16 x 16 x 16, weighted acquisition,
- Sonata, software MR 2002B

Discussion

This case is an example from the IMAPS study (International Multi-Centre Assessment of Prostate MR Spectroscopy) which investigates the capabilities of ^1H CSI to detect prostate carcinoma in vivo. For this case the MRS-examination confirms the existence and spread of the cancerous tissue. As the MRS data is absolutely free from mayor lipid contamination and of excellent spectral resolution, it is an outstanding demonstration of the data quality which is achievable with this technique.

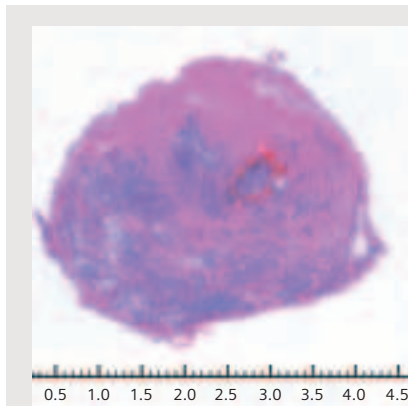


Figure 1 Histopathology result indicated adenocarcinoma of the prostate. The cancerous region is marked.

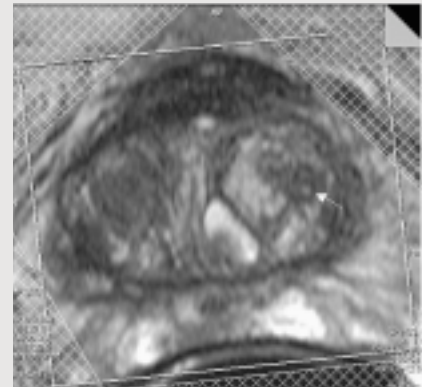


Figure 2 MRS results from the same prostate section as the histopathologic slice of Fig. 1.

Figure 2a T2 weighted axial reference image, which reveals a hypo intense spot in the region of the lesion.

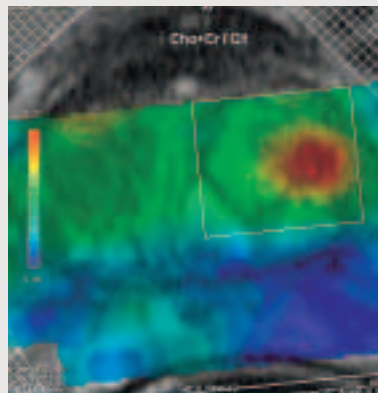


Figure 2b Metabolite map of the ratio (choline+creatine)/citrate. Tumor spectra are characterized by high (cholin+creatin)/citrate ratios.

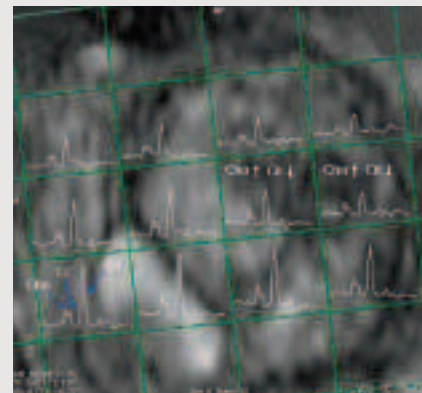


Figure 2c Spectral map, which reflects the alteration of the metabolite composition from suspicious tissue (central right part with higher choline levels and lower citrate levels) to inconspicuous tissue. Its expansion is indicated by the white rectangle in b). (Cit: Citrate, Cho: Choline, Cr: Creatine).

Courtesy of Dr. Matthias Lichy,
Universitätskrankenhaus Tübingen
Radiologie

* WIP: The information about this product is preliminary. The product is under development and is not commercially available in the US and its future availability cannot be ensured.

Case Report: Prostate Carcinoma Stage T3b

Dr. Tom Scheenen

University Medical Centre
Nijmegen
Dept. of Radiology
Nijmegen, The Netherlands

Patient History

Age: 62 years, PSA = 5.9, Biopsy: Gleason 6/10, Suspected stage: T1c. With his stage, PSA and Gleason score the pretest probability of having limited disease (confined to the prostate) is 71%, according to the Partin coefficient tables. Upon personal request, we called this patient, who was under treatment in a different institution, for an MRI/MRSI exam.

Image Findings

We found a large tumor predominantly in the left peripheral zone, minimally extending into the left seminal vesicle (T3b). The tumor shows relatively high choline over citrate ratios (which is a pathologic marker), also centrally around the urethra. There is a smaller limited tumor more close to the apex without extracapsular spread. The tumors show some pathological enhancement. Based upon MRI/MRS findings, the diagnosis is stage T3b.

At the patient's treating institution, the urologist performed a prostate and seminal vesicles resection with intrafacial nerve sparing on the right side and an extra facial nerve sparing on the left side. The pathology of this patient was indeed pT3b. The pathologists found an extra prostatic extension in front of the left and right basis, and the left seminal extension that was detected with MRI/MRS. The margins were negative. The post

operative PSA was 0.1 and the patient had recovered erection. The possibility of recurrence is monitored.

Measurement Details

- 3D_CSI_SE_prostate_special sequence with spectral lipid and water saturation (MEGA-pulses)
- endorectal coil
- automatic adjustments, of which shimming was repeated twice
- acquisition time = 12:40 min
- TR = 650 ms, TE = 120 ms, $\alpha = 90^\circ$, vectorsize = 512 samples, acquisition bandwidth = 1250 Hz, acquisition-weighted k-space sampling with 6 averages in the center of k-space, field of view 70 x 60 x 60 mm, matrix size = 14 x 12 x 12, filtered and zero-filled to 16 x 16 x 16 matrix.

Sonata, software MR 2002B

Discussion

This case is an example from the IMAPS study (International Multi-Centre Assessment of Prostate MR Spectroscopy) which investigates the capabilities of ^1H CSI to detect prostate carcinoma in vivo. Despite the small chance for seminal invasion based on the Partin tables, the combination of MRI and MRSI predicted extension of the tumour into the seminal vesicles, which was confirmed by histopathology of the removed prostate. In this case the MRS-examination confirms the existence and spread of the cancerous tissue, whereas also healthy tissue can be characterized as such.

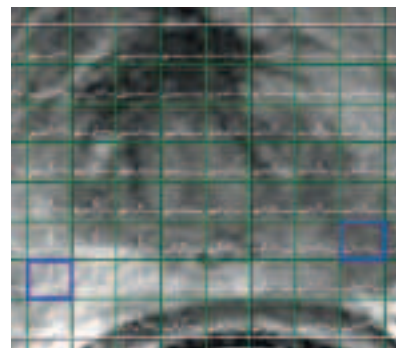


Figure 1a Spectral map (range 1.5 to 4 ppm) from one out of 16 slices from the 3D MRSI dataset, overlaid on an axial T2-weighted image of the prostate of the patient. The voxels indicated in blue are enlarged in Fig. 1b and Fig. 1c.

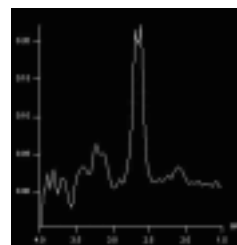


Figure 1b Spectrum from tissue in the healthy peripheral zone of the prostate. The citrate signal is centered at 2.60 ppm, the choline signal at 3.20 ppm overlaps with the creatine signal at 3.04 ppm.

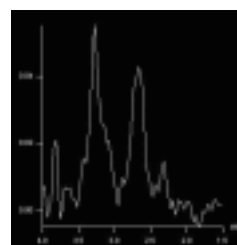


Figure 1c Spectrum from tumour tissue. Notice the relative increase in choline, and decrease in citrate signals.

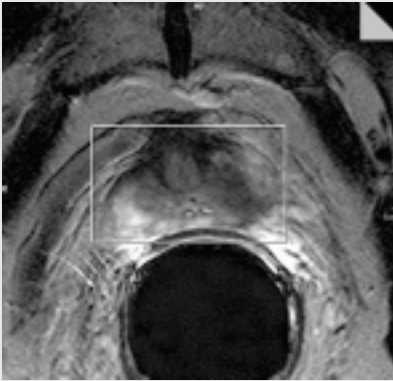


Figure 2a Axial T2-weighted image through the base of the prostate. The white box is the volume of interest, or the PRESS box, of the 3D MRSI measurement.

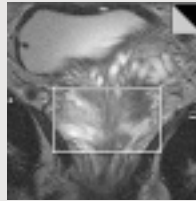


Figure 2b Coronal T2-weighted image of the prostate and surrounding tissues. A hypo-intense lesion extends from the prostate into the left seminal vesicles.

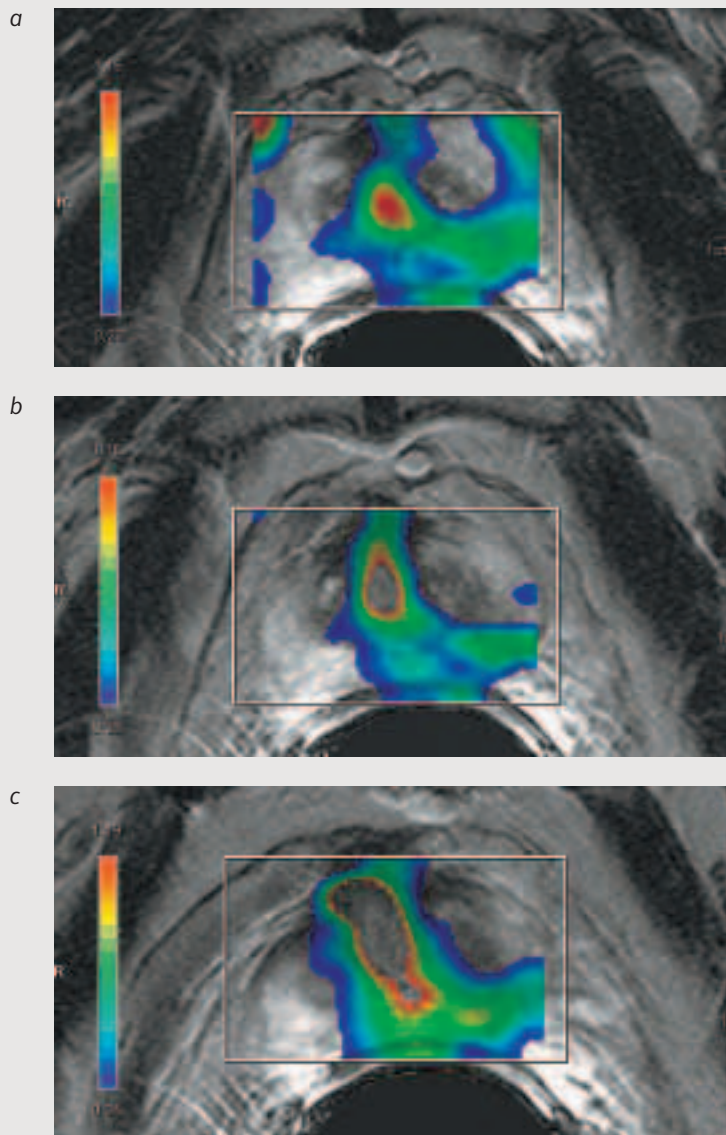


Figure 3a to c Three metabolite ratio images of the base of the prostate, overlaid on adjacent T2-weighted images. Deviating Choline over citrate ratios are detected in the center of the prostate, extending to the left peripheral zone towards the seminal vesicles.

Prostate Carcinoma Detected with Single Voxel Spectroscopy

O. Soellner M.D.¹,
W. Pegios M.D.¹,
Th.J. Vogl M.D.¹,
M. Wolfram M.D.²,
D. Jonas M.D.²

¹ Dept. Diagn. and Intervent.
Radiology,

² Dept. Urology
University Hospital Frankfurt a.M.,
Germany

The patient had a PSA-value of 13.2. The MR exam was carried out after a first biopsy of the prostate showing a negative result. While the left hand side of the prostate appeared normal in the spectrum (Figs. 1a and b), the spectrum of the right hand side showed clearly elevated choline and reduced citrate levels (Figs. 2a and b). The spectral resolution achieved by automatized shimming is excellent. A second biopsy confirmed a trabecular prostate adeno-carcinoma between G2 to G3 (combined Gleason-grade 10).

This is one of our early prostate MRS examinations, carried out at a time when the prostate CSI package was not yet available. While 3D-CSI is the method-of-choice used today, this case still shows that even an SVS exam can lead to clinically relevant results.

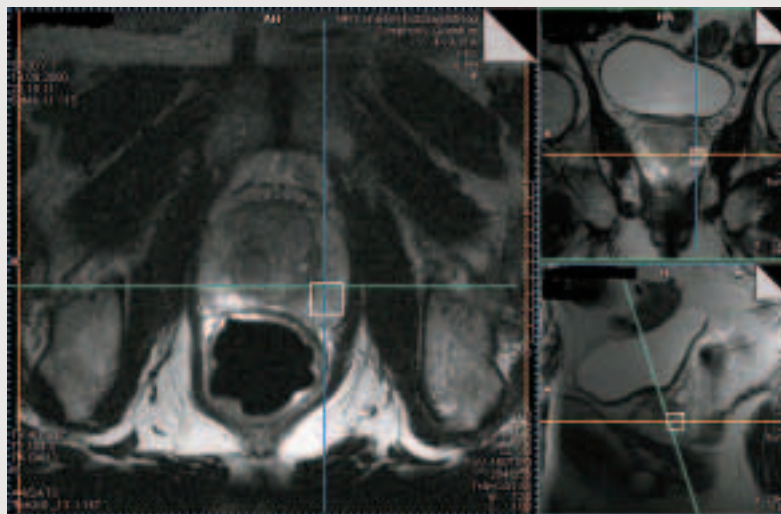


Figure 1a Voxel location of spectrum of healthy tissue.

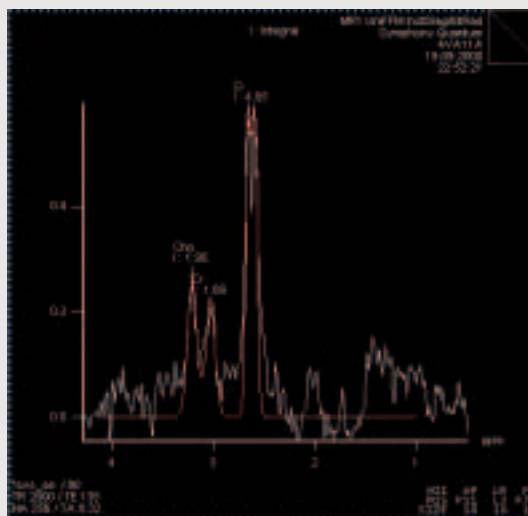


Figure 1b Spectrum of healthy tissue.

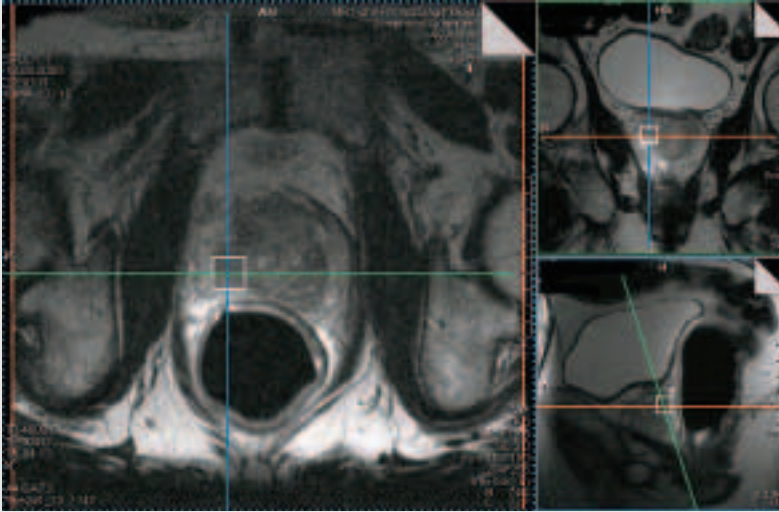


Figure 2a Voxel location of spectrum of suspected carcinoma.

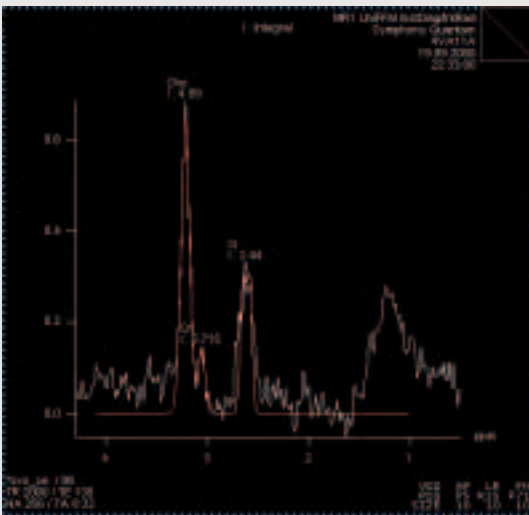


Figure 2b Spectrum of suspected prostate carcinoma.
Elevated choline, reduced citrate.

^1H -MR Spectroscopic Imaging of the Human Prostate: from 1.5 to 3T

Tom W. J. Scheenen, Ph.D.
Jurgen J. Fütterer, M.D.
Jelle O. Barentsz, M.D., Ph.D.
Arend Heerschap, Ph.D.

Department of Radiology,
University Medical Center
Nijmegen, The Netherlands

Proton MR spectroscopic imaging (SI) of the prostate is a challenge: the organ is small, resides in the centre of the male body, is embedded in lipid tissue, and is close to intestines containing air. The use of an endo-rectal surface coil, positioned very close to the prostate, enables an adequate SNR and spatial resolution of the MRSI measurement. Lipid signals are suppressed with a combination of saturation slabs and dual frequency-selective rf pulses in the pulse sequence. Automated shimming algorithms produce acceptable line widths of the water resonance before the actual MRSI measurement starts.

The clinical value of prostate spectroscopy at 1.5T with a dedicated pulse sequence on different Maestro Class scanners is currently being evaluated. Siemens Medical Solutions, together with Medrad Inc. and around ten other participating clinical institutions, have organized an International Multi-centre Assessment of Prostate Spectroscopy (IMAPS) trial, the primary objectives of which are to prove that 3D MRSI of the prostate can detect and localize prostate cancer on the basis of the ratio of the choline signal integral over the citrate signal integral (for more information, please look at the IMAPS home page <http://get.to/IMAPS>).

Since the MR signal of citrate at 1.5 and 3T originates from a strongly coupled spin system, its spectral shape depends on magnetic field strength and PRESS (Point RESolved Spectroscopy) pulse sequence timing. At an echo time of 120 ms at 1.5T, the citrate resonances appear as a singlet; almost all intensity in two largely overlapping peaks around 2.60 ppm and hardly any intensity in the two surrounding satellite peaks. However at 3T, the spectral resolution increases twofold, more clearly revealing the complex shape of the citrate signals that can appear with either positive or negative inner lines and non-zero satellite peaks. After understanding the spectral shape of citrate at 3T, the advantages of moving prostate spectroscopy to 3T can be appreciated. Apart from an increase in spectral resolution, which increases the separation of individual resonances, the SNR of the metabolites also increases, which can be used to either decrease total measurement time or increase spatial resolution.

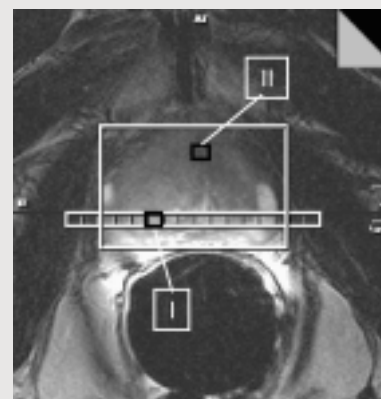


Figure 1a Axial T2 weighted TSE image (TE 132 ms) of the prostate of a patient with prostate cancer at 1.5 T. The white box indicates the PRESS box selection of the 3D MRSI measurement; voxels I and II are the positions of figures 1b and 1c.

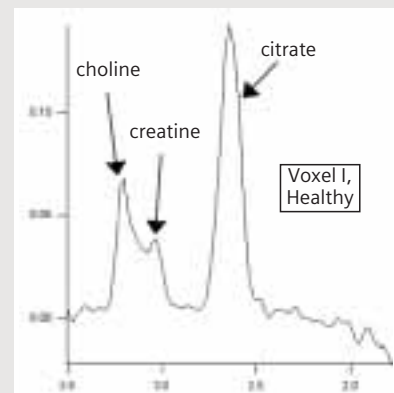


Figure 1b Spectrum of a voxel in healthy tissue of the peripheral zone of the prostate. In the spectral range of 1.8 to 3.5 ppm resonances from citrate, creatine and choline are present. Polyamines could be present between choline and creatine, connecting these resonances with each other.

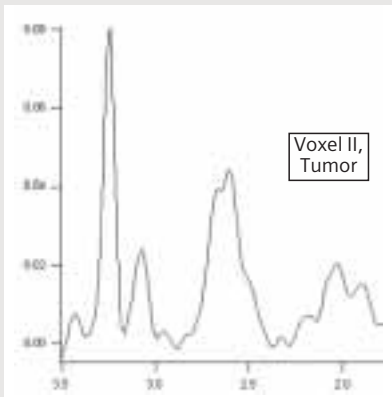


Figure 1c Spectrum of a voxel in possible tumor tissue in the central gland of the prostate. Notice the relative difference in choline and citrate signal intensities: increased choline and decreased citrate, combined in the choline/citrate ratio, are markers for tumor tissue.

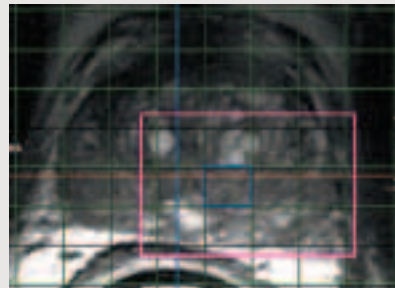


Figure 3a T2 weighted TSE image (TE 109 ms) of a patient with prostate cancer at 3T. MRSI voxels from one out of 16 MRSI slabs from the 3D matrix are overlaid in green. The purple box is enlarged in 3b, the blue voxel is the origin of the spectrum in 3d.

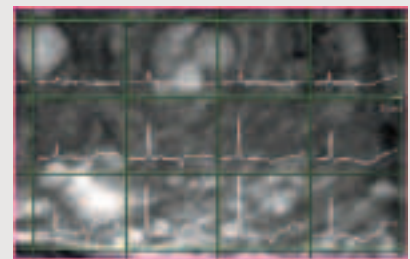


Figure 3b Enlargement from fig. 3a of 12 nominal voxels. For every voxel the corresponding spectrum is shown from 2.0 to 3.5 ppm. The large choline signal intensities compared to citrate are indicative for the presence of tumor tissue.

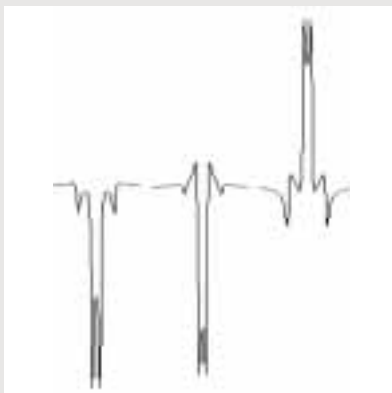


Figure 2 Useful theoretical shapes of the citrate resonance at 3T. The three different spectral shapes correspond to three different PRESS pulse sequence timings: TE of 75, 100 and 145 ms respectively.

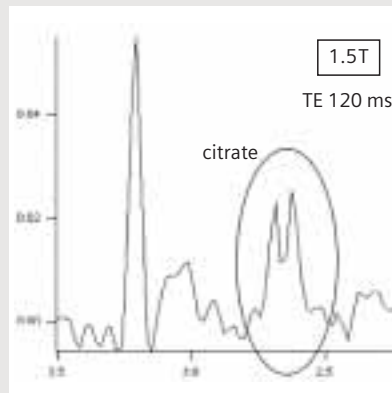


Figure 3c Spectrum from the blue voxel (Fig. 3a) at 1.5T. The line-widths are small enough to see the splitting of the citrate resonance, even at 1.5T.

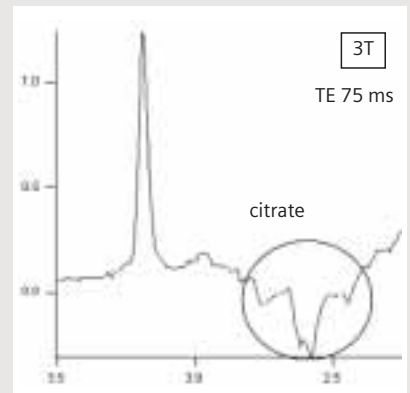


Figure 3d Spectrum from the blue voxel (Fig. 3a) at 3T. Notice the high SNR of this spectrum, and the inversion of the citrate signal at an echo time of 75 ms at 3T.

The Potential of ^1H MRS of the Breast*

Stefan Roell
Marianne Vorbuchner

MRS Application Development
Siemens Medical Solutions
Erlangen, Germany

Today, contrast-enhanced MRI of the breast achieves a high sensitivity for detecting suspicious masses. However, variable specificities have been reported using this technique. MR spectroscopy has the ability to detect metabolic changes in tissue and may provide an added measure of confidence in the characterization of breast lesions. *In vivo* investigations of the phospholipid metabolism by ^{13}C - or ^{31}P -MRS appear to be restricted to cases of advanced cancer, due to the low sensitivity of these methods. The much higher sensitivity of ^1H -MRS allows the detection of smaller carcinoma. Using *in vivo* ^1H MRS, the singlet signal of choline-containing compounds at 3.2 ppm appears to be significant for the detection of carcinoma. Other *in vivo* ^1H signals of breast tissue origin from water and lipid compartments. An additional lactose signal is seen in spectra of lactating breast. Whilst it was previously suspected that choline is only detectable in malignancies, high field studies have now shown that healthy breast tissue also produces a weak signal at 3.2 ppm. Hence, it is necessary to calibrate the detected choline signal. One suggested method involves the use of the unsuppressed water signal as an internal standard, i.e. estimating the concentration of choline in its solvent (water), thereby correcting for the partial volume of adipose tissue. Among the other technical requirements of ^1H breast MRS are an effective suppression of the lipid

signal, and the correction for signal variations induced by breathing. Currently, a WIP SVS Spin-Echo sequence, complemented with additional spectral (lipid) suppression pulses, is used for examining the sensitivity of choline detection in the breast.

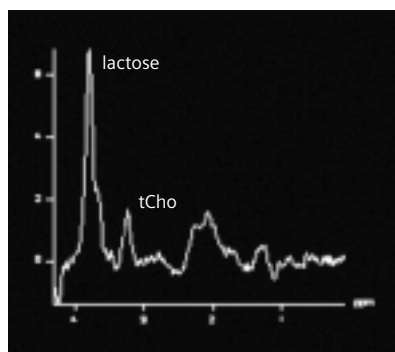


Figure 1 ^1H *in vivo* spectrum of a lactating breast. tCho refers to total choline; MAGNETOM Sonata (1.5T), voxel size 8 cc, acq. time 3 min 12 sec. Courtesy of Dr. B. Joe and Dr. T. Bae, Washington University School of Medicine, St. Louis, MO, USA.

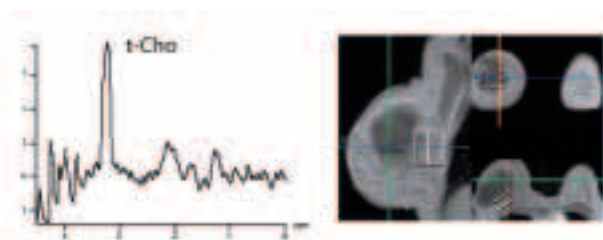


Figure 2 tCho signal detected in ductal carcinoma; MAGNETOM Symphony (1.5T), voxel size 3.4 cc, acq. time 3 min 12 sec. Courtesy of Dr. I. Gribbestad et al., St. Olavs Hospital, Trondheim, Norway.

*WIP: The information about this product is preliminary. The product is under development and is not commercially available in the US and its future availability cannot be ensured.



Siemens
Women's Health

³¹P-MR Spectroscopy of the Heart – Current Status and Future Potential

Stefan Neubauer, M.D. FRCP

University of Oxford Centre
for Clinical Magnetic Resonance
Research
United Kingdom

Introduction

Cardiac magnetic resonance (CMR) imaging (MRI) is an excellent method for obtaining anatomical and functional information on the heart, but offers little insight into the biochemical state of cardiac tissue. In contrast, ³¹P-MR spectroscopy (³¹P-MRS) is the only available method for the non-invasive study of cardiac energy metabolism without need for the application of external radioactive tracers (as required in PET). Non-invasive imaging of cardiac metabolism is a long-standing Cardiologists' dream, and the main reason why ³¹P-MRS has not yet fulfilled its promise in clinical Cardiology is the limited resolution of the method: the MR sensitivity of the ³¹P-nucleus is 6.6% that of ¹H. Even more significantly, in the heart, ³¹P-containing metabolites [(adenosinetriphosphate (ATP), phosphocreatine (PCr), inorganic phosphate (Pi)] are present in concentrations that are several orders of magnitude lower than those of ¹H nuclei of water and fat (1-15 mM vs. 110 M). Thus, the signals we aim to interrogate in ³¹P-MRS are ~6 orders of magnitude weaker than those used in ¹H-MRI.

Cardiac Energetics

³¹P-MRS is suitable for the repeated measurement of cardiac high-energy phosphate metabolism, to non-invasively monitor the energetic state of the heart. ATP is the only

substrate for all energy-consuming reactions in the cell. Phosphocreatine, the other major high-energy phosphate compound, acts as an energy reservoir and has at least two additional roles: First, phosphocreatine serves as an energy transport molecule in the "creatine kinase / phosphocreatine energy shuttle" [1, 2]. The high-energy phosphate bond is transferred from ATP to creatine at the site of ATP production (i.e. the mitochondria), yielding phosphocreatine and ADP. This reaction is catalyzed by the mitochondrial creatine kinase isoenzyme. Phosphocreatine, which is a smaller molecule than ATP, then diffuses through the cytoplasm to the site of ATP utilization, the myofibrils, where the back reaction occurs, ATP is reformed and is used for contraction. This reaction is catalyzed by the myofibrillar-bound MM-creatine kinase isoenzyme. Free creatine then diffuses back to the mitochondria. This "energy shuttle" is required, because the low free cytosolic ADP concentration (40-80 μM) does not provide the necessary capacity for back diffusion to the mitochondria [1, 3], while free creatine is present at concentrations that are at least two orders of magnitude greater. The second crucial cellular function of phosphocreatine and creatine kinase is to maintain free cytosolic ADP at low concentration. When ATP is hydrolysed, inorganic phosphate is formed. Inorganic phosphate increases when ATP utilization exceeds ATP production, for example during ischemia.

Experimental ³¹P-MR Spectroscopy

³¹P-MRS has been a standard method in experimental cardiology since the 1970s [4]. A large body of literature exists on experimental applications of ³¹P-MRS to the heart, and the

principles of ³¹P-MRS are best explained in the experimental setting. The most widely used animal model for ³¹P-MRS is the isolated buffer-perfused rodent heart. MRS is performed using a high field (7-18 Tesla) MR spectrometer. The magnet bore holds the nucleus-specific probe head with the radio frequency (RF) coils, which are used for MR excitation and signal reception. The magnet is interfaced with a control computer, a gradient system, and an RF transmitter and receiver. After shimming the magnetic field, a radio frequency impulse is sent into the RF coils for spin excitation. The resulting MR signal, the free induction decay (FID) is recorded. Using "Fourier transformation", the FID is converted to an MR spectrum, which relates resonance frequency and signal intensity. Due to the low sensitivity of ³¹P-MRS, many FIDs have to be signal-averaged to obtain MR spectra with a sufficient signal-to-noise ratio. MR spectra have to be corrected for the effects of partial saturation.

A typical ³¹P-MR spectrum from an isolated, beating rat heart is shown in Figure 1 (upper left panel). A ³¹P-spectrum shows six resonances, corresponding to the three ³¹P-atoms of ATP, phosphocreatine (PCr), inorganic phosphate (Pi) and monophosphate esters (MPE; mostly AMP and glycolytic intermediates). "Chemical shift" (quantified relative to the B0 field in ppm = parts per million) describes the phenomenon that different metabolites resonate at distinct frequencies, allowing their discrimination from each other. The area under each resonance is proportional to the amount of each ³¹P-nucleus in the sample, and metabolite resonances are therefore quantified by integrating peak areas. Relative metabolite levels are calculated directly (such as the phosphocreatine/ATP ratio), but absolute metabolite

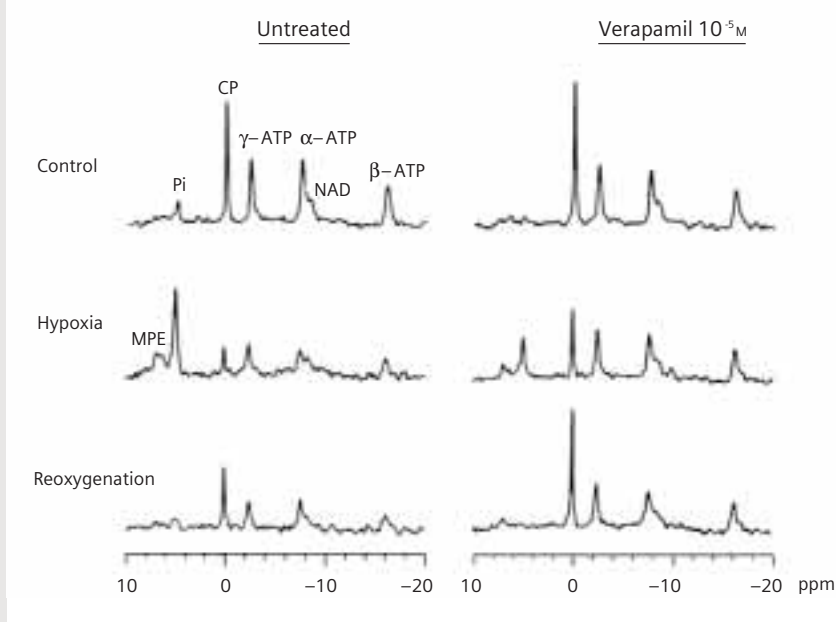


Figure 1 ^{31}P -MR spectra from an untreated perfused rat heart and a heart treated with Verapamil during control, at the end of 30 min. of hypoxia and at the end of 30 min. of reperfusion. NAD = Nicotine adenine dinucleotide. See the depletion of phosphocreatine and ATP during hypoxia, and the recovery of phosphocreatine, but not of ATP, during reoxygenation in the untreated heart. These changes of cardiac energetics are attenuated by the presence of the Ca^{++} antagonist Verapamil. CP or CrP = creatine phosphate, a term synonymous with phosphocreatine.

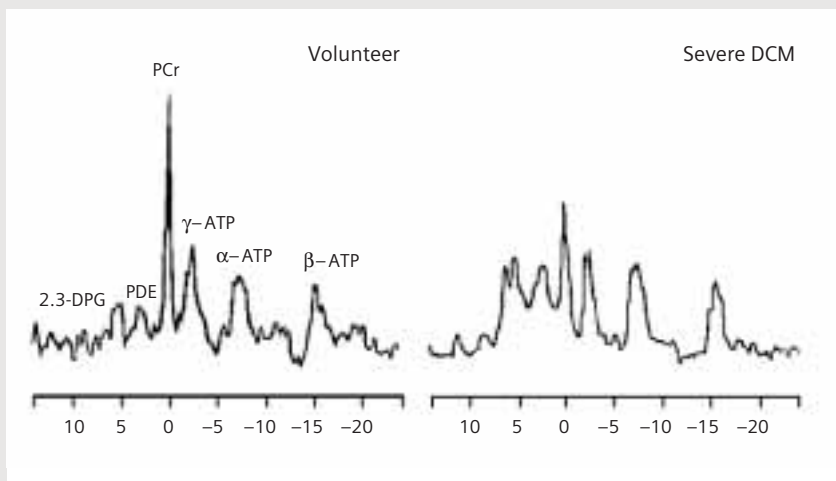


Figure 2 ^{31}P -MR spectrum from the human heart of a volunteer and of a patient with dilated cardiomyopathy. The reduction of the phosphocreatine resonance in the patient is apparent. From Neubauer S et al. *Eur Heart J* 1995;16(Suppl O): 115-118. Reproduced with permission from European Society of Cardiology.

concentrations are evaluated by comparing the tissue ^{31}P -resonance areas to those of an external ^{31}P -reference standard. ^{31}P -MRS also allows the quantification of intracellular pH (pH_i), from the chemical shift difference between phosphocreatine and inorganic phosphate, which is pH-sensitive. Because the method is non-invasive, spectra can be acquired sequentially, and the dynamic response of energy metabolites to ischemia, hypoxia or inotropic stimulation can be followed in one experiment (Fig. 1).

Clinical Cardiac ^{31}P -MRS Studies

Methodological aspects

Clinical cardiac ^{31}P -MR spectroscopy faces major technical challenges: total examination time should not be more than one hour, and the time for signal acquisition is thereby limited. The heart is a rapidly moving organ, requiring gating to the heart beat, and, when resolution is further improved, ultimately to respiration as well [6]. The cardiac muscle lies behind the chest wall skeletal muscle

which by itself creates a strong ^{31}P -signal that requires suppression. This necessitates the use of localization techniques such as DRESS (depth-resolved surface coil spectroscopy), rotating frame, 1D-CSI (chemical shift imaging), ISIS (image-selected in vivo spectroscopy), and 3D-CSI, which are described in detail elsewhere [7]. For most spectroscopic techniques, ^1H scout images are first obtained, which are used to select the spectroscopic volume(s). The low sensitivity of ^{31}P -MRS has required large voxel sizes, typically ~30 ml. A

typical ^{31}P -MR spectrum of a healthy volunteer is shown in Figure 2. Compared to the rat heart spectrum, two additional resonances are detected: 2,3-diphosphoglycerate (2,3-DPG), due to the presence of blood (erythrocytes) in the interrogated voxel, and phosphodiesters (PDE), a signal due to membrane as well as serum phospholipids. The 2,3-diphosphoglycerate resonances overlap with the inorganic phosphate peak, which therefore cannot be detected in blood-contaminated human ^{31}P -MR spectra. For relative quantification of human ^{31}P -spectra, the phosphocreatine/ATP ratio is calculated. Phosphocreatine/ATP is an index of the energetic state of the heart, because any imbalance between oxygen supply and demand will lead to substantial depletion of phosphocreatine before ATP levels start to decline (due to the CK equilibrium constant). For area integration of resonances in human ^{31}P -spectra, a Lorentzian line fitting algorithm is applied.

Absolute quantification of phosphocreatine and ATP is technically demanding, but is clearly a necessity in the long term, as the phosphocreatine/ATP ratio cannot detect simultaneous decreases of both phosphocreatine and ATP that occur, for example, in the failing [8] or in the infarcted myocardium [9]. The most sophisticated method for this is SLOOP ("spectral localisation with optimum pointspread function"), which allows for curved regions of interest and absolute quantification with high accuracy [10]. SLOOP requires use of a ^{31}P reference standard, flip angle calibration, precise B₁ field mapping and determination of myocardial mass in the interrogated voxel (Fig. 3). However, almost all previous clinical ^{31}P -MRS studies have used the phosphocreatine/ATP ratio for quantification.

It has been impossible up to now to interrogate the posterior wall of the human heart due to its distance from the ^{31}P -surface coil. However, Pohmann and von Kienlin [11] have recently implemented acquisition-weighted ^{31}P -chemical shift imaging in volunteers at 2T. Acquisition-weighting significantly reduced the signal contamination between adjacent voxels, and it has been possible to obtain human heart ATP and phosphocreatine images with 16 ml spatial resolution within 30 min. Furthermore, for the first time, ^{31}P -spectra from the posterior wall could be obtained.

In a normal human heart, the phosphocreatine/ATP ratio is ~1.8 [7] although, due to different methods being used, the range of "normal" phosphocreatine/ATP ratios reported in the literature is considerable, from about 1.1 to 2.4.

Ischemic Heart Disease

There are, in principle, two applications of ^{31}P -MRS in ischemic heart disease:

"Biochemical Ergometry" for Detection of Exercise-Induced Ischemia.

A decrease of phosphocreatine and an increase of inorganic phosphate are amongst the very earliest metabolic responses in myocardial ischemia. Thus, a "biochemical stress test", able to measure these metabolites in human myocardium with high temporal and spatial resolution, would allow detection of the regional biochemical consequences of myocardial ischemia at rest, during exercise and recovery. The principal feasibility of this approach has been demonstrated: Weiss et al. showed that in patients with high grade LAD stenosis, phosphocreatine/ATP ratios were normal at rest; phosphocreatine/ATP decreased during hand grip exercise from 1.5 ± 0.3 to 0.9 ± 0.2 , and returned towards normal during

recovery [12]. After revascularization, phosphocreatine/ATP ratios no longer changed with exercise. If high spatial (1-5 ml) and temporal (stress duration <15 min.) resolution for this approach could be achieved, then this method might well find its way into routine cardiology. A ^{31}P -MRS stress test would, for example, allow the non-invasive study of the efficiency of revascularization procedures or of various anti-anginal therapies. Pohost's group [13] recently reported on the pathophysiologic mechanisms of exercise-induced chest pain in women with normal coronary arteries: in 7/35 women with chest pain and normal coronary arteries, the phosphocreatine/ATP ratio decreased by $29 \pm 5\%$ during hand grip exercise. These findings provide direct evidence of exercise-induced myocardial ischemia in women with chest pain and normal coronary arteries.

Assessment of Myocardial Viability.

Both biochemical [14] and ^{31}P -MRS measurements [15, 16] (Fig. 4) in animal models have shown that myocardial scar tissue contains negligible amounts of ATP (<1% of normal levels), while in stunned and hibernating [17] myocardium, ATP levels remain close to normal. Therefore, a non-invasive method that allows measurement of myocardial ATP levels with high spatial (1-5 ml) and acceptable temporal resolution (<30 min.) should be quite suitable for evaluation of myocardial viability. Only a few clinical studies have previously addressed this issue [18, 19]. For example, Kalil-Filho et al. studied 29 patients with anterior infarction 4 and 39 days after MI. All patients showed akinetic anterior myocardium, which had recovered function at the time of the second examination. Phosphocreatine/ATP ratios were normal in stunned myocardium (1.51 ± 0.17 vs. 1.61

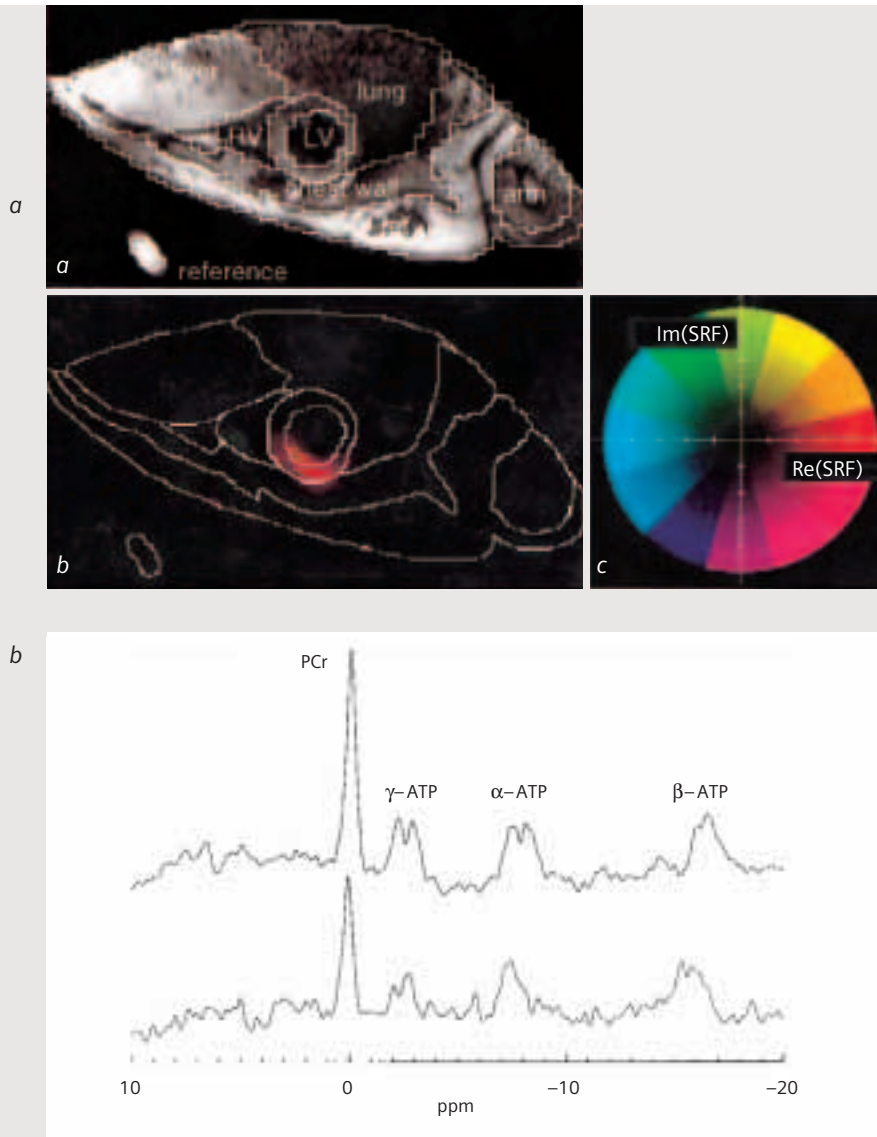


Figure 3 SLOOP MR spectroscopy. a) B_1 -corrected proton short-axis image of the heart as used for segmentation. A threshold filter was applied to cut off the noise in the image regions distant from the coil. After segmentation, the matrix size was reduced to limit computational burden. The contours of this compartment map with decreased resolution are overlaid. b: For the same slice the spatial response function (SRF) of the left ventricular myocardium is overlaid with the original compartment borders. c: The color encoding scheme for the complex value of the SRF. b) ^{31}P -spectra from the left ventricular wall, obtained from SLOOP reconstruction of 3D-CSI datasets, acquired with NOE (top), and without (bottom), and calculated with T1 and the off-resonance effect of PCr. These spectra were reconstructed from the localized time domain signals using zero-filling to 2048 data points and an exponential filter with a line-broadening of 7 Hz prior to fast Fourier transform.

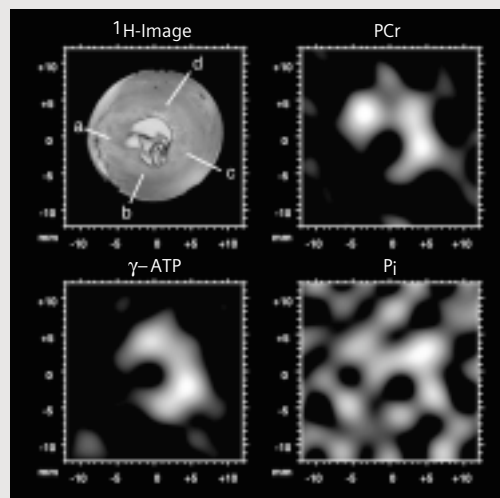


Figure 4 Central slices of a 3D- ^{31}P -chemical shift imaging experiment in an isolated, chronically infarcted rat heart. 12 Tesla, nominal voxel size 54 μl . On the ^1H image (upper left), the infarcted area in the anterior wall (a) appears just barely brighter than the unaffected myocardium. In ^{31}P -images, however, the infarcted area can be identified due to the complete absence of phosphocreatine (PCr; upper right) and of γ -ATP (lower left). Inorganic phosphate cannot be detected due to its low concentration (lower right).

+/- 0.18 in volunteers) and did not change during the recovery of contractile function (1.51 ± 0.17 vs. 1.53 ± 0.17). However, loss of myocardial tissue, such as following a non-viable infarct leading to necrosis and scar formation, primarily leads to a reduction of both phosphocreatine and ATP, and detection of this requires measurement of absolute concentrations of high-energy phosphates. Feasibility for this approach was shown by Yabe et al. [9]: absolute myocardial ATP content was significantly reduced in patients with fixed thallium defects (non-viable) but was unchanged in patients with reversible defects (viable myocardium). While these initial results are promising, technical advances are required to achieve the necessary resolution to make ^{31}P -MRS evaluation of viability clinically practicable.

Hypertension

Very few studies have examined patients with left ventricular hypertrophy due to chronic hypertension. Lamb et al. demonstrated reduced phosphocreatine/ATP ratios in patients with hypertension both at rest and during dobutamine-stress testing [20]. Furthermore, phosphocreatine/ATP ratios correlated inversely with indices of diastolic function (E deceleration peak). In contrast, another study showed no significant changes of cardiac energetics in hypertension [21]. It is likely that differences in patient characteristics, such as severity and duration of hypertension, are responsible for this discrepancy, since experimental data clearly suggest that cardiac energetics are impaired in longstanding hypertension [22]. In advanced hypertensive heart disease, ^{31}P -MRS should allow the energetic correlates of hypertrophy regression during various forms of antihypertensive therapy to be followed.

Heart Failure

Experimental studies have universally shown reduced phosphocreatine levels in chronically failing myocardium (e.g. [14, 23]). Hardy et al. first demonstrated that the myocardial phosphocreatine/ATP ratio is significantly reduced (from 1.80 ± 0.06 to 1.46 ± 0.07) in symptomatic patients with heart failure of ischemic or non-ischemic origin [24]. We reported that the decrease of phosphocreatine/ATP ratios in dilated cardiomyopathy correlated with the clinical severity of heart failure, according to the New York Heart Association (NYHA) class [25] and also with left ventricular ejection fraction [26]. Thus, phosphocreatine/ATP ratios decrease for the more symptomatic stages of heart failure. However, in heart failure, both phosphocreatine and ATP levels decrease in parallel [8], and this cannot be detected by measurement of phosphocreatine/ATP ratios. Using the SLOOP technique for absolute quantification, we have recently studied patients with heart failure due to dilated cardiomyopathy (ejection fraction 18%), and found that absolute phosphocreatine levels were reduced by 51%, ATP levels by 35%, while the phosphocreatine/ATP ratio decreased by 25% only [21] (Fig. 5). Thus, the true extent of changes in energy metabolism in heart failure is underestimated when phosphocreatine/ATP ratios are measured rather than absolute concentrations. Therefore, measurement of absolute concentrations of high-energy phosphates should become the standard approach for human ^{31}P -MRS studies in heart failure as well as for other cardiac pathologies.

The energy-deprivation hypothesis in heart failure has recently gained fresh support, since an analysis of heart failure trials from the past decade shows that any treatment that is

energy-costly, such as beta-receptor mimetic or phosphodiesterase inhibitor drugs, while increasing cardiac output in the short term, has ultimately increased mortality, while any treatment that is energy-sparing, such as betablockers, ACE-inhibitors, or Angiotensin-II-receptor blockers, has improved survival in long-term studies. For clinical heart failure trials, it would thus be highly attractive to monitor the early energetic response of the myocardium to new classes of agents for the treatment of heart failure, and it is conceivable that the phosphocreatine/ATP ratio or absolute concentrations of phosphocreatine and ATP may be powerful surrogate parameters for mortality in heart failure trials. Our initial observation was that in 6 patients with dilated cardiomyopathy treated with standard medical therapy including ACE inhibitors, digitalis, diuretics and, in 4 patients, beta-blockers, clinical recompensation occurred over 3 months. Over this time, the phosphocreatine/ATP ratio of the patients improved significantly from 1.51 ± 0.32 to 2.15 ± 0.27 [25]. Apart from this early anecdotal evidence, no systematic study has been published so far using ^{31}P -MRS to monitor cardiac energetics during heart failure treatment and such trials are eagerly awaited.

In line with the concept that energy-sparing forms of therapy improve prognosis in heart failure, is our observation that phosphocreatine/ATP ratios hold prognostic information on survival of patients with heart failure that extends beyond the prognostic relevance of clinical and hemodynamic variables. We showed that in dilated cardiomyopathy, the myocardial phosphocreatine/ATP ratio was a better predictor of long-term survival than left ventricular ejection fraction or New York Heart Association (NYHA) class [27] (Fig. 6).

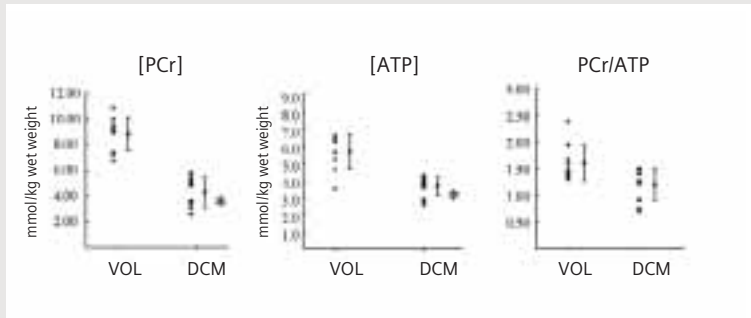


Figure 5 Absolute and relative concentrations of phosphocreatine (PCr) and adenosine triphosphate (ATP) in volunteers (VOL) and in patients with dilated cardiomyopathy (DCM). Individual as well as mean \pm SD values are shown for each group. PCr: VOL vs. DCM $p < 0.000001$; ATP: VOL vs. DCM $p < 0.0003$; PCr/ATP ratio: VOL vs. DCM $p = 0.06$. Reproduced with permission from *Journal of the American College of Cardiology*.

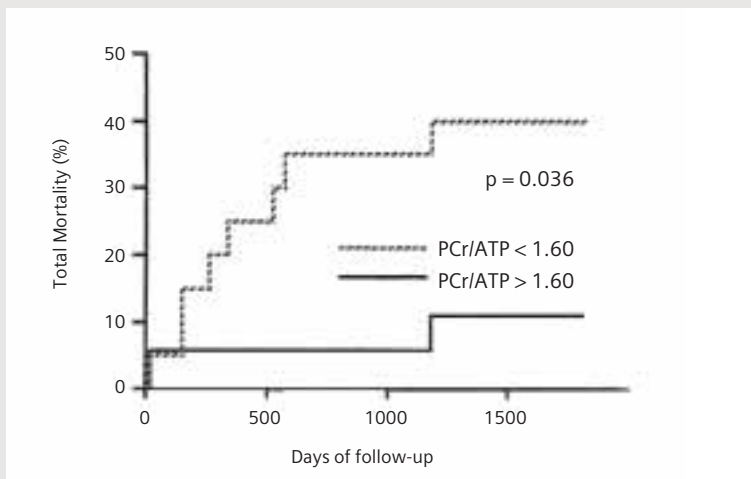


Figure 6 Kaplan-Meier life table analysis for total mortality of dilated cardiomyopathy patients divided into two groups split by the myocardial phosphocreatine/ATP ratio (<1.60 vs. >1.60). Patients with an initially low PCr/ATP ratio showed increased mortality over the study period of, on average, 2.5 years.

Thus, ^{31}P -MRS may become a tool for prognosis evaluation in heart failure.

Diabetic Cardiomyopathy

Most recently, ^{31}P -MRS has been applied to the study of the unique metabolic alterations present in diabetic cardiomyopathy, which develops on the basis of combined hyperglycaemia and increased plasma free fatty acids. Whereas cardiac glucose uptake is reduced due to insulin resistance, uptake of free fatty acids and their β -oxidation within the mitochondrion is increased. This further inhibits glucose uptake, glycolytic ATP synthesis and the generation of glucose derived Acetyl-CoA. Additionally, β -oxidation of free fatty acids increases the expression of uncoupling proteins, which shunt protons away from the respiratory (electron transport) chain, leading to reduced ATP generation. Scheuermann-Freestone et al. reported recently that myocardial phosphocreatine/ATP ratios are substantially reduced in patients with type II diabetes in the presence of maintained left ventricular function [28], and that phosphocreatine/ATP ratios correlate with acute plasma levels of free fatty acids and glucose (Fig. 7). Diamant et al [29] confirmed these findings and also demonstrated the phosphocreatine/ATP ratios correlated with indices of diastolic function. Metzler's group [30] demonstrated similar reductions of phosphocreatine/ATP ratios in otherwise normal type I diabetics. Together, these findings suggest that altered cardiac energetics contribute to the development of diabetic cardiomyopathy.

Genetic Heart Disease

One of the most promising areas for clinical cardiac ^{31}P -MRS is the non-invasive phenotyping of cardiomyopathies due to specific gene defects. While it is still early days, it is conceiv-

able that specific gene defects may eventually be identifiable by a specific metabolic profile, as detected non-invasively by MRS. Most work in this area has so far concentrated on hypertrophic cardiomyopathy (HCM). The Watkins group has recently proposed a new energy depletion paradigm as the one unifying pathophysiological mechanism underlying HCM due to various gene mutations [31]. Human studies in HCM have shown reduced phosphocreatine/ATP ratios in myocardial tissue affected by hypertrophy. Jung et al. [32] demonstrated that young, asymptomatic patients with HCM show a significantly reduced phosphocreatine/ATP ratio, indicating that energetic imbalance occurs at an early stage of the disease process. Crilley et al. showed reduced phosphocreatine/ATP ratios in patients with three different mutations causing HCM [33]. Importantly, the phosphocreatine/ATP ratio was reduced whether hypertrophy was present or not, suggesting that hypertrophy is not per se the primary mechanism reducing phosphocreatine/ATP ratios in HCM. In the future, large patient cohorts with HCM and identified specific gene defects will have to be studied to test the hypothesis that metabolic phenotyping using ^{31}P -MRS can non-invasively predict specific genetic mutations in individual HCM patients.

Summary and Future Perspective

^{31}P -MR spectroscopy is a fascinating technique, allowing insight into cardiac energy metabolism in normal and diseased heart. The main obstacles for routine implementation of cardiac ^{31}P -MRS are its technical complexity and limited resolution. Thus, a major technological effort is required to improve spatial and temporal resolu-

tion. This will include advances in coil and sequence design, and implementation of MRS at higher field strength [34, 35]. In addition, high signal/noise spectra need to be acquired so that measurement variability is reduced, and standardized acquisition and quantification protocols will have to be developed, so that the method produces measurements that are robust and universally accepted. If these development

Figure 7 a) Typical cardiac ^{31}P -MR spectra from a normal control (upper spectrum) and a patient with type 2 diabetes (lower spectrum), showing lower PCr/ATP ratio in the patient. 2,3-DGP indicates 2,3-diphosphoglycerate; PDE, phosphodiester; PCr, phosphocreatine; α , β , and γ indicate the three phosphate groups of ATP. b) Cardiac PCr/ATP ratios correlated negatively with the plasma free fatty acid (FFA) concentrations ($r^2 = 0.32$, $P = 0.01$) for all subjects and correlated positively with the plasma glucose concentrations ($r^2 = 0.55$, $P = 0.05$) for the patients with type 2 diabetes, but there was no correlation for control subjects.

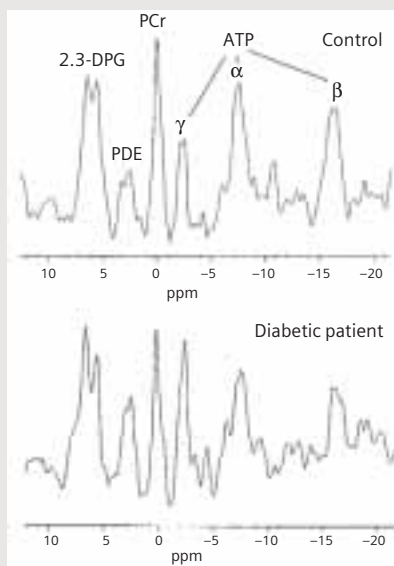


Figure 7a

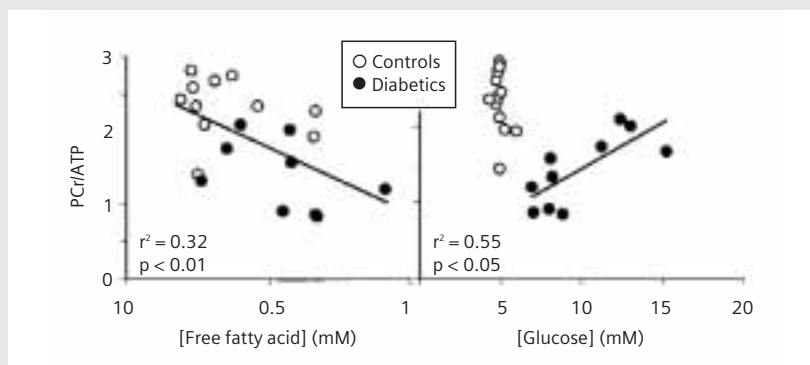


Figure 7b

goals can be achieved, high resolution metabolic imaging of the heart may become part of standard diagnostic pathways in Cardiology.

References

- [1] Wallimann T, Wyss M, Brdiczka D, Nicolay K, Eppenberger HM. Intracellular compartmentation, structure and function of creatine kinase isoenzymes in tissues with high and fluctuating energy demands: The 'phosphocreatine circuit' for cellular energy homeostasis. *Biophys J*. 1992; 281:21-40.

- [2] Ingwall JS, Kramer MF, Fifer MA, Lorell BH, Shemin R, Grossman W, Allen PD. The creatine kinase system in normal and diseased human myocardium. *N Engl J Med*. 1985; 313:1050-4.
- [3] Jacobus WE. Respiratory control and the integration of heart high-energy phosphate metabolism by mitochondrial creatine kinase. *Annu Rev Physiol*. 1985; 47:707-25.
- [4] Garlick PB, Radda GK, Seeley PJ. Phosphorus NMR studies on perfused heart. *Biochem Biophys Res Commun*. 1977; 74:1256-62.
- [5] Neubauer S. Cardiac magnetic resonance spectroscopy: potential clinical applications. *Herz*. 2000; 25:452-60.
- [6] Kozerke S, Schar M, Lamb HJ, Boesiger P. Volume tracking cardiac 31P spectroscopy. *Magn Reson Med*. 2002; 48:380-4.
- [7] Bottomley PA. MR spectroscopy of the human heart: the status and the challenges. *Radiology*. 1994; 191:593-612.
- [8] Shen W, Asai K, Uechi M, Mathier MA, Shannon RP, Vatner SF, Ingwall JS. Progressive loss of myocardial ATP due to a loss of total purines during the development of heart failure in dogs: a compensatory role for the parallel loss of creatine. *Circulation*. 1999; 100:2113-8.
- [9] Yabe T, Mitsunami K, Inubushi T, Kinoshita M. Quantitative measurements of cardiac phosphorus metabolites in coronary artery disease by 31P magnetic resonance spectroscopy [see comments]. *Circulation*. 1995; 92:15-23.
- [10] Meininger M, Landschutz W, Beer M, Seyfarth T, Horn M, Pabst T, Haase A, Hahn D, Neubauer S, von Kienlin M. Concentrations of human cardiac phosphorus metabolites determined by SLOOP 31P NMR spectroscopy. *Magn Reson Med*. 1999; 41:657-63.
- [11] Pohmann R, von Kienlin M. Accurate phosphorus metabolite images of the human heart by 3D acquisition-weighted CSI. *Magn Reson Med*. 2001; 45:817-26.
- [12] Weiss RG, Bottomley PA, Hardy CJ, Gerstenblith G. Regional myocardial metabolism of high-energy phosphates during isometric exercise in patients with coronary artery disease [see comments]. *N Engl J Med*. 1990; 323:1593-600.
- [13] Buchthal SD, den Hollander JA, Merz CN, Rogers WJ, Pepine CJ, Reichel N, Sharaf BL, Reis S, Kelsey SF, Pohost GM. Abnormal myocardial phosphorus-31 nuclear magnetic resonance spectroscopy in women with chest pain but normal coronary angiograms. *N Engl J Med*. 2000; 342:829-35.
- [14] Neubauer S, Horn M, Naumann A, Tian R, Hu K, Laser M, Friedrich J, Gaudron P, Schnackerz K, Ingwall JS, et al. Impairment of energy metabolism in intact residual myocardium of rat hearts with chronic myocardial infarction. *J Clin Invest*. 1995; 95:1092-100.
- [15] Friedrich J, Apstein CS, Ingwall JS. 31P nuclear magnetic resonance spectroscopic imaging of regions of remodeled myocardium in the infarcted rat heart. *Circulation*. 1995; 92:3527-38.
- [16] von Kienlin M, Rosch C, Le Fur Y, Behr W, Roder F, Haase A, Horn M, Illing B, Hu K, Ertl G, Neubauer S. Three-dimensional 31P magnetic resonance spectroscopic imaging of regional high-energy phosphate metabolism in injured rat heart. *Magn Reson Med*. 1998; 39:731-41.
- [17] Flameng W, Vanhaecke J, Van Belle H, Borgers M, De Beer L, Minten J. Relation between coronary artery stenosis and myocardial purine metabolism, histology and regional function in humans. *J Am Coll Cardiol*. 1987; 9:1235-1242.
- [18] Kalil-Filho R, de Albuquerque CP, Weiss RG, Mocelim A, Bellotti G, Cerri G, Pileggi F. Normal high-energy phosphate ratios in stunned human myocardium. *J Am Coll Cardiol*. 1997; 30:1228-1232.
- [19] Beer M, Sandstede J, Landschutz W, Viehrig M, Harre K, Horn M, Meininger M, Pabst T, Kenn W, Haase A, von Kienlin M, Neubauer S, Hahn D. Altered energy metabolism after myocardial infarction assessed by 31P-MR-spectroscopy in humans. *Eur Radiol*. 2000; 10:1323-8.
- [20] Lamb HJ, Beyerbach HP, van der Laarse A, Stoel BC, Doornbos J, van der Wall EE, de Roos A. Diastolic Dysfunction in Hypertensive Heart Disease Is Associated With Altered Myocardial Metabolism. *Circulation*. 1999; 99:2261-2267.
- [21] Beer M, Sandstede J, Landschutz W, Seyfarth T, Lipke C, Köstler H, Pabst T, Kenn W, Meininger M, von Kienlin M, Horn M, Harre K, Hahn D, Neubauer S. Absolute concentrations of myocardial high-energy phosphate metabolites in normal, hypertrophied and failing human myocardium, measured non-invasively with 31P-SLOOP-magnetic resonance spectroscopy. *J Am Coll Cardiol*. 2002; 40:1267-74.
- [22] Perings SM, Schulze K, Decking U, Kelm M, Strauer BE. Age-related decline of PCr/ATP-ratio in progressively hypertrophied hearts of spontaneously hypertensive rats. *Heart Vessels*. 2000; 15:197-202.
- [23] Nascimben L, Friedrich J, Liao R, Pauletto P, Pessina AC, Ingwall JS. Enalapril treatment increases cardiac performance and energy reserve via the creatine kinase reaction in myocardium of Syrian myopathic hamsters with advanced heart failure. *Circulation*. 1995; 91:1824-33.
- [24] Hardy CJ, Weiss RG, Bottomley PA, Gerstenblith G. Altered myocardial high-energy phosphate metabolites in patients with dilated cardiomyopathy. *Am Heart J*. 1991; 122:795-801.
- [25] Neubauer S, Krahe T, Schindler R, Horn M, Hillenbrand H, Entzeroth C, Mader H, Kromer EP, Riegger GA, Lackner K, Ertl G. 31P magnetic resonance spectroscopy in dilated cardiomyopathy and coronary artery disease. Altered cardiac high-energy phosphate metabolism in heart failure. *Circulation*. 1992; 86:1810-8.
- [26] Neubauer S, Horn M, Pabst T, Gödde M, Lübke D, Illing B, Hahn D, Ertl G. Contributions of 31P-magnetic resonance spectroscopy to the understanding of dilated heart muscle disease. *Eur Heart J*. 1995; 16 (Suppl O):115-118.
- [27] Neubauer S, Horn M, Cramer M, Harre K, Newell JB, Peters W, Pabst T, Ertl G, Hahn D, Ingwall JS, Kochsiek K. Myocardial phospho-creatine-to-ATP ratio is a predictor of mortality in patients with dilated cardiomyopathy. *Circulation*. 1997; 96:2190-6.
- [28] Scheuermann-Freestone M, Madsen PL, Manners D, Blamire AM, Buckingham RE, Styles P, Radda GK, Neubauer S, Clarke K. Abnormal cardiac and skeletal muscle energy metabolism in patients with type 2 diabetes. *Circulation*. 2003; 107:3040-6.
- [29] Diamant M, Lamb HJ, Groeneveld Y, et al. Diastolic dysfunction is associated with altered myocardial metabolism in asymptomatic normotensive patients with well-controlled type II diabetes mellitus. *J Am Coll Cardiol*. 2003; 42:328-35.
- [30] Metzler B, Schöckel MF, Steinboeck P, Wolf C, Judmaier W, Lechleitner M, Lukas P, Pachinger O. Decreased high-energy phosphate ratios in the myocardium of men with diabetes mellitus type I. *J Cardiovasc Magn Reson*. 2002; 4:493-502.
- [31] Ashrafian H, Redwood C, Blair E, Watkins H. Hypertrophic cardiomyopathy: a paradigm for myocardial energy depletion. *Trends Genet*. 2003; 19:263-8.
- [32] Jung WJ, Sieverding L, Breuer J, Hoess T, Widmaier S, Schmidt O, Bunse M, van Erckelens F, Apitz J, Lutz O, Dietze GJ. 31P NMR spectroscopy detects metabolic abnormalities in asymptomatic patients with hypertrophic cardiomyopathy. *Circulation*. 1998; 97:2536-2542.
- [33] Crilly JG, Boehm EA, Blair E, Rajagopalan B, Blamire AM, Styles P, McKenna WJ, Ostman-Smith I, Clarke K, Watkins H. Hypertrophic cardiomyopathy due to sarcomeric gene mutations is characterized by impaired energy metabolism irrespective of the degree of hypertrophy. *J Am Coll Cardiol*. 2003; 41:1776-82.
- [34] Lee RF, Giaquinto R, Constantinides C, Souza S, Weiss RG, Bottomley PA. A broadband phased-array system for direct phosphorus and sodium metabolic MRI on a clinical scanner. *Magn Reson Med*. 2000; 43:269-77.
- [35] Hetherington HP, Luney DJ, Vaughan JT, Pan JW, Ponder SL, Tschendel O, Twieg DB, Pohost GM. 3D 31P spectroscopic imaging of the human heart at 4.1 T. *Magn Reson Med*. 1995; 33:427-31.

³¹P-Chemical Shift Imaging for Myocardial Infarction

Frank Kober Ph.D.
J. Quilici, E. Guedj, T. Caus,
J.L. Bonnet, P.J. Cozzone, M. Bernard

Centre d'Exploration Métabolique
par Résonance Magnétique
(CEREM)
Marseilles, France

Introduction

Phosphorus-31 magnetic resonance spectroscopy (³¹P-MRS) gives non-invasive access to the concentrations of high-energy phosphates (HEP). The ratio of the concentrations of ATP and phosphocreatine (PCr) is a well-established marker of cardiac and muscular ischemia. In the future, ³¹P-MRS could complement the set of parameters measured by other techniques in order to improve the regional characterization of myocardial tissue. In particular, it could contribute to an early prediction of functional recovery after surgical intervention in myocardial infarction.

Clinical Method Description

3D ³¹P chemical shift imaging (CSI) provides spatially localized information of the entire heart in one single exam, allowing the selection of regions of interest for spectral evaluation after completion of the exam. In the past, the localization quality of CSI techniques was substantially affected by contamination of the spectra from surrounding tissue (skeletal muscle, liver) and blood, making human studies difficult and prone to errors. Acquisition-weighted CSI helps to partly overcome the problem of spectral contamination and therefore to increase the sensitivity of the experiment. Moreover, 3D-CSI enables the concentration of HEP metabolites to be mapped spatially. We present the PCr metabo-

lite images and spectra of a patient with anterior wall infarction. All MR experiments were conducted on a Siemens Vision Plus system operating at 1.5T.

Spectra and Images

The figure shows a short-axis proton turbo-FLASH image and a spatially corresponding PCr image of a patient (70 years, 84 kg) with apical anterior wall infarction (small antero-apical necrosis) after LAD occlusion. Spectra taken from two different regions in the myocardium are shown. The patient has an akinetic anterior wall. The shape drawn in red and purple represents the voxel contours at 64 and 33 percent maximum of the point spread function at the location where the spectra were obtained and that enables an estimate to be made of the localization quality. The presented image slice is located in the middle part of the left ventricle that does not contain necrotic tissue. The spectra, however, show a visibly lower PCr/ATP ratio in the anterior wall than in the inferior wall, indicating metabolic alteration in viable tissue adjacent to the necrosis. The PCr image demonstrates the localization quality achieved with acquisition-weighted 3D-CSI.

Sequence Details

CEREM-developed implementation derived from factory ³¹P 3D-CSI sequence.

3D Hanning acquisition-weighted ³¹P chemical shift imaging with pulsed NOE.

2228 phase encoding steps acquired in radial order, four accumulations in the center of k-space.

FOV: 240x240x200 mm³.

Spatial resolution:
2.1x2.1x3.0 cm³ = 13 ml.

ECG-gating, total exam time:
around 45 minutes with positioning and acquisition of proton reference images.

Post-processing: institute-developed 3D-CSI software.

Date and Location of Scan:
04-22-2002 CEREM Marseilles, France.

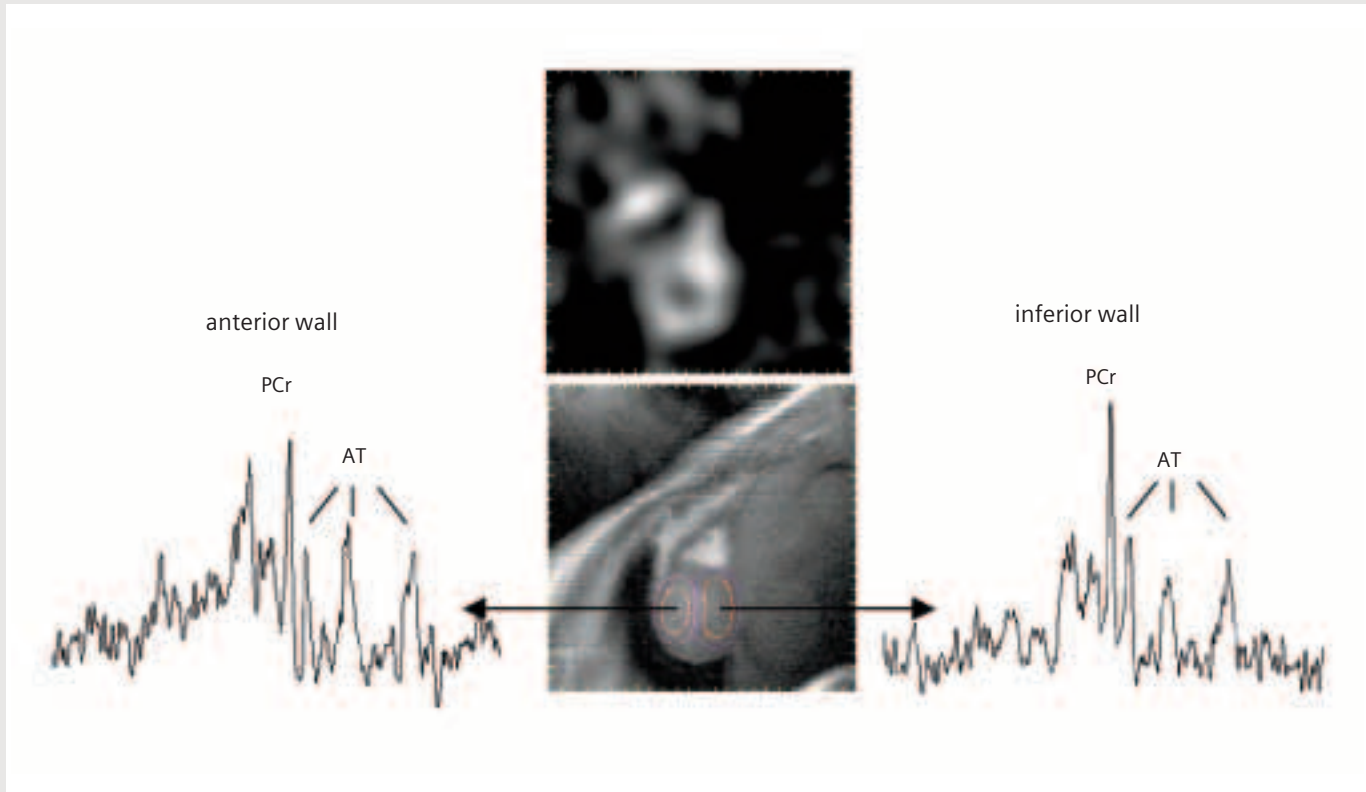
Scanner Model: MAGNETOM Vision Plus at 1.5T with broadband option.

Coil used: Siemens ³¹P-heart/liver surface coil.

Software Version:
Numaris 3.5 VB 33.

Discussion

3D acquisition-weighted CSI has enabled the acquisition of regional spectra with good localization quality – here demonstrated by a PCr metabolic image. The spectra show metabolic differences between different locations around the necrotic area in the apex. CSI here gives non-invasive and direct access to metabolism. The spatial resolution achieved in the metabolic map is low compared with conventional MRI, but close to routinely practised SPECT image resolutions. Metabolic mapping of HEP might enable localization of jeopardized tissue and help in the decision whether or not to revascularize in case of severe coronary stenosis.



Functional investigation of exercising muscle: A non-invasive Magnetic Resonance Spectroscopy – Magnetic Resonance Imaging approach

David BENDAHAN, M.D.,
Benoît GIANNESINI, M.D.,
Patrick J. COZZONE, Ph.D.

Centre de Résonance Magnétique
Biologique et Médicale (CRMBM)

Faculté de Médecine de Marseilles,
Marseilles, France

The main results related to both issues, i.e. the metabolic and electrical aspects of fatigue and the MRI functional investigation of exercising muscle, are discussed in this work. All experimental data were acquired on a Siemens vision Plus system operating at 1.5 teslas.

Key words: skeletal muscle, fatigue, recruitment, MRS, MRI, energetics

I. Introduction

Functional non-invasive investigation of exercising muscle actually began in 1974 when Hoult et al reported that high-energy phosphate compounds could be detected in vivo using 31-phosphorus (^{31}P) magnetic resonance spectroscopy (MRS) [1]. Since then, a large number of studies have been devoted to the investigation of several metabolic aspects of exercising muscle and so forth under a variety of conditions ranging from muscular diseases to high-level training (for review see [2-4]. However, the acute effects of exercise on muscle MR images contrast were first reported in 1988 by Fleckenstein et al. [5]. From then onwards, it has been recognized that MRI could be used to distinguish between active and non-active muscle groups, thereby providing some functional assessments of exercising muscle.

In this report, we will describe in particular the muscle fatigue investigated using magnetic resonance

spectroscopy combined with surface electromyography. A paragraph covers the issue of functional investigations of muscle using MR Imaging (MRI). For each paragraph, a short section will be devoted to technological issues.

II. Combined investigations of muscle fatigue using MR spectroscopy and surface electromyography

Muscle fatigue is usually defined as the loss of maximum force-generating capacity and may occur at the various sites along the pathway from the central nervous system through to the intramuscular contractile machinery. As well as core factors [6], there are peripheral factors that could interfere with force production, including metabolic inhibition of the contractile process and E-C coupling failure [7; 8]. Therefore, isolated metabolic investigations offer a limited window towards the investigation of peripheral factors and a few groups have reported combined investigations of electrical and metabolic changes associated with the failure of muscle force production in order to widen the experimental field of research related to fatigue.

Electromyographic components of fatigue: During the transition from rest to exercise, typical electromyographic changes, such as a rise in the integrated EMG (iEMG) and a shift of the power spectrum towards low

Summary

Magnetic Resonance Spectroscopy and Imaging can be used in order to investigate muscle function non-invasively. Most of the hypotheses related to muscle fatigue – defined as the decline in muscle performance during exercise – have been elaborated on the basis of experimental results obtained in vitro and their physiological relevance has never been clearly demonstrated in vivo. In that context, non-invasive methods such as 31-phosphorus magnetic resonance spectroscopy (^{31}P MRS) and surface electromyography (EMG) have been used to understand both metabolic and electrical aspects of muscle fatigue under physiological conditions. However, muscle activation during exercise can be mapped in terms of both localisation and intensity, using MR Imaging and more particularly T2 changes.

frequencies, have been reported [9; 10]. While the iEMG rise may indicate an increase in the firing rate of the motor unit's discharge and/or recruitment of additional muscle fibers, the reasons accounting for the shift of the mean frequency of the EMG power spectrum remains a matter of debate. Alterations in the frequency components of the [11] EMG power spectrum have been reported during static and dynamic contractions [12; 13] and variously related to accumulation of muscle lactate [14] but not systematically to intracellular acidosis [10] and muscle conduction velocity [15]. Overall, metabolic causes have sometimes been put forward as reasons for surface EMG (sEMG) alterations and combined ^{31}P MRS and sEMG investigations have been performed in order to identify the link, if any.

Methodological issues: From a mainly methodological point of view, this type of combined experiment is actually challenging. On the one hand, surface electrodes have to be positioned beneath the muscles investigated and these could introduce additional noise in MR spectra. Similarly, radiofrequency field interferes with sEMG signals. On the other hand, the magnitudes of sEMG changes are relatively small and the signal must be amplified very close to the source. In summary, technically challenging adaptations are necessary in order to perform such combined experiments. Several types of solutions have been proposed by a few research groups and convincing combined measurements have been reported.

Main results: sEMG recordings can be analyzed in the time domain (root mean square) and in the frequency domain (mean power frequency) and exercise-induced changes associated with both variables provide informa-

tion related to the amount and chronological activation of different motor units. When muscle contractions are not performed voluntarily, electrical stimulations may be used to acquire information regarding peripheral activation i.e. the excitability of the neuromuscular junction and muscle membrane. In that case, supramaximal stimulations are used and corresponding compound muscle action potentials (CMAP or M-wave) are recorded. These variables – or more exactly alterations of these variables – have been reported during fatiguing exercise and analyzed in the light of simultaneous metabolic changes such as depletion of high-energy phosphates and accumulation of metabolic products, for example ADP, Pi and H⁺ as determined from ^{31}P MR spectra recorded in exercising muscle (Fig. 1). Since the first study reported by Miller et al, a few combined analyses have been devoted to the study of both metabolic and electrical changes linked to muscle fatigue. As underlined below, the results are highly controversial and an unified position cannot be proposed at the moment. Miller's results were mainly based on the analysis of the recovery phase following exercise and not on the exercise period per se. They proposed at least three components of fatigue following the completion of exercise with one of them i.e. the recovery rate of MVC being associated with time-dependent changes in both PCr and intracellular pH [8]. They also reported altered M-wave (reduced in amplitude and prolonged in duration) reflecting impaired muscle membrane excitation and a decrease in neuromuscular efficiency (NME) that persists for a longer time as compared to both M-wave and metabolic changes. However, neither variable was closely associated with metabolic changes. Furthermore, the delayed recovery of

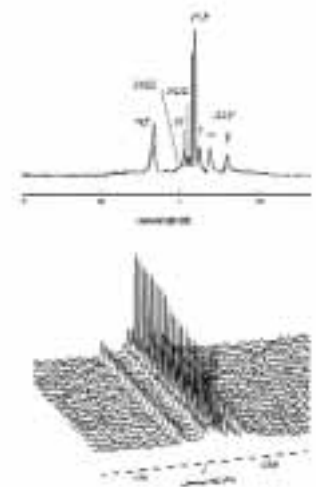


Figure 1 Typical series of ^{31}P MR spectra recorded on a Siemens Vision Plus system (surface coil) with a time resolution of 2 s at end of exercise (first bottom spectrum) and during the following recovery period. Assignments of signals are specified on the top spectrum: ref: reference compound, PME: phosphomonoesters, PDE: phosphodiesters, Pi: inorganic phosphate, PCr: phosphocreatine, a,b,g phosphate groups of ATP. Horizontal axis represents the chemical shifts expressed in Hz. Spectra are recorded from the thigh muscles.

NME indicates a component of impaired muscular function that is independent of high-energy phosphates and intracellular pH. Interestingly, in both adductor pollicis and tibialis anterior muscles, low-intensity exercise produced a marked depression of twitch tension with only minimal changes in MVC, M-wave, PCr and pH [16]. These observations clearly indicate that for a low intensity-exercise, fatigue is largely due to changes in E-C coupling with no contribution of either central factors, impairment of the contractile mechanism, altered membrane properties or impaired neuromuscular transmission [16]. However, the exact mechanism is poorly understood. Similar conclusions have been advanced by Bendahan et al from combined measurements performed during isometric contractions of the forearm flexor muscles [17]. On the basis of their measurements, the existence of

causal relationships between the extent of acidosis and EMG signs of fatigue could not be firmly established. A shift of the median frequency of the EMG power spectrum was indeed observed as a sign of fatigue, but its time-dependent evolution was not linked at all to pH of PCr time-dependent changes given that EMG changes characterizing fatigue were only noted beyond critical metabolic values [17]. Also of interest was their observation of a large scattering of data in a group of untrained subjects despite a standardization of the exercise protocol using the MVC [17]. The effect of oxygen availability on a potential relationship between electrical signs of fatigue and muscle energetics alterations has also been investigated [18]. Hypoxemia did not affect the magnitude of metabolic changes and the duration of contraction. However, the rate of changes in integrated sEMG was significantly modified, thereby changing the correlated evolution of metabolic and electrical changes [18]. The downward shift of the relationships between myoelectrical and metabolic changes under hypoxemia points to the existence of a better E-C coupling and could indicate an adaptive mechanism [18].

However, a relationship between the loss of MVC and accumulation of Pi – or more exactly its diprotonated form – has been reported [19] although the exact causative nature of this relationship is unclear. While Wilson et al [19] and Miller et al [8] have reported such a relationship in a single group of subjects and suggested that accumulation of $H_2PO_4^-$ could account for the failure of muscle force production in agreement with experiments conducted in skinned fibers [20], Kent-Braun et al have recently reported that this relationship is modulated by age and gender, indicating that the causative

links and the underlying mechanisms could differ among various groups of subjects [21]. Accumulation of $H_2PO_4^-$ has been advocated as accounting for the loss of MVC but also for the shift of the mean power frequency (MPF) of the EMG spectrum [22; 23]. A quasi-linear decrease in mean power frequency (MPF) was found during an exhaustive calf muscle exercise test and it was significantly correlated with $H_2PO_4^-$ concentration, which can be considered as resulting from both Pi accumulation and intramuscular acidosis. A similar inverse relationship has been reported between muscle lactate accumulation and the MPF shift in the vastus lateralis muscle, but surprisingly the expected link with intracellular pH was not observed [10]. Bouissou et al also reported that systemic alkalosis was associated with a greater spectrum shift toward lower frequencies at exhaustion despite a level of muscle acidosis similar to that in placebo condition although muscle lactate concentration was higher in alkalosis [10]. It is noteworthy that the shift in EMG power spectrum toward lower frequencies can also account for the increased RMS. When the low frequency component of the EMG signal is increased, more myoelectrical signals will be recorded since muscle tissue and skin act as low-pass filters [24]. In addition, for submaximal (higher than 25% of MVC) exercise, the drop in MPF is independent of force output [12].

More recently, combined analyses of central and peripheral contributions to muscle fatigue have been reported by Kent-Braun et al [21; 25]. In order to quantify the respective contributions of central and peripheral factors to fatigue development, they performed simultaneous non-invasive measurements of central activation (using electromyography), neuromus-

cular junction and muscle membrane excitability (using electrical stimulation) and muscle energetics (using ^{31}P MRS). Their main conclusion was that during a 4-min maximum isometric exercise involving the ankle dorsiflexor muscles, central factors contributed modestly (16%) to fatigue development. The remaining 80% was apparently due to intramuscular sources, primarily increased proton concentration, given that intracellular acidosis was significantly linked to both the fall in MVC and the integrated EMG decrease [25]. The role of H^+ accumulation in muscle fatigue has often been considered as minor, but Kent-Braun's study [21; 25] and other studies [23; 26] have reported that a decline in force was closely related to it. Likewise, Miller et al observed such a relationship [26]. This strong association between fatigue and pH would be consistent with the role of pH in feedback to the central nervous system and a subsequent alteration in central motor drive during the development of fatigue. Similar measurements have been performed during an incremental isometric exercise with the purpose of comparing the magnitude and mechanisms of ankle dorsiflexor muscle fatigue in young and older subjects [21]. From this study, the authors' main conclusion was that young subjects fatigued more than older subjects regarding MVC measurements. However, at the conclusion of the exercise, there was a significant gender effect in that men had a higher Pi and/or PCr (i.e. larger energy consumption) than women. Meanwhile, intracellular pH fell more and accumulation of Pi and/or $H_2PO_4^-$ were larger in the young compared with older subjects and in men compared with women. Whatever the group, a significant linear relationship was found between $H_2PO_4^-$ and the fall in MVC regardless of the

magnitude of fatigue or degree of metabolites accumulation. Although men had a nearly twofold greater increase in H_2PO_4^- during exercise, they developed no greater fatigue than women. As a result, the slope of the relationship between fatigue and $[\text{H}_2\text{PO}_4^-]$ appears to be steeper for women. Similar observations were reported for pH and the overall Pi concentration. Kent-Braun et al suggested that alterations in contractile function did not explain the age-related difference in fatigue. During their moderately fatiguing exercise, whatever the group, CMAP amplitude did not change, suggesting that peripheral excitability was not affected, whereas its duration was shorter as a sign of an increased conduction velocity across the neuromuscular junction or along the muscle membrane. Overall, neither central nor peripheral (compound muscle action potential) played a significant role in fatigue in any group. The varied metabolic responses to exercise suggest that the mechanisms of fatigue change with age and gender [21].

III. Functional investigation of exercising muscle using MRI

As previously mentioned, the acute effects of exercise on muscle MR images contrast were first reported in 1988 by Fleckenstein et al. [5] and from then onwards, it has been recognized that MRI could be used to distinguish between active and non-active muscle groups, thereby providing some functional assessments of exercising muscle. This information comes in addition to the well-known anatomical content of T1-weighted MR images (Fig. 2).

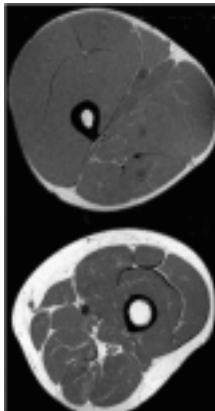


Figure 2 Typical T1-weighted ^1H MR images recorded on a Siemens Vision Plus system (extremity coil) representing transverse sections of the thigh recorded at rest in a professional cyclist (A) and an age and sex-matched control subject.

III.A. ^1H MRI

Contrast differences in MR images come from differences in T1, T2 values and nuclear density. Bone, fat, muscle, connective tissue and blood have different proton nuclear density, which, together with T1 and T2 relaxation processes, will have a significant impact on the final contrast obtained on the image produced. In muscle MR images, signals arise from the protons of water, lipids and bone marrow (Fig. 3). The MR behaviour of intracellular water is believed to result from interactions between the surface of macromolecules and a bound water layer and exchange between this layer and the relatively free cellular water. Proton motion within the free cellular water is itself fast enough to average out molecular interactions; accordingly, this large fraction of cellular water may not contribute to the MR relaxation process. The smaller slowly exchanging bound water fraction may determine much of the MR relaxation character of muscle cells. Muscle cell

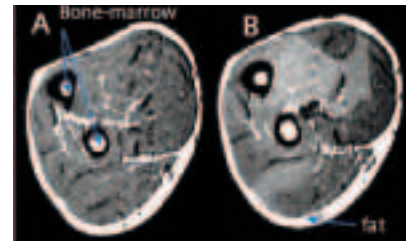


Figure 3 Typical T2-weighted ^1H MR images recorded on a Siemens Vision Plus system (extremity coil) representing transverse sections of the forearm recorded at rest (A) and after a finger flexions exercise (B). Areas with a higher contrast on the image B indicate the activated muscles during exercise.

contraction involves conformational changes in the large contractile proteins as well as mechanical alterations in intracellular surfaces [27]. Such surface alterations may affect the bound water layer, which in turn may determine MR relaxation [28]. In addition to alteration in the size, shape and charge of surfaces in muscle cells, contraction involves the production and translocation of ions and metabolites. These processes would have osmotic effects that alters the concentration and the MR relaxation of water.

III.B. T2 changes in exercising muscle

The changes in proton signal intensity cause exercised muscles to appear "lit up" in T2 weighted images as shown in figure 3. The mechanism of the T2 increase underlying muscle functional MRI is still poorly understood, but is definitely different from the well-known blood oxygenation level dependent (BOLD) effect under-

lying brain functional MRI investigations. T2 measurements in muscle have been performed in order to elucidate the signal shift in muscle that is related to exercise. More particularly, MRI measurements focus on the intrinsic property of water and its exchange between compartments as well as the binding capacity of the water molecule to subcellular structures. Changes in T2 accounting for the discrimination between active and inactive muscles result from the dependence of relaxation on the local molecular environment of the nuclei under study [28]. Given that T2 changes affect exclusively muscle and neither fat nor bone marrow, it is reasonable to conclude that the signal changes arise from one or more of the water compartments in muscle i.e. from intra and extracellular spaces.

T2 and volume changes: As an example, different T2 values in resting muscle have been reported as an indication of different size in extracellular spaces [29]. Increased perfusion would therefore seem an obvious factor, which could account for exercise-induced T2 changes. The volume of exercising muscle is known to increase because of redistribution of body water [30; 31]. This redistribution could be attributed to increased perfusion and the production and translocation of ionic species which could alter the osmotic behaviour of muscle cells [32; 33]. Low intensity exercise is believed to be associated with an increase in extracellular water, whereas high intensity exercise is primarily associated with change in intracellular water [31; 34]. Changes in either intra or extracellular water would be expected to alter the relaxation characteristics of the excited nuclei in a muscle sample [28]. However, changes in muscle volume can be induced by venous occlusion in the same extent as

exercise and similar T2 changes could be expected. Fisher et al [35] demonstrated that venous occlusion had little effect on T2 despite significant changes in muscle volume, thereby clearly indicating that exercise-induced enhanced MRI contrast does not result from the simple increase in fluid volume linked to increased perfusion. More complex, probably intracellular events would be responsible for exercise-induced contrast enhancement.

Exercise-induced changes in MRI T2 contrast result from some complex combination of several processes occurring during muscle contraction and several studies have been devoted to the determination of the mechanisms involved in such changes.

T2 and metabolic changes: As indicated above, it has been known from invasive studies that the volume of exercising muscle increases as a result of redistribution of body water [30; 34]. While changes in muscle volume as a factor involved in post-exercise T2 changes have been refuted on the basis of venous occlusion experiments [11], it has been clearly demonstrated that T2 changes were graded with exercise intensity during dorsiflexion exercises [35], thereby indicating that T2 changes during exercise are dependent on generated force. Furthermore, a direct relationship between changes in osmotically active metabolites – such as lactate and inorganic phosphate – have also been correlated with the extent of T2 changes [36; 37], indicating that they are likely to be related to fluid-shift osmotically driven. This relationship between the extent of T2 and pH changes in exercising muscle has been confirmed from a functional analysis of McArdle patients. Such patients suffer from glycogenolysis deficiency and are unable to produce lactate [38]. As a result of this deficiency, intracellular

pH cannot change upon exercise, as clearly shown by ³¹P MR measurements [38]. In association with the absence of intracellular acidosis, a couple of studies have reported an absence of T2 changes in these patients, thereby confirming the close relationship between MRI T2 contrast changes and pH [39]. The cause-effect relationships between exercise intensity, pH and MRI contrast measurements have been further illustrated from a combined MRI and electromyography study [11]. This study has suggested that shifts in MRI contrast after exercise are an excellent measure of muscle use. Indeed, EMG and T2 changes were both different in eccentric and concentric actions. Interestingly, both measurements were linked [11]. To go further with the determination of mechanisms underlying T2 changes in activated muscles and in keeping with the hypothesis that these changes must result primarily from altered relaxation within the active muscle cells and not from changes in the extracellular fluid space [40; 41], a series of experiments in humans and animals have looked at the metabolic dependence of T2 increase. These studies were based on the hypothesis that an increase in intracellular fluid during exercise is likely to be caused by the accumulation of osmolites such as inorganic phosphate (Pi, resulting from phosphocreatine (PCr) degradation) and lactate. Therefore, if the osmotic expansion of an intracellular fluid compartment is linked to post-exercise T2 changes, these intensity changes ought to vary according to the metabolic changes. In that respect, it has been reported that T2 changes are linked to the exercise intensity [11] and aerobic capacity of a given muscle [42; 43]. However, experiments conducted in marine invertebrates have provided interes-

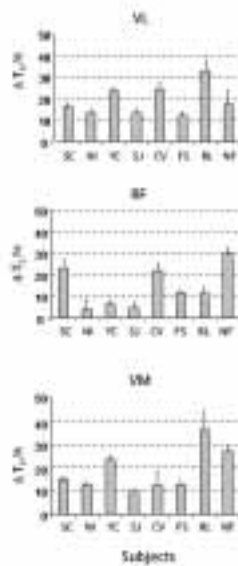


Figure 4 Relative T2 changes (expressed in % of the value measured at rest) in exercising muscles (VL: vastus lateralis, RF: rectus femoris, VM: vastus medialis) of six professional cyclists. It is noteworthy that despite their similar aerobic aptitudes, T2 changes largely vary from one subject to another.

ting information as to the relation between T2 and metabolic changes [44]. Contraction of tail muscle of crayfish (an osmoregulator species with osmolarity near 340mosM) was linked to T2 changes, whereas contraction of lobster tail (a marine osmoconformer with osmolarity equal to that of seawater i.e. 1 osmolar) was not linked to any. These results clearly point to T2 changes being linked to a redistribution of tissue fluid caused by accumulation of intracellular osmolites as previously indicated in rat muscles [43]. However, pH changes occurred only in lobster tail muscle upon contraction and not in crayfish tail muscle, thereby suggesting that muscle acidification per se is not a necessary or dominant cause of the T2 increase during stimulation [44]. Overall, one can conclude that the T2 increase in active mammalian muscles is caused by osmotically driven fluid shifts between subcellular compartments. However, in order to exploit these changes as either a mapping tool or an index of exercise intensity, one has to address the issue of normalising the T2 changes between different muscles and different individuals. Indeed, heterogeneous exercise-induced T2 changes have been reported among subjects with different training status or among muscles within the same subject with no clear interpretation regarding the underlying mechanisms [36; 45]. For instance, we have observed a large range of T2 changes after exercise in professional cyclists with similar aerobic aptitudes (Fig. 4). It has been clearly shown from comparative analysis between eccentric and concentric exercises that the T2 increase after exercise is not dependent on absolute work rate per se but is linearly linked to exercise intensity relative to maximum aerobic power [42; 46]. In addition, Prior et al [43]

have recently reported that the T2 increase after exercise varied inversely with the known aerobic aptitudes. In keeping with the results published by Reid et al [42], such a standardisation should allow reliable comparison.

IV. Conclusion

For many years, there has been considerable interest in trying to determine whether or not biochemical changes occurring in exercising muscle actually contributed to the subjective manifestation of fatigue. The development of fatigue is attributable to both central and peripheral factors. The relative contributions of these factors may be estimated using a combination of voluntary and electrically stimulated force measurements, ³¹P MRS and surface EMG. This type of approach should improve and shed some light on our understanding of the mechanisms of human muscle fatigue by simultaneously assessing functions at the various stages along the pathway of force production.

With regard to the mapping of muscles activated during exercise, investigation of T2 changes using MRI provides reliable information as long as standardisation procedure are properly used. Although it has been quite clearly established that the mechanisms underlying these T2 changes are linked to altered relaxation within the active muscle cells likely due to accumulation of osmotic metabolites, the exact nature of these metabolites still remain to be precisely identified.

References

- [1] Hoult, D. I.; Busby, S. J.; Gadian, D. G.; Radda, G. K.; Richards, R. E.; Seeley, P. J. (1974). Observation of tissue metabolites using ³¹P nuclear magnetic resonance. *Nature* 252, 285-7.
- [2] Argov, Z.; Arnold, D. L. (2000). MR spectroscopy and imaging in metabolic myopathies. *Neurol Clin* 18, 35-52.
- [3] Bendahan, D.; Mattei, J. P.; Kozak-Ribbens, G.; Cozzzone, P. J. (2002). [Non-invasive investigation of muscle diseases using ³¹P magnetic resonance spectroscopy: potential in clinical applications]. *Rev Neurol (Paris)* 158, 527-40.
- [4] Cozzzone, P. J.; Vion-Dury, J.; Bendahan, D.; Confort-Gouny, S. (1996). [Future path of magnetic resonance spectroscopy in clinical medicine]. *Rev. Prat.* 46, 853-8.
- [5] Fleckenstein, J. L.; Canby, R. C.; Parkey, R. W.; Peshock, R. M. (1988). Acute effects of exercise on MR imaging of skeletal muscle in normal volunteers. *AJR Am J Roentgenol* 151, 231-7.
- [6] Bigland-Ritchie, B.; Jones, D. A.; Hosking, G. P.; Edwards, R. H. (1978). Central and peripheral fatigue in sustained maximum voluntary contractions of human quadriceps muscle. *Clin. Sci. Mol. Med.* 54, 609-14.
- [7] Degroot, M.; Massie, B. M.; Boska, M.; Gober, J.; Miller, R. G.; Weiner, M. W. (1993). Dissociation of [H+] from fatigue in human muscle detected by high time resolution ³¹P-NMR. *Muscle Nerve* 16, 91-8.
- [8] Miller, R. G.; Giannini, D.; Milner-Brown, H. S.; Layzer, R. B.; Koretsky, A. P.; Hooper, D., et al. (1987). Effects of fatiguing exercise on high-energy phosphates, force, and EMG: evidence for three phases of recovery. *Muscle Nerve* 10, 810-21.

- [9] Moritani, T.; Muro, M.; Kijima, A. (1985). Electromechanical changes during electrically induced and maximal voluntary contractions: electrophysiologic responses of different muscle fiber types during stimulated contractions. *Exp. Physiol.* 88, 471-483.
- [10] Bouissou, P.; Estrade, P. Y.; Goubel, F.; Guezennec, C. Y.; Serrurier, B. (1989). Surface EMG power spectrum and intramuscular pH in human vastus lateralis muscle during dynamic exercise. *J. Appl. Physiol.* 67, 1245-9.
- [11] Adams, G. R.; Duvoisin, M. R.; Dudley, G. A. (1992). Magnetic resonance imaging and electromyography as indexes of muscle function. *J Appl Physiol* 73, 1578-83.
- [12] Hagberg, M.; Ericson, B. E. (1982). Myoelectric power spectrum dependence on muscular contraction level of elbow flexors. *Eur. J. Appl. Physiol. Occup. Physiol.* 48, 147-56.
- [13] Moritani, T.; Muro, M.; Nagata, A. (1986). Intramuscular and surface electromyogram changes during muscle fatigue. *J. Appl. Physiol.* 60, 1179-85.
- [14] Horita, T.; Ishiko, T. (1987). Relationships between muscle lactate accumulation and surface EMG activities during isokinetic contractions in man. *Eur. J. Appl. Physiol. Occup. Physiol.* 56, 18-23.
- [15] Mortimer, J. T.; Magnusson, R.; Petersen, I. (1970). Conduction velocity in ischemic muscle: effect on EMG frequency spectrum. *Am. J. Physiol.* 219, 1324-9.
- [16] Moussavi, R. S.; Carson, P. J.; Boska, M. D.; Weiner, M. W.; Miller, R. G. (1989). Nonmetabolic fatigue in exercising human muscle. *Neurology* 39, 1222-6.
- [17] Bendahan, D.; Jammes, Y.; Salvan, A. M.; Badier, M.; Confort-Gouny, S.; Guillot, C., et al. (1996). Combined electromyography-31P-magnetic resonance spectroscopy study of human muscle fatigue during static contraction. *Muscle Nerve* 19, 715-21.
- [18] Bendahan, D.; Badier, M.; Jammes, Y.; Confort-Gouny, S.; Salvan, A. M.; Guillot, C., et al. (1998). Metabolic and myoelectrical effects of acute hypoxaemia during isometric contraction of forearm muscles in humans: a combined 31P-magnetic resonance spectroscopy-surface electromyogram (MRS-SEMG) study. *Clin Sci (Colch)* 94, 279-86.
- [19] Wilson, J. R.; McCully, K. K.; Mancini, D. M.; Boden, B.; Chance, B. (1988). Relationship of muscular fatigue to pH and diprotonated Pi in humans: a 31P-NMR study. *J. Appl. Physiol.* 64, 2333-9.
- [20] Nosek, T. M.; Fender, K. Y.; Godt, R. E. (1987). It is diprotonated inorganic phosphate that depresses force in skinned skeletal muscle fibers. *Science* 236, 191-3.
- [21] Kent-Braun, J. A.; Ng, A. V.; Doyle, J. W.; Towse, T. F. (2002). Human skeletal muscle responses vary with age and gender during fatigue due to incremental isometric exercise. *J. Appl. Physiol.* 93, 1813-23.
- [22] Vestergaard-Poulsen, P.; Thomsen, C.; Sinkjaer, T.; Henriksen, O. (1994). Simultaneous 31P NMR spectroscopy and EMG in exercising and recovering human skeletal muscle: technical aspects. *Magn. Reson. Med.* 31, 93-102.
- [23] Laurent, D.; Portero, P.; Goubel, F.; Rossi, A. (1993). Electromyogram spectrum changes during sustained contraction related to proton and diprotonated inorganic phosphate accumulation: a 31P nuclear magnetic resonance study on human calf muscles. *Eur. J. Appl. Physiol. Occup. Physiol.* 66, 263-8.
- [24] Lindstrom, L.; Kadefors, R.; Petersen, I. (1977). An electromyographic index for localized muscle fatigue. *J. Appl. Physiol.* 43, 750-4.
- [25] Kent-Braun, J. (1999). Central and peripheral contributions to muscle fatigue in humans during sustained maximal effort. *Eur. J. Appl. Physiol.* 80, 57-63.
- [26] Cady, E. B.; Jones, D. A.; Lynn, J.; Newham, D. J. (1989). Changes in force and intracellular metabolites during fatigue of human skeletal muscle. *J. Physiol. (Lond.)* 418, 311-25.
- [27] Fung, B. M. (1977). Correlation of relaxation time with water content in muscle and brain tissues. *Biochim Biophys Acta* 497, 317-22.
- [28] Fullerton, G. D.; Potter, J. L.; Dornbluth, N. C. (1982). NMR relaxation of protons in tissues and other macromolecular water solutions. *Magn Reson Imaging* 1, 209-26.
- [29] Polak, J. F.; Jolesz, F. A.; Adams, D. F. (1988). Magnetic resonance imaging of skeletal muscle. Prolongation of T1 and T2 subsequent to denervation. *Invest Radiol* 23, 365-9.
- [30] Lundvall, J.; Mellander, S.; Westling, H.; White, T. (1972). Fluid transfer between blood and tissues during exercise. *Acta Physiol Scand* 85, 258-69.
- [31] Sjogaard, G.; Saltin, B. (1982). Extra- and intracellular water spaces in muscles of man at rest and with dynamic exercise. *Am J Physiol* 243, R271-80.
- [32] Rowell, L. B. (1988). Muscle blood flow in humans: how high can it go? *Med Sci Sports Exerc* 20, S97-103.
- [33] altin, B.; Sjogaard, G.; Gaffney, F. A.; Rowell, L. B. (1981). Potassium, lactate, and water fluxes in human quadriceps muscle during static contractions. *Circ Res* 48, 118-24.
- [34] Sjogaard, G. (1986). Water and electrolyte fluxes during exercise and their relation to muscle fatigue. *Acta Physiol Scand Suppl* 556, 129-36.
- [35] Fisher, M. J.; Meyer, R. A.; Adams, G. R.; Foley, J. M.; Potchen, E. J. (1990). Direct relationship between proton T2 and exercise intensity in skeletal muscle MR images. *Invest Radiol* 25, 480-5.
- [36] Weidman, E. R.; Charles, H. C.; Negro-Vilar, R.; Sullivan, M. J.; MacFall, J. R. (1991). Muscle activity localization with 31P spectroscopy and calculated T2-weighted 1H images. *Invest Radiol* 26, 309-16.
- [37] de Kerviler, E.; Leroy-Willig, A.; Jehenson, P.; Duboc, D.; Eymard, B.; Syrota, A. (1991). Exercise-induced muscle modifications: study of healthy subjects and patients with metabolic myopathies with MR imaging and P-31 spectroscopy. *Radiology* 181, 259-64.
- [38] Bendahan, D.; Confort-Gouny, S.; Kozak-Ribbens, G.; Cozzzone, P. J. (1992). 31-P NMR characterization of the metabolic anomalies associated with the lack of glycogen phosphorylase activity in human forearm muscle. *Biochem Biophys Res Commun* 185, 16-21.
- [39] Fleckenstein, J. L.; Haller, R. G.; Lewis, S. F.; Archer, B. T.; Barker, B. R.; Payne, J., et al. (1991). Absence of exercise-induced MRI enhancement of skeletal muscle in McArdle's disease. *J Appl Physiol* 71, 961-9.
- [40] Conley, M. S.; Foley, J. M.; Ploutz-Snyder, L. L.; Meyer, R. A.; Dudley, G. A. (1996). Effect of acute head-down tilt on skeletal muscle cross-sectional area and proton transverse relaxation time. *J Appl Physiol* 81, 1572-7.
- [41] Ploutz-Snyder, L. L.; Nyren, S.; Cooper, T. G.; Potchen, E. J.; Meyer, R. A. (1997). Different effects of exercise and edema on T2 relaxation in skeletal muscle. *Magn Reson Med* 37, 676-82.
- [42] Reid, R. W.; Foley, J. M.; Jayaraman, R. C.; Prior, B. M.; Meyer, R. A. (2001). Effect of aerobic capacity on the T(2) increase in exercised skeletal muscle. *J Appl Physiol* 90, 897-902.
- [43] Prior, B. M.; Ploutz-Snyder, L. L.; Cooper, T. G.; Meyer, R. A. (2001). Fiber type and metabolic dependence of T2 increases in stimulated rat muscles. *J Appl Physiol* 90, 615-23.
- [44] Meyer, R. A.; Prior, B. M.; Siles, R. I.; Wiseman, R. W. (2001). Contraction increases the T(2) of muscle in fresh water but not in marine invertebrates. *NMR Biomed* 14, 199-203.
- [45] Le Rumeur, E.; Carre, F.; Bernard, A. M.; Bansard, J. Y.; Rochongar, P.; De Certaines, J. D. (1994). Multiparametric classification of muscle T1 and T2 relaxation times determined by magnetic resonance imaging. The effects of dynamic exercise in trained and untrained subjects. *Br J Radiol* 67, 150-6.
- [46] Shellock, F. G.; Fukunaga, T.; Mink, J. H.; Edgerton, V. R. (1991). Acute effects of exercise on MR imaging of skeletal muscle: concentric vs eccentric actions. *AJR Am J Roentgenol* 156, 765-8.



FAQs

Marianne Vorbuchner

MRS Application Development
Siemens Medical Solutions
Erlangen, Germany

Matrix Spectroscopy:

When is the matrix spectroscopy available?

Matrix spectroscopy (signal combination of MRS data originating from multi-array coils) is available with the Tim-SW *syngo* MR 2004V.

All localization methods – *csi*, *svs* and *fid* – are supported.

A stripped-down version of this product feature is available as a WIP package for the software versions 2002B, 2003T and 2004A (Multiple Array).

A transmit/receive head coil is available on 1.5 Tesla MAGNETOM Symphony/Sonata and on the MAGNETOM Avanto system.

Delta Frequency / OVS:

For brain spectroscopy, should we use a -2.7 delta shift to place NAA (2.0 ppm) in the center?

This depends on the pathology. For example, for a lateral lesion close to the bone, the delta frequency can shift to fat ($4.7 \text{ minus } 3.4 = 1.3 \text{ ppm}$).

For prostate spectroscopy, should we use a -2.1 delta shift to place Citrate in the center?

Yes, the Citrate peak ($= 2.6 \text{ ppm}$) can be used: set the delta shift at -2.1 ($4.7 \text{ minus } 2.1 = 2.6 \text{ ppm}$). The range between Citrate and Choline can also be used, in this case set the delta frequency to -1.8.

Is there a separate parameter for a delta shift for the sat bands, according to what signal we want to eliminate?

The regional sat bands in the prostate protocol are used to suppress the local fat signal (set at -3.4) and NOT the water signal. Use a minimal sat band thickness in order to avoid chemical shift artifacts, and keep in mind that the first sat band is the most effective (this is time dependent).

Do the 4 invisible sats apply only to CSI, or also to svcs? Are these 4 sats automatically on or is there a key that has to be toggled on?

This new feature is the “fully excited VOI” (shown also on the Contrast Card). If you select the check box there are 4 internal, invisible saturation bands: this enables the acquisition of a bigger volume in order to keep the chemical shift artifact between water/fat a little lower. Fully excited VOI is only available for CSI spin echo protocols.

Spectral suppression pulses, what are they for?

Using the CSI_SE sequence with the ‘spectral suppression’ feature you can either suppress lipid signals or water signals or both. These pulses are very effective global suppression pulses, mainly used for prostate applications. Note, however, that the minimum echo time is only 90 ms.

Licenses:

Is prostate MRS a separate package?

Prostate spectroscopy is a part of the ^1H CSI-option and is included with the *syngo* MR 2004A/2004V.

Multinuclear

The multinuclear option contains the hardware and system driving, tune-up and adjustment SW for obtaining images and spectra of the following nuclei:

^{13}C , ^{19}F , ^3He , ^7Li , ^{23}Na , ^{39}K , ^{17}O (3T only), ^{129}Xe

Additionally, proton NOE and pulsed CW proton decoupling experiments can be run.

The multinuclear option is available for Symphony and Sonata systems (including upgrades) from *syngo* MR 2002B onwards, and for Trio and Allegra with 2004A. For the Avanto system, it will be available with the next major SW release.

The multinuclear option itself is intended for research users who are willing to create dedicated setups using special sequences and coils.

Recommended multinuclear coil providers for Siemens systems are:

- Advanced Imaging Research, Cleveland, Ohio, USA.
<http://www.advimg.com>
- Bruker Biospin MRI, Ettlingen, Germany.
<http://www.bruker-biospin.de>
- Rapid Biomedical, Wuerzburg, Germany.
<http://www.rapidbiomed.de/>

The application development environment IDEA is required for creating special multinuclear sequences.

³¹P MRS

³¹P MRS is a ready-to-use application package for heart, liver and calf muscle ³¹P-spectroscopy. It contains the double resonant ³¹P/¹H heart-liver surface coil, and dedicated acquisition and post-processing protocols based on the csi_fid and the fid sequence. ¹H NOE and decoupling parameters are activated or available in those protocols.

The ³¹P MRS option requires the multinuclear option among other options. It is available for Symphony and Sonata systems (including upgrades) from syngo MR 2002B onwards and will be available for the Avanto system with the next major SW release. It is planned to offer the ³¹P MRS option also with our 3T systems Trio and Allegra.

Shim:

How is the best shim value calculated during interactive shimming?

The best shim value is calculated as a maximum of T2*. The T2* is more stable than the Full Width Half Maximum. In the optimal case, FWHM should be as small as possible, and T2* as large as possible.

How can the shim result be controlled?

To achieve a highest possible spectra quality, a homogeneous magnetic field is required. Therefore "Advanced Shim" is the default setting in all spectroscopy protocols. The Advanced Shim field Map measurement is an iterative procedure. On all 1T, 1.5T and 3T systems three different shim modes are available: push-button

mode, semi automatic mode, manual mode (the Advanced Shim is independent from the hardware option "Advanced High Order Shim").

Within this shim modes, there is the helpful possibility of using the semi automatic shim. In this mode, all adjustments are automatically executed. Then the user can control and improve the results if necessary before the real start of the measurement. This is recommended in critical anatomic areas, or in off-center positions.

Water Suppression:

Please distinguish between water suppression during measurement and the post-processing step of water reference processing.

Sequence:

What is the difference between our spin echo sequence and the PRESS technique?

The spin echo and the PRESS technique are precisely the same thing.

Measurement:

Please explain how the new water suppression adjustment of syngo MR 2004A works?

The water suppression in syngo MR 2002B was iterative. In the new version, this is replaced by non-iterative searching for the optimum flip-angle. The aim is to shorten the measurement time and to increase the robustness of the adjustment procedure.

Export Rawdata:

How do we get data – such as spectra and even raw data – from the MRI system?

You can copy the whole patient/study/series, including spectra image or raw data, from the Patient Browser to a CD-Rom. Export to offline in a DICOM or BITMAP format is also possible via Patient Browser. From the Spectroscopy Card, the Export to offline function allows the raw data-export in a private ASCII format (explained in the Spectro Application Guide, VA21B).

Important: The switch "implicit raw data transfer" in the service UI must be switched on (Local service / Configuration / Next / Dicom / General / >).

Postprocessing:

In syngo MR 2002B boundary CSI voxels may not be evaluated, and the message "water suppression failed" is displayed.

The problem will be solved in SW 2004A. For older SW versions, open the post-processing protocol and switch off the first step "water reference processing". The cause of this problem is a strong water peak or water hump. The software will search the highest signal at 4.7 +/- 0.5 ppm. If there is a "bad" water signal, then the error message appears.

Life

Sean Harrison
Installed Base Manager

MR Marketing,
Siemens AG Medical Solutions,
Erlangen, Germany

Life. Life is our customer care solution. There are seven key programs to Life. In the most general sense our programs support both the continuous development of your skills, as well as the continuous development of your product. Both essential to helping you extract every bit of value from your investment. These seven programs are focused on helping you meet your clinical and business objectives. Delivering Proven Outcomes. Today. And far into the future.

We would like to introduce a key ingredient of Life with respect to MR. **MAGNETOM Elevate.** Our upgrade program.

There are currently many challenges confronting modern diagnostic imaging. Declining reimbursements, staffing shortages and decreased capital budgets are among these external factors which affect administrative decisions regarding the purchase of imaging systems. These market conditions support exploring cost effective alternatives which maximize system performance and workflow optimization.

MAGNETOM Elevate. It's all about Life. And Life is about getting the most out of your MR investment and maintaining cutting-edge technology at all levels. Siemens has a proven history of MR upgrades spanning over 25 years! Beginning with the first MRI systems installed in the early 80s, we have consistently offered MR upgrades to support EACH platform since. It's a tradition in MR. We

continue to demonstrate our commitment to this tradition by offering simple, easy and smart upgrades to serve almost any MAGNETOM product that you may be using. We are proud to offer the following Elevate programs:

TECHNOLOGY Elevate. Such as **Tim***, for our MAGNETOM Symphony and Trio systems will increase your performance with the latest in MR advancements. Your Symphony only needs the Quantum gradient package in order to be able to move into the **Tim** world of performance. Please contact your local sales representative regarding the Quantum gradient upgrade and the additional benefits you will experience.

SYSTEM Elevate for our classic products such as the MAGNETOM Vision and Impact will utilize your existing magnet vessel technology however transformed to the latest IPA and syngo performance levels. Restoring Life and protecting your investment. Elevate to a MAGNETOM Harmony or Symphony or Sonata.

MANAGED Elevate simplifies the replacement of your previous generation system and provides the latest cutting-edge technology and performance. Elevate to a MAGNETOM Avanto. The first **Tim** system.

There has never been a better time to consider upgrading your MAGNETOM system.

Please contact your local sales organization and inquire as to which MAGNETOM Elevate program will best meet your needs.

*WIP: The information about this product is preliminary. The product is under development and is not commercially available in the US and its future availability cannot be ensured.

Life

Get the most from your investment

Continuous development with Life

Continuous development of your **skills**

Continuous development of your **productivity**

Continuous development of your **technology**



MAGNETOM Flash – Reader Service

Letters to the Editor – We welcome your comments about the content of MAGNETOM Flash. Please send comments to the Editor. Include your name, address, and phone number or e-mail.

World Wide Web – Visit us at www.SiemensMedical.com and www.SiemensMedical.com/MAGNETOM-World. These sites provide information about all Siemens medical products.

Publish articles? – You are invited to publish articles in the newsletter to share your experience with MAGNETOM MR users all over the world. To submit an article please contact the Editor.

Subscription – You have seen the newsletter and want to get it on a regular basis? In the US, please contact the Applications Helpline (phone 800-888-SIEM) and give us your name and business address (no home addresses, please). Outside the US, MAGNETOM Flash is distributed through the local Siemens offices. Please contact the Editor and we will make sure that you are included on your local support office's distribution list.

Editor

Ali Nejat Bengi, M.D., AliNejat.Bengi@siemens.com

Published by

Siemens AG Medical Solutions
P.O. Box 3260, D-91052 Erlangen

Correspondence and

International Distribution

Ali Nejat Bengi, M.D., Editor in Chief

MAGNETOM FLASH

Siemens AG Medical Solutions

MR Marketing

Karl-Schall-Str. 6

D-91052 Erlangen

Phone: 49 - 91 31 - 84 - 75 99

Fax: 49 - 91 31 - 84 - 21 86

US Distribution

MR APPLICATIONS HELPLINE

Siemens Uptime Service Center

110 MacAlyson Court

Cary, NC 27511

Phone: 800 - 888 - SIEM

Fax: 919 - 319 - 28 64

All articles represent the techniques and opinions of the authors and may not represent specific recommendations or endorsements from Siemens Medical Solutions. Contact the authors directly for further information about their techniques and opinion.

The information in this document contains general descriptions of the technical options available, which do not always have to be present in individual cases.

The required features should therefore be specified in each individual case at the time of closing the contract.

Siemens reserves the right to modify the design and specifications contained herein without prior notice. Please contact your local Siemens sales representative for the most current information.

Original images always lose a certain amount of detail when reproduced.

This brochure refers to both standard and optional features. Availability and packaging of options varies by country and is subject to change without notice. Some of the features described are not available for commercial distribution in the US.

Siemens AG, Medical Solutions
Henkestr. 127, D-91052 Erlangen
Germany
Telephone: +49 9131 84-0
www.siemens.com/medical

Please contact in the USA:

Siemens Medical Solutions USA, Inc.
51 Valley Stream Parkway
Malvern, PA 19355
Tel.: +1 888-826-9702
Tel.: 610-448-4500
Fax: 610-448-2254

in Asia:

The Siemens Centre
60 MacPherson Road
Singapore 348615
Tel.: +65 6341 0990
Fax: +65 6778 6722

in Japan:

Siemens-Asahi
Medical Technologies Ltd.
Takanawa Park Tower 14 F
20-14, Higashi-Gotanda 3-chome
Shinagawa-ku
Tokyo 141-8641
(03) 54 23 40 01

**Or contact your local Siemens
Sales Representative**

Siemens AG, Medical Solutions
Magnetic Resonance
Henkestr. 127, D-91052 Erlangen,
Germany
Telephone: ++49 9131 84-0
www.siemens.com/medical

Siemens **Medical**
Solutions that help

© 2004 Siemens Medical Solutions
Order No. A91100-M2220-F691-7-7600
Printed in Germany
GP 65558 WS 050420.